

JSCSEN 74(10)1021–1153(2009)

Journal of the Serbian Chemical Society

ersion
lectronic

VOLUME 74

No 10

BELGRADE 2009

Available on line at



www.shd.org.rs/JSCS/

The full search of JSCS
is available through

DOAJ DIRECTORY OF
OPEN ACCESS
JOURNALS
www.doaj.org



CONTENTS

K. Vytřas, I. Švancara and R. Metelka: Carbon paste electrodes in electroanalytical chemistry (Authors' review)..... 1021

Organic Chemistry and Biochemistry

V. Tešević, S. Milosavljević, V. Vajs, I. Đorđević, M. Soković, V. Lavadinović and M. Novaković: Chemical composition and antifungal activity of the essential oil of Douglas fir (*Pseudotsuga menziesii* Mirb. Franco) from Serbia 1035

S. F. Barbuceanu, G. L. Almajan, I. Saramet, C. Draghici, R. Socoteanu and F. Barbuceanu: New S-alkylated 1,2,4-triazoles incorporating diphenyl sulfone moieties with potential antibacterial activity 1041

M. V. Zlatović, V. V. Škalović, G. M. Roglić, S. V. Kostić-Rajačić and D. B. Andrić: The influence of dispersive interactions on the binding affinities of ligands with an aryl-piperazine moiety to the dopamine D2 receptor 1051

M. A. Nasar, A. Jarrari, M. A. Naseer, T. F. Subhani, B. V. Shetty and F. Shakeel: Anti-oxidant status of atorvastatin in hypercholesterolemic patients 1063

Inorganic Chemistry

L. Mitu, N. Raman, A. Kriza, N. Stănică and M. Dianu: Template synthesis, characterization and antimicrobial activity of some new complexes with isonicotinoyl hydrazone ligands 1075

G. N. Krishnamurthy and N. Shashikala: Synthesis of ruthenium(II) carbonyl complexes with 2-monosubstituted and 1,2-disubstituted benzimidazoles 1085

C. Zhuang, X. Tang, D. Wang, A. Xia, W. Lian, Y. Shi and T. Shi: An unsymmetrical porphyrin and its metal complexes: synthesis, spectroscopy, thermal analysis and liquid crystal properties 1097

R. Ghiasi: Theoretical insights into the properties of the borazine···X⁻ complexes (X⁻ = H, F, Cl, CN, NC or NCO) 1105

Physical Chemistry

S. Mentus, Z. Mojović and V. Radmilović: The use of NaX zeolite as a template to obtain a mono-atomic Pt dispersion by impregnation with Pt(II) acetylacetonate/acetone solution 1113

D. R. Sekulić, B. M. Babić, Lj. M. Kljajević, J. M. Stašić and B. V. Kaludjerović: The effect of gamma radiation on the properties of activated carbon cloth 1125

Analytical Chemistry

Z. J. Huang, X. G. Wang and J. Zhang: Solid phase extraction and a spectrophotometric method for the determination of trace amounts of gold with 4-rhodanineazo benzoic acid..... 1133

Z. B. Todorović, M. L. Lazić, V. B. Veljković and D. M. Milenović: Validation of an HPLC–UV method for the determination of digoxin residues on the surface of manufacturing equipment 1143

Published by the Serbian Chemical Society
Karnegijeva 4/III, 11000 Belgrade, Serbia
Printed by the Faculty of Technology and Metallurgy
Karnegijeva 4, P.O. Box 35-03, 11120 Belgrade, Serbia



J. Serb. Chem. Soc. 74 (10) 1021–1033 (2009)
JSCS–3896

AUTHORS' REVIEW

Carbon paste electrodes in electroanalytical chemistry#

KAREL VYTRÁS*, IVAN ŠVANCARA and RADOVAN METELKA

*Department of Analytical Chemistry, Faculty of Chemical Technology, University of
Pardubice, CZ – 532 10 Pardubice, Czech Republic*

(Received 17 April 2009)

Abstract: An overview is given dealing with the applications of carbon paste electrodes in equilibrium potentiometry as well as in electrochemical stripping analysis using both voltammetric and potentiometric modes. Various modifications of carbon pastes and carbon paste-based biosensors are also mentioned. The main emphasis in this article is directed at summarizing recent results of the authors' research group during the past few years.

Keywords: carbon paste electrodes; potentiometry; electrochemical stripping analysis; flow injection analysis; electrode modification; heavy metals determination; biosensors.

CONTENT

1. INTRODUCTION
2. CONSTRUCTION OF CARBON PASTE ELECTRODES
3. POTENTIOMETRY
 - 3.1. Electrochemical stripping analysis with unmodified paste electrodes
 - 3.2. Modified carbon pastes in stripping analysis
4. CARBON PASTE AS A SUPPORT FOR METALLIC FILM ELECTRODES
5. AMPEROMETRIC (BIO)SENSORS
6. CONCLUSION

1. INTRODUCTION

Carbon paste electrodes (CPEs) belong to promising electrochemical or bio-electrochemical sensors of wide applicability. In 2008, it was exactly a half century since Ralph Norman Adams from the University of Kansas published a short one-page report¹ in which he introduced this kind of electrode, which was originally designed as an alternative to the dropping mercury electrode. Although the concept of a dynamic renewable electrode surface was not successful, it turned

* Corresponding author. E-mail: karel.vytras@upce.cz

Presented as Invited Lecture at 47th Meeting of the Serbian Chemical Society, Belgrade, Serbia, 2009.

doi: 10.2298/JSC0910021V

out that the material with paste-like consistency could be practically employed in voltammetric analysis. After the pioneering work of Kuwana,^{2,3} who actually first modified a CPE by introducing an electrochemically active surface into the material and, after the first chemical modification of an electrode for electrosynthesis,⁴ the modification was soon applied to carbon paste electrodes.^{5,6} Finally, Baldwin described a simple method of direct mixing of a solid modifier to the paste,⁷ which was the commencement of explosive research activity in this field. Quite a few reviews are exclusively devoted to CPEs.^{8–14} Presently, CPEs represent one of the most frequent types of working electrodes. The overwhelming number of CPEs used worldwide belongs to pastes with insulating liquids (paraffin oil, silicon oil, bromonaphthalene, tricresyl phosphate and others). The basic requirements for a pasting liquid are its practical insolubility in the solution under measurement, a low vapor pressure to ensure both mechanical stability and long lifetime, and further, in the case of voltammetric and amperometric applications, its electrochemical inactivity in the potential window of interest. In contrast to the relatively complicated modifications of solid substrates, carbon pastes can be modified simply to obtain quantitatively new sensors with desired, often predefined, properties.¹⁵ Very recently, a review with 333 references was published¹⁶ in the form of a retrospective compilation presenting the field by means of various facts, notes, data, surveys, and summaries that illustrate individual achievements and milestones. A brief overview based mainly on the authors' group contributions is thus given in this paper.

2. CONSTRUCTION OF CARBON PASTE ELECTRODES

Common types of carbon pastes are soft and non-compact, and have to be kept in special bodies. A holder for carbon pastes can be realized as a well drilled into a short Teflon rod,¹⁷ a glass tube¹⁸ or a polyethylene syringe¹⁹ filled with a paste, which is electrically contacted *via* a conducting wire. Such constructions are very simple; however, there is one aspect which makes them not very convenient for practical use and this is the necessity of refilling the carbon paste in experiments requiring a regular removal of the electrode surface layer. More sophisticated constructions circumventing this time-consuming procedure were designed by Monien *et al.*²⁰ and Lindquist,²¹ who proposed piston-driven electrode holders where the desired amount of the used paste could simply be extruded from the electrode body and smoothed away or cut off. Similar types of home-made piston-driven carbon paste holders are used by our research team.^{15,22}

Recently, our research group also devoted particular attention to the development of novel or innovated carbon paste electrode holders. Two typical examples of these activities are illustrated in Fig. 1. Image "1A" shows two variants of the so-called carbon paste groove electrode (CPGrE) as atypical construction of CPE, copying the planar design of some screen-printed electrodes.²³ The CPGrE

assembly comprises a miniature plastic prismatic bar with a horizontal channel for carbon paste filling, a metal contact and additional plastic insert(s) defining the electrode surface *via* its mechanical coverage/exposure. The whole construction can be devised as an electrically heated electrode (left), applicable for batch measurements and allowing the sensitivity of measurements that have to be made in still solutions to be enhanced or as the working electrode for hydrodynamic amperometry, and as the detector in flowing streams (right). The usefulness of the latter was demonstrated in a very recent study concerning its intimate testing in the FIA mode.²⁴

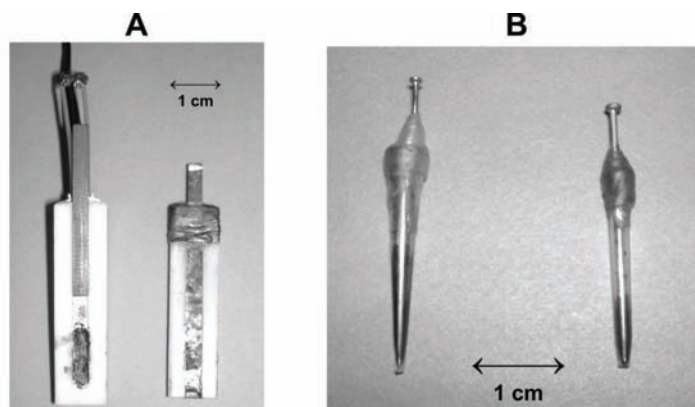


Fig. 1. Some novel construction types of electrode holders for carbon paste. Two assembled carbon paste groove electrodes; the electrically heated variant (A – left) and set-up for detection in the FIA-mode (A – right); two carbon paste mini-electrodes; with an uncut tip (B – left), cut-off variant offering a larger surface diameter (B – right). For further specification, see original reports.²³⁻²⁵

A new type of carbon paste mini-electrode (CPmE) which can be made from common plastic pipette tips, the vertical cutting of which provides the desired surface area,²⁵ is depicted in photograph “1B”. The advantage of this small design is the minimization of the consumption of carbon paste(s), which can be economic when using some mixtures from rather expensive carbon nanotubes, for example.

3. POTENTIOMETRY

From the viewpoint of equilibrium potentiometry, the composition of carbon pastes enables the classification of CPEs as ion-selective liquid membrane type electrodes. The pasting liquid usually exhibits good extraction ability against neutral electroactive species of non-dissociated weak acids, neutral metal chelates or ion associates. Then, the potential of an electrode containing such an organic solvent extract is predominantly governed by ionic exchange at the interface between the organic phase of the electrode and the sample solution, resulting in the

so-called Donnan potential.²⁶ Carbon paste-based ion-selective electrodes (CPISEs) were reported and applied for the determination of several ions (see Refs.^{14,26} and references therein). For example, four ion-exchangers were prepared for new perchlorate and fluoroborate CPISEs, which found their application in the direct potentiometric determinations of the two anions, as well as monitoring sensors for potentiometric ion-pair formation-based titrations.²⁷ Similarly, the ion-pairing principle was used in titrations of complex anions of trivalent thallium²⁸ or elements forming heteropolyanions.^{29,30} An application of the CPGRE type construction (see above) in potentiometric pH measurements³¹ is presented in Fig. 2.

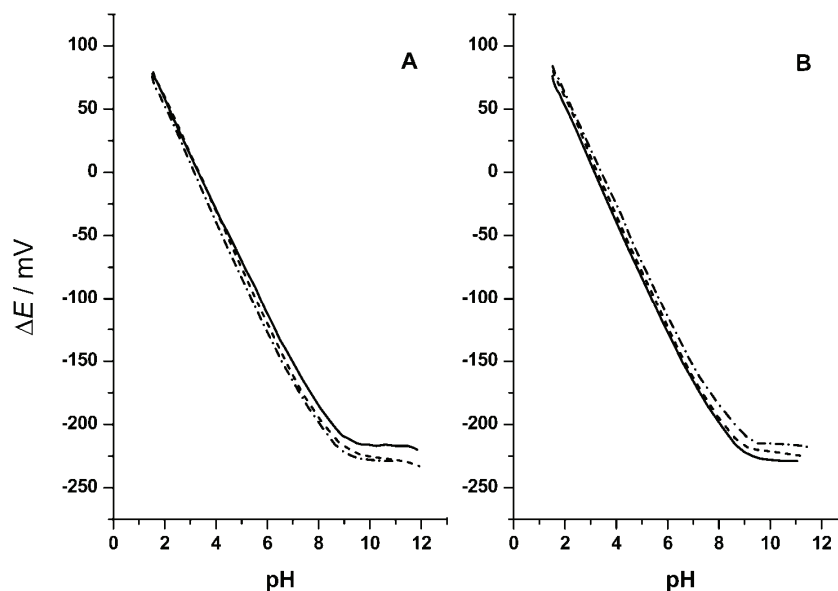


Fig. 2. Potentiometric responses of carbon paste groove electrodes with dispersed bismuth powder (17 % w/w) in Britton–Robinson buffer solution (three repeated measurements).

The electrode surface was renewed after each set of measurements (A);
all sets measured at the same surface (B).

A distinct advantage of carbon paste-based electrodes is their very low ohmic resistance (less than 10Ω instead of up to $\text{M}\Omega$ values for electrodes equipped with polymeric membranes). Thus, experimental work with CPISEs is more convenient and simpler potentiometers allowing voltage measurements of potentiometric cells with lower inner resistance may be applied. This fact accompanied with a very quick response time is especially appreciated in automatic titration procedures.³² Thus, all procedures elaborated for potentiometric indication of ion-pair formation-based titrations with polymeric membrane electrodes³³ can simply be monitored using CPISEs; the determination of surfactants can serve as an excellent example.³⁴

3.1. Electrochemical stripping analysis with unmodified paste electrodes

In voltammetric stripping analysis, the choice of the main constituents for the preparation of the carbon paste was rather conservative and, in fact, there were no attempts to seek new alternative materials. The properties of conventional paste mixtures from spectroscopic graphite and paraffin oils were found satisfactory for the majority of applications. An example can be given dealing with application of such an electrode for trace iron(III) determination in compounds of pharmaceutical significance.³⁵ In 1993, some new types of CPEs containing more polar organic liquids, often used as plasticizers of polymeric membrane-based ion-selective electrodes, were introduced.³⁶ Consequently, it was shown that these pasting liquids act as anion exchangers in acidic media due to the presence of some protonizable functional groups. For example, a CPE containing tricresyl phosphate was found suitable for the accumulation of some lipophilic anions, forming ion-pairs with the protonized pasting liquid. At that time, some interesting applications of these pastes in both stripping voltammetry^{37,38} and stripping chronopotentiometry³⁹⁻⁴² were introduced.

3.2. Modified carbon pastes in stripping analysis

Carbon pastes undoubtedly represent one of the most convenient materials for the preparation of modified electrodes. A modifier can be dissolved in a binder or admixed mechanically to the paste during its homogenization. For example, a CPE modified with cobalt(II) phthalocyanine was used for voltammetric determination of ascorbic acid in foodstuffs.⁴³ *In situ* modification of the electrode paste surface is often used as well; examples may be given dealing with applications of an anionic surfactant for voltammetric determination of silver(I) at ultratrace levels.⁴⁴ Recently, some procedures utilizing cationic surfactants for *in situ* modifications of CPEs were reported for determinations of chromium(VI),⁴⁵ osmium(IV)⁴⁶ and other platinum metals,⁴⁷ whereby negatively charged complex anions were formed.

4. CARBON PASTE AS A SUPPORT FOR METALLIC FILM ELECTRODES

In order to prepare electrodes plated with metallic films, numerous conductive materials have been proposed for use; glassy carbon is probably the most frequently employed material. It was confirmed that carbon paste as a support for plating with metallic films is able to offer results similar to those of well established solid electrodes and, in addition, their easy and inexpensive preparation and no risk of mechanical damage of the electrode surface are very advantageous.

Mercury film electrodes were very popular and mostly employed in electrochemical stripping determinations of heavy metal ions instead of stationary mercury electrodes. For example, a CPE containing tricresyl phosphate was found to

be especially suitable for this purpose; both voltammetric and chronopotentiometric modes were applied.^{48,49} It was also confirmed that a mercury film with properties similar to those of a mercury film generated from solutions of mercury(II) salts may be obtained by reduction of mercury(II) oxide dispersed in a paste.⁵⁰ Since 1996, investigations on gold film-plated CPEs represents a new subject of our research because, hitherto, no report on such electrodes had been published. They were found useful for the determination of mercury⁵¹ and arsenic.⁵²

Bismuth film electrodes (BiFEs) were first prepared by Schwabe⁵³ and used in potentiometric pH measurements. Into electrochemical stripping analysis, they were introduced by Wang *et al.* in 2000.⁵⁴ This whole topic has already achieved a relevant position within research activities devoted to the development and application of mercury-free electrodes. Their most significant advantage is that they are environmentally friendly, since the toxicity of bismuth and its salts is significantly lower than that of salts of other heavy metals. Furthermore, the advantageous analytical properties of BiFEs in electrochemical stripping analysis, roughly comparable to those of mercury film electrodes, are attributed to the property of bismuth to form alloys with various metals (which is analogous to the amalgams formed by mercury). Many papers appearing since introduction of BiFEs are referred to in recent reviews.^{55–59} Unfortunately, numerous authors simply followed the original procedure;⁵⁴ this means that BiFEs were prepared using either different substrates or different varieties in their constructions but they were only applied in the determinations of the same metal ions - lead(II) and cadmium(II) – in the same medium – a pH 4.5 acetate buffer. However, it has been shown that bismuth film-plated CPEs may also be applied in alkaline media, such as ammonia buffers⁶⁰ or even 0.10 M KOH solution.⁶¹

The role of the plating regime in the deposition of bismuth films onto a carbon paste surface was also investigated. It should be noted that the term “film” does not correspond with the real situation as it is not compact: analogously to mercury “films” deposited in form of isolated droplets, bismuth is deposited in form of isolated crystals. The new observations performed by scanning electron microscopy were focused mainly on morphological transformations of the microstructure of the bismuth film in dependence on the deposition process and its intensity during potentiostatic electrolysis.⁶² To overcome such electrolytic depositions, bismuth powder-dispersed CPEs were introduced.⁶³ The electrode paste was prepared as a mixture of finely powdered metallic bismuth together with graphite powder and silicon oil and was characterized in solutions containing Cd(II) and Pb(II) at the microgram/liter level in conjunction with square-wave anodic stripping voltammetry. The electrode exhibited well-defined and separated stripping signals for both metals accompanied with a low background contribution. Moreover, it exhibited superior performance in comparison to the bare CPE and,

surprisingly, yielded a response higher than that of an *in situ* prepared bismuth film CPE.

The introduction of bismuth(III) salts and bismuth films into electroanalysis also instigated the novel approach of potentiometric stripping analysis based on total substitution of mercury by bismuth. First, Bi(III) salts could be applied to form bismuth films. Secondly, bismuth(III) salts could substitute mercury(II) in its role as an oxidant. These facts offer quite new possibilities of an attractive use of “mercury-free”, environmentally friendly PSA procedures for the determinations of some heavy metals. The highest signals were observed when working in solutions containing anions forming complexes with bismuth(III), such as chlorides or bromides.⁶⁴

Similarly to bismuth, antimony bulk electrodes are also well known from equilibrium potentiometry. Concerning voltammetry, attempts with modifications of screen-printed carbon electrodes using either Bi₂O₃ or Sb₂O₃ were also realized,⁶⁵ but the first antimony film electrode prepared *in situ* on a glassy carbon electrode substrate and employed in combination with either stripping voltammetry or stripping potentiometry was reported very recently.⁶⁶ Simultaneously, initial studies with antimony-modified CPEs, focusing on their performance in anodic stripping voltammetry, were performed; the investigations comprised the first experiments with Sb film-plated and Sb powder-dispersed CPEs.^{67,68} Again, antimony films generated *in situ* on CPEs with excess antimony(III) salts as chemical oxidants were introduced as new procedures for potentiometric stripping analysis following previous electrolytic preconcentration of the to be determined metals.⁶⁹ Moreover in acidic solutions containing halide ions, the oxidation ability of Sb(III) is adequately limited because of the formation of its corresponding halide complexes. Compared with similar total substitution of traditionally used mercury(II) by bismuth(III), the use of antimony(III) offers a higher sensitivity in the detection of heavy metals.

Typical stripping voltammetric responses of metallic film, metal powder, and metal oxide-modified CPEs obtained by analyzing an equimolar mixture of Cd(II) and Pb(II) ions in model water samples are depicted in Fig. 3. The figure shows a comparison of the individual electrode configurations in two sets of voltammograms (A and B), taken from previous studies,^{59,67,70} in which the respective experimental conditions and, especially, the supporting electrolyte were optimized for the antimony-modified variants.

5. AMPEROMETRIC (BIO)SENSORS

In collaboration with Austrian colleagues, the first modifications of carbon pastes with manganese dioxide films in order to obtain sensors for the determination of hydrogen peroxide commenced at the end of the nineties.^{71–73} However, for application in procedures utilizing flow injection analysis, it seemed

more effective to transfer all experience obtained with such CPE-based sensors to their analogous screen-printed configurations.⁷⁴ Such sensors enabled the detection of hydrogen peroxide by either mediated oxidation or mediated reduction (Fig. 4).

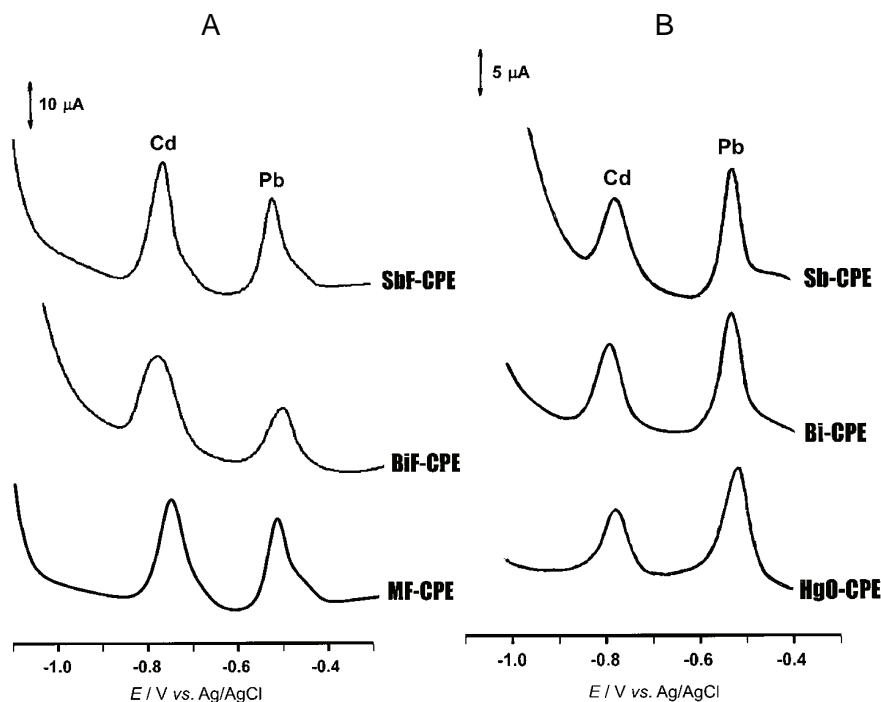


Fig. 3. Anodic stripping voltammograms of Cd(II) + Pb(II) at different types of metal film-plated and metal or metal oxide powder-dispersed carbon paste electrodes.

Mercury, bismuth or antimony film-plated carbon paste electrode (MF-CPE, BiF-CPE, or SbF-CPE) (A); HgO (5 %), Bi (20 %) or Sb (20 % w/w) powder-dispersed CPE (B); supporting electrolyte, 0.01 M HCl; $c(\text{Cd,Pb}) = 50 \text{ ppb}$; $c(\text{Hg,Bi,Sb}) = 1 \times 10^{-5} \text{ mol L}^{-1}$ (for A); accumulation potential, $-1.2 \text{ V vs. Ag/AgCl/3M KCl}$; accumulation time, 120 s; equilibrium time, 15 s; potential range from -1.1 to -0.30 V .

Furthermore, in combination with a proper biocatalyst (glucose oxidase was used in the initial experiments), they served as basic units in the construction of the corresponding biosensors;^{75,76} a similar biosensor based on sarcosine oxidase was also reported.⁷⁷ Modification with other metal oxides were also studied.^{78–80} Recently, biosensors possessing very good properties were obtained when electrocatalysts based on the oxides of platinum group metals were used as modifiers/mediators.^{81–85} Biosensors based on dehydrogenases were also studied.⁸⁶

Finally, CPEs were applied in studies involving DNA sensing,^{87–89} as well as for the electrochemical detection of bacterial cells.^{90,91}

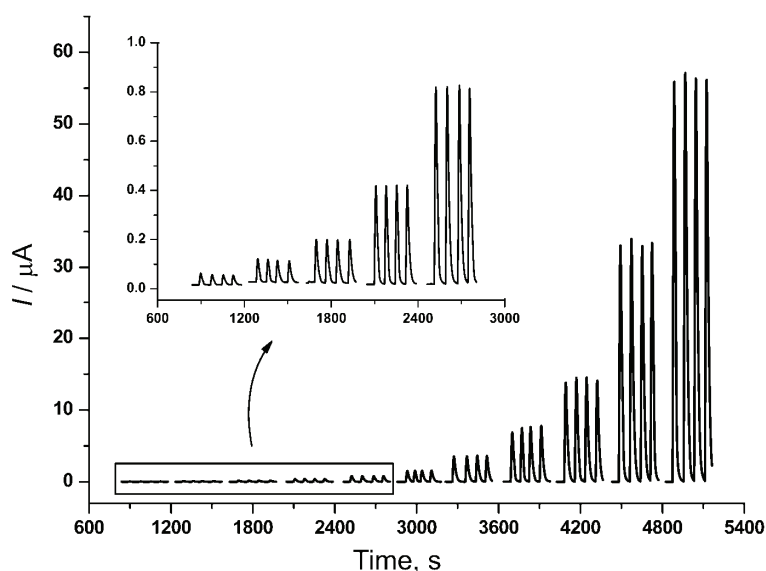


Fig. 4. Flow injection analysis of hydrogen peroxide with amperometric detection. Sensing element, CPGRE with dispersed RuO_2 powder (5 % w/w); $c(\text{H}_2\text{O}_2)$: 0.5–1000 mg L^{-1} ; measured in a stream of 0.10 M phosphate buffer (pH 7.0); flow rate, 0.50 mL min^{-1} ; detection potential, 0.5 V vs. Ag/AgCl/3M KCl.

In some case, however, carbon ink used for the fabrication of screen-printed layers, although similar to carbon pastes, can cause some different properties of sensors when compared with those based on original carbon pastes. To avoid this sometimes unexpected behavior, groove electrodes (GrEs) were recently introduced as a new alternative to using carbon pastes in electroanalysis (see above).³¹ Compared to conventional CPEs, the construction specifics of GrEs offer simpler preparation and quicker exchange of the carbon paste mixture, whereas the small size and planar configuration compete with screen-printed electrodes. First experiments dealing with their application in flow injection analysis were recently presented.^{23,24,31}

6. CONCLUSION

Over the past decades, as indicated in a very recent review,¹⁶ carbon paste has become one of the most popular electrode materials used for the laboratory preparation of various electrodes, sensors, and detectors. Such a position is undoubtedly the result of the optimum constellation of physicochemical and electrochemical properties of this carbonaceous substrate. The authors also believe

that a contribution coming from our laboratories, outlined in this paper, may offer an interesting insight into the field.

Acknowledgement. Financial support of the Ministry of Education, Youth and Sports of the Czech Republic under project MSM0021627502 is gratefully acknowledged.

ИЗВОД

ЕЛЕКТРОДЕ ОД УГЉЕНИЧНЕ ПАСТЕ У ЕЛЕКТРОАНАЛИТИЧКОЈ ХЕМИЈИ

KAREL VYTRÁS, IVAN ŠVANCARA и RADOVAN METELKA

*Department of Analytical Chemistry, Faculty of Chemical Technology,
University of Pardubice, CZ – 532 10 Pardubice, Czech Republic*

Дат је преглед примена електрода од угљеничне пасте у равнотежној потенциометрији као и у електрохемијској линеарној промени потенцијала и волтаметрији. Поменуте су такође и различите модификације угљеничних паста и биосензора заснованих на угљеничним пастама. Основни циљ овог рада је да сумира новије резултате истраживачке групе аутора током неколико протеклих година.

(Примљено 17. априла 2009)

REFERENCES

1. R. N. Adams, *Anal. Chem.* **30** (1958) 1576
2. T. Kuwana, W. G. French, *Anal. Chem.* **36** (1964) 241
3. F. A. Schultz, T. Kuwana, *J. Electroanal. Chem.* **10** (1965) 95
4. G. T. Cheek, R. F. Nelson, *Anal. Lett. A* **11** (1978) 393
5. T. Yao, S. Musha, *Anal. Chim. Acta* **110** (1979) 203
6. K. Ravichandran, R. P. Baldwin, *J. Electroanal. Chem.* **126** (1981) 293
7. K. Kalcher, *Electroanalysis* **2** (1990) 419
8. I. Švancara, K. Vytřas, F. Renger, M. R. Smyth, *Sb. Ved. Pr., Vys. Sk. Chem.-Technol., Pardubice* **56** (1992/93) 21
9. K. Kalcher, X. H. Cai, G. Koelbl, I. Švancara, K. Vytřas, *Sb. Ved. Pr., Vys. Sk. Chem.-Technol., Pardubice* **57** (1994) 5
10. I. Švancara, K. Vytřas, *Chem. Listy* **88** (1994) 138
11. K. Vytřas, I. Švancara, *Chem. Listy* **88** (1994) 412
12. K. Kalcher, J.-M. Kauffmann, J. Wang, I. Švancara, K. Vytřas, C. Neuhold, Z. P. Yang, *Electroanalysis* **7** (1995) 5
13. K. Kalcher, K. Schachl, I. Švancara, K. Vytřas, H. Alemu, *Sci. Pap. Univ. Pardubice, Ser. A* **3** (1997) 57
14. K. Vytřas, K. Kalcher, I. Švancara, K. Schachl, E. Khaled, J. Jeřková, J. Konvalina, R. Metelka, *Electrochem. Soc. Proc.* **18** (2001) 277
15. K. Kalcher, I. Švancara, R. Metelka, K. Vytřas, A. Walcarius, *Heterogeneous Carbon Electrochemical Sensors*, in *Encyclopedia of Sensors*, C. A. Grimes, E. C. Dickey, M. V. Pishko, Eds., American Scientific Publishers, Stevenson Ranch, 2006, Vol. 4, p. 283
16. I. Švancara, K. Vytřas, K. Kalcher, A. Walcarius, J. Wang, *Electroanalysis* **21** (2009) 7
17. R. N. Adams, *Electrochemistry at Solid Electrodes*, Dekker, New York, 1969, p. 280
18. T. Z. Peng, H. P. Li, S. W. Wang, *Analyst* **118** (1993) 1321
19. J. H. Pei, Q. Jin, J. Y. Zhong, *Talanta* **38** (1991) 1185

20. H. Monien, H. Specker, K. Zinke, *Fresenius Z. Anal. Chem.* **225** (1967) 342
21. J. Lindquist, *J. Electroanal. Chem.* **18** (1968) 204
22. I. Švancara, R. Metelka and K. Vytřas, *Piston-Driven Carbon Paste Electrode Holders for Electrochemical Measurements*, in *Sensing in Electroanalysis*, K. Vytřas, K. Kalcher, Eds., University of Pardubice, Pardubice, 2005, p. 7
23. I. Švancara, P. Kotzian, M. Bartoš, K. Vytřas, *Electrochem. Commun.* **7** (2005) 657
24. R. Metelka, M. Žeravík, K. K. Vytřas, in *Monitorování cizorodých látek v životním prostředí - X*, J. Fischer, J. Kellner, K. Vytřas, Eds., University of Pardubice, Pardubice, 2008, p. 153 (in Czech)
25. L. Baldrianová, I. Švancara, S. Sotiropoulos, *Anal. Chim. Acta* **599** (2007) 249
26. K. Vytřas, I. Švancara, in *Sensing in Electroanalysis*, K. Vytřas, K. Kalcher, Eds., University of Pardubice, Pardubice, 2007, Vol. 2, p. 7
27. J. Ježková, J. Musilová, K. Vytřas, *Electroanalysis* **9** (1997) 1433
28. K. Vytřas, E. Khaled, J. Ježková, H. N. A. Hassan, B. N. Barsoum, *Fresenius J. Anal. Chem.* **367** (2000) 203
29. K. Vytřas, J. Ježková, J. Skořepa, *Talanta* **64** (1998) 1619
30. R. Metelka, S. Slavíková, K. Vytřas, *Talanta* **58** (2002) 147
31. R. Metelka, M. Žeravík, K. Vytřas, in *Programme and Abstract Book of the Zing Conference "Electrochemistry Exploring the Frontiers"*, (2009), Playa del Carmen, Mexico, 2009, p. 33
32. K. Vytřas, J. Ježková, V. Dlabka, J. Kalous, *Sci. Pap. Univ. Pardubice, Ser. A* **3** (1997) 307
33. K. Vytřas, *Ion-Sele. Electrode Rev.* **7** (1985) 77
34. K. Vytřas, J. Ježková, J. Kalous, *Egypt. J. Anal. Chem.* **6** (1997) 1433
35. A. Komersová, M. Bartoš, K. Kalcher, K. Vytřas, *J. Pharm. Biomed. Anal.* **16** (1998) 1373
36. I. Švancara, K. Vytřas, *Anal. Chim. Acta* **273** (1993) 195
37. K. Vytřas, I. Švancara, F. Renger, M. Srey, R. Vaňková, M. Hvizdalová, *Collect. Czech. Chem. Commun.* **58** (1993) 2039
38. I. Švancara, J. Konvalina, K. Schachl, K. Kalcher, K. Vytřas, *Electroanalysis* **10** (1998) 435
39. K. Vytřas, J. Konvalina, *Electroanalysis* **10** (1998) 787
40. J. Konvalina, E. Khaled, K. Vytřas, *Collect. Czech. Chem. Commun.* **65** (2000) 1047
41. I. Švancara, B. Ogorevc, S. B. Hočevar, K. Vytřas, *Anal. Sci.* **18** (2002) 301
42. I. Švancara, B. Ogorevc, M. Nović, K. Vytřas, *Anal. Bioanal. Chem.* **372** (2002) 795
43. M. Nováková, K. Kalcher, K. Schachl, A. Komersová, M. Bartoš, K. Vytřas, *Sci. Pap. Univ. Pardubice, Ser. A* **3** (1997) 41
44. I. Švancara, K. Kalcher, W. Diewald, K. Vytřas, *Electroanalysis* **8** (1996) 336
45. I. Švancara, P. Foret, K. Vytřas, *Talanta* **64** (2004) 844
46. M. Galík, M. Cholota, I. Švancara, A. Bobrowski, K. Vytřas, *Electroanalysis* **18** (2006) 2218
47. I. Švancara, M. Galík, K. Vytřas, *Talanta* **72** (2007) 512
48. I. Švancara, M. Pravda, M. Hvizdalová, K. Vytřas, K. Kalcher, *Electroanalysis* **6** (1994) 663
49. J. Konvalina, E. Khaled, K. Vytřas, *Collect. Czech. Chem. Commun.* **65** (2000) 1047
50. R. Metelka, K. Vytřas, A. Bobrowski, *J. Solid State Electrochem.* **4** (2000) 348

51. I. Švancara, M. Matoušek, E. Sikora, K. Schachl, K. Kalcher, K. Vytřas, *Electroanalysis* **9** (1997) 827
52. P. Chadim, I. Švancara, B. Pihlar, K. Vytřas, *Collect. Czech. Chem. Commun.* **65** (2000) 1035
53. a) K. Schwabe, *Pharmazie* **3** (1948) 449; b) K. Schwabe, *Z. Elektrochem.* **53** (1949) 125; c) K. Schwabe, *Z. Elektrochem.* **55** (1951) 411
54. J. Wang, J. M. Lu, S. B. Hočevar, P. A. M. Farias, B. Ogorevc, *Anal. Chem.* **72** (2000) 3218
55. A. Economou, *Trends Anal. Chem.* **24** (2005) 334
56. J. Wang, *Electroanalysis* **17** (2005) 1341
57. I. Švancara, K. Vytřas, *Chem. Listy* **100** (2006) 90
58. K. Vytřas, I. Švancara, R. Metelka, L. Baldrianová, E. Tesařová, M. Stočes, in *International Conference on Electroanalytical Chemistry and Allied Topics*, S. K. Aggarwal, K. Chander, N. Gopinath, Eds., ISEAC, Mumbai, 2007, p. 230
59. I. Švancara, L. Baldrianová, E. Tesařová, S. B. Hočevar, S. A. A. Elsuccary, A. Economou, S. Sotiropoulos, B. Ogorevc, K. Vytřas, *Electroanalysis* **18** (2006) 177
60. I. Švancara, L. Baldrianová, E. Tesařová, T. Mikysek, K. Vytřas, *Sci. Pap. Univ. Pardubice, Ser A* **12** (2006) 5
61. S. A. A. Elsuccary, I. Švancara, R. Metelka, L. Baldrianová, M. E. M. Hassouna, K. Vytřas, *Sci. Pap. Univ. Pardubice, Ser A* **9** (2003) 5
62. I. Švancara, L. Baldrianová, M. Vlček, R. Metelka, K. Vytřas, *Electroanalysis* **17** (2005) 120
63. S. B. Hočevar, I. Švancara, K. Vytřas, B. Ogorevc, *Electrochim. Acta* **31** (2005) 706
64. K. Vytřas, I. Švancara, R. Metelka, *Electroanalysis* **14** (2002) 1359
65. R. Pauliukaite, R. Metelka, I. Švancara, A. Królicka, A. Bobrowski, E. Norkus, K. Kalcher, K. Vytřas, *Sci. Pap. Univ. Pardubice, Ser A* **10** (2004) 47
66. S. B. Hočevar, I. Švancara, B. Ogorevc, K. Vytřas, *Anal. Chem.* **79** (2007) 8639
67. I. Švancara, S. B. Hočevar, L. Baldrianová, E. Tesařová, B. Ogorevc, K. Vytřas, *Sci. Pap. Univ. Pardubice, Ser A* **13** (2007) 5
68. E. Tesařová, L. Baldrianová, S. B. Hočevar, I. Švancara, K. Vytřas, B. Ogorevc, *Electrochim. Acta* **54** (2009) 1506
69. E. Tesařová, K. Vytřas, *Electroanalysis* **21** (2009), in press (DOI: 10.1002/elan.200804518)
70. I. Švancara, R. Metelka, M. Stibůrková, J. Seidlová, G. Jansová, K. Vytřas, B. Pihlar, *Sci. Pap. Univ. Pardubice, Ser. A* **8** (2002) 19
71. K. Schachl, H. Alemu, K. Kalcher, J. Ježková, I. Švancara, K. Vytřas, *Analyst* **122** (1997) 985
72. K. Schachl, H. Alemu, K. Kalcher, J. Ježková, I. Švancara, K. Vytřas, *Anal. Lett.* **30** (1997) 2655
73. K. Schachl, H. Alemu, K. Kalcher, J. Ježková, I. Švancara, K. Vytřas, *Sci. Pap. Univ. Pardubice, Ser. A* **3** (1997) 41
74. K. Schachl, H. Alemu, K. Kalcher, H. Moderegger, I. Švancara, K. Vytřas, *Fresenius J. Anal. Chem.* **362** (1998) 194
75. E. Turkušić, K. Kalcher, K. Schachl, A. Komersová, M. Bartoš, H. Moderegger, I. Švancara, K. Vytřas, *Anal. Lett.* **34** (2001) 2633
76. N. W. Beyene, P. Kotzian, K. Schachl, H. Alemu, E. Turkušić, A. Čopra, H. Moderegger, I. Švancara, K. Vytřas, K. Kalcher, *Talanta* **64** (2004) 1151

77. P. Kotzian, N. W. Beyene, L. F. Llano, H. Moderegger, P. Tuñón-Blanco, K. Kalcher, K. Vytřas, *Sci. Pap. Univ. Pardubice, Ser. A* **8** (2002) 93
78. T. T. Waryo, S. Begić, E. Turkušić, K. Vytřas, K. Kalcher, *Sci. Pap. Univ. Pardubice, Ser. A* **11** (2005) 265
79. T. T. Waryo, S. Begić, E. Turkušić, K. Vytřas, K. Kalcher, in *Sensing in Electroanalysis*, K. Vytřas, K. Kalcher, Eds., University of Pardubice, Pardubice, 2005, p. 14
80. T. Waryo, P. Kotzian, S. Begić, P. Brázdilová, N. Beyene, P. Baker, B. Kgarebe, E. Turkušić, E. Iwuoha, K. Vytřas, K. Kalcher, *IFMBE Proc.* **23** (2009) 283
81. P. Brázdilová, P. Kotzian, K. Kalcher, K. Vytřas, *Anal. Lett.* **38** (2005) 1099
82. P. Brázdilová, P. Kotzian, K. Vytřas, *Bull. Potravn. Výsk.* **44** (2005) 75
83. P. Kotzian, P. Brázdilová, S. Řezková, K. Kalcher, K. Vytřas, *Electroanalysis* **18** (2006) 1499
84. P. Kotzian, P. Brázdilová, K. Kalcher, K. Handlř, K. Vytřas, *Sens. Actuators B* **124** (2007) 297
85. P. Kotzian, T. Janků, K. Kalcher, K. Vytřas, *Anal. Chim. Acta* **599** (2007) 287
86. V. Polan, J. Soukup, K. Vytřas, in *Analyza organických látek v životním prostředí*, (2008), V. Helán, Ed., 2THETA, Český Těšín, Czech Rep., 2008, p. 125 (in Czech)
87. P. Kotzian, I. Ch. Ghergi, S. T. Girousi, K. Vytřas, in *Sensing in Electroanalysis*, K. Vytřas, K. Kalcher, Eds., University of Pardubice, Pardubice, 2005, p. 109
88. P. Horáková-Brázdilová, M. Fojtová, K. Vytřas, M. Fojta, *Sensors* **8** (2008) 193
89. P. Šnévajsová, L. Tisoň, J. Vytřasová, I. Brožková, M. Pejchalová, K. Vytřas, in *Proceedings of YISAC2008 - 15th Young Investigators' Seminar on Analytical Chemistry*, H. Prosen, Ed., University of Ljubljana, Slovenia, 2008, p. 26
90. M. Hrubeš, K. Klodová, J. Vytřasová, K. Vytřas, in *Proceedings of YISAC2008 - 15th Young Investigators' Seminar on Analytical Chemistry*, H. Prosen, Ed., University of Ljubljana, Slovenia, 2008, p. 37
91. M. Hrubeš, P. Šnévajsová, L. Červenka, J. Vytřasová, K. Vytřas, in *Current Research Topics in Applied Microbiology and Microbial Biotechnology*, A. Mendez-Vilaz, Ed., Wiley-VCH, Weinheim, 2009, p. 136.



J. Serb. Chem. Soc. 74 (10) 1035–1040 (2009)
JSCS–3897

Chemical composition and antifungal activity of the essential oil of Douglas fir (*Pseudotsuga menziesii* Mirb. Franco) from Serbia

VELE TEŠEVIĆ^{1*#}, SLOBODAN MILOSAVLJEVIĆ^{1#},
VLATKA VAJS^{2#}, IRIS ĐORĐEVIĆ³, MARINA SOKOVIĆ⁴,
VERA LAVADINOVIC⁵ and MIROSLAV NOVAKOVIĆ²

¹Faculty of Chemistry, University of Belgrade, Studentski trg 16, 11000 Belgrade, ²Institute for Chemistry, Technology and Metallurgy, University of Belgrade, Njegoševa 12, 11000 Belgrade, ³Faculty for Veterinary Medicine, University of Belgrade, Bulevar oslobođenja 18, 11000 Belgrade, ⁴Institute for Biological Research “S. Stanković”, University of Belgrade, Bulevar despota Stefana 142, 11000 Belgrade and ⁵Institute of Forestry, Kneza Višeslava 3, 11030 Belgrade, Serbia

(Received 25 February, revised 8 April 2009)

Abstract: The chemical composition of the essential oil of fresh young needles with twigs of Douglas fir (*Pseudotsuga menziesii* Mirb. Franco) obtained by hydrodistillation were analyzed by gas chromatography (GC) and gas chromatography–mass spectrometry (GC–MS). Ten compounds, accounting for 94.26 % of the oil, were identified. The main compounds found were bornyl acetate (34.65 %), camphene (29.82 %), α -pinene (11.65 %) and santene (5.45 %). The antifungal activity of the essential oil was tested against various fungal species. The minimum inhibitory concentration of Douglas fir essential oil ranged from 1.5 to 4 $\mu\text{g mL}^{-1}$. The fungi most sensitive to the tested oil were *Phomopsis helianthi*, while *Penicillium* species, along with *Microsporum canis*, were the most resistant. Compared to the commercial fungicidal agent bifonazole, the studied essential oil demonstrated higher antifungal activity.

Keywords: antifungal activity; bornyl acetate; Douglas fir; essential oil.

INTRODUCTION

Douglas fir (*Pseudotsuga menziesii* Mirb. Franco) is an autochthonous conifer species from North America and Canada, belonging to the family Pinaceae. It is the most introduced species in Europe since 1825 because of its high wood yield, fast growth and wide uses. Douglas fir is a large to very large tree with a narrow, pointed crown of slightly drooping branches, the crown becoming flat-

* Corresponding author. E-mail: vtesevic@chem.bg.ac.rs

Serbian Chemical Society member.

doi: 10.2298/JSC0910035T

tened with age in large specimens. The needles are petiolate and leave a small, raised scar on the twig.

Douglas fir was often employed medicinally by various native North American Indian tribes, who used it to treat a variety of complaints. An antiseptic resin is obtained from the trunk. It is used as a poultice to treat cuts, burns, wounds and other skin ailments. The resin is used for the treatment of coughs and can be chewed as a treatment for sore throats. An infusion of the green bark has been used in the treatment of excessive menstruation, bleeding bowels and stomach problems. An infusion of the leaves has been used as a wash and a sweat bath for rheumatic and paralyzed joints. An infusion of the young sprouts has been used in the treatment of colds. A decoction of the buds has been used in the treatment of venereal disease. A mouthwash is made by soaking the shoots in cold water. The fresh leaves have a pleasant balsamic odour and are used as a coffee substitute.¹

Antimicrobial and vermifugal activities of essential oils of Douglas fir against bacteria, fungi and worms are well known.²⁻⁶

Previous studies of the volatiles from *P. menziesii* include essential oils from Bulgaria,^{7,8} Austria,⁹ Slovakia¹⁰ and the United States.¹¹ In the oils from Bulgaria, the main constituents were the monoterpenes β -pinene, sabinene, (*Z*)- β -ocimene, (*E*)- β -ocimene, α -terpinolene, α -terpineol, citronellyl acetate, α -terpinene and limonene.^{7,8}

The main constituents of the investigated Austrian samples of *P. menziesii* were β -pinene, sabinene (both dominant in samples of needles) and terpinen-4-ol, α -pinene, 3-carene, limonene, terpinolene, α -terpineol, α -terpinene, γ -terpinene, and myrcene in twigs.⁹ Compounds identified in samples from California included α -pinene, camphene, β -pinene, 3-carene, myrcene, limonene, 2-hexenal, ethyl caproate, γ -terpinene, terpinolene, ethyl caprylate, citronellal, linalool, fenchyl alcohol, bornyl acetate, terpinen-4-ol, β -caryophyllene, citronellyl acetate, α -terpineol, citronellol, geranyl acetate, farnesyl acetate, *p*-cymene and farnesol.¹²

The composition of the volatiles of Douglas fir depends on seasonal, geographic and ecological conditions. Urban conditions cause notable changes in the α -pinene to β -pinene, α -phellandrene and terpineol ratios vs. the relatively clean (arboretum) locality.¹⁰

The aim of this study was to obtain, for the first time, information on the composition and antifungal activity of the essential oils of fresh needles with twigs of Serbian Douglas fir.

EXPERIMENTAL

Plant material

Needles with twigs of *Pseudotsuga menziesii* Mirb. Franco (Pinaceae) were collected from a provenance experiment in Serbia during August 1999 at the mountain Juhor, 745 m. Vou-

cher specimens, accession number PM0899, are deposited in the Herbarium of the Faculty of Biology, University of Belgrade, Herbarium code: BEOU.

The provenance experimental plot in central Serbia on the mountain Juhor (745 m) was established with original material from the native area of the species from Oregon and Washington.

Isolation of the essential oil

Fresh needles with twigs (500 g) were crushed and steam distilled in a Clevenger apparatus for about four hours to obtain a yellow coloured oil (yield: 0.67 %).

Analysis of the essential oil

Gas chromatographic analysis was performed using an HP 5890 gas chromatograph equipped with a flame ionization detector (FID) and a split/splitless injector. The separation was achieved using a HP-5 (5 % diphenyl- and 95 % dimethylpolysiloxane) fused silica capillary column, 30 m×0.25 mm i.d., 0.25 µm film thickness. The GC oven temperature was programmed from 50 °C (6 min) to 285 °C at a rate of 4.3 °C/min. Hydrogen was used as the carrier gas; flow rate: 1.6 mL/min at 45 °C; injector temperature: 250 °C; detector temperature: 280 °C; injection mode: splitless.

Gas chromatographic–mass spectrometric analysis (EI) was performed using an Agilent 5973 Network chromatograph coupled to an Agilent 5973 MSD spectrometer. The separation was achieved using an Agilent 19091S-433 HP-5MS fused silica capillary column, 30 m×0.25 mm i.d., 0.25 µm film thickness. The GC oven temperature was programmed from 60 °C to 285 °C at a rate of 4.3 °C/min. Helium was used as the carrier gas; the inlet pressure was 25 kPa; the linear velocity was 1ml/min at 210 °C; injector temperature: 250 °C; injection mode: splitless. MS scan conditions: source temperature, 200 °C; interface temperature, 250 °C; energy, 70 eV; mass scan range, 40–350 amu.

The components were identified based of their retention index and comparison with reference spectra (Wiley and NIST databases). The percentage (relative) of the identified compounds was computed from their GC peak area.

Antifungal activity

The fungi used in this study were *Aspergillus niger* (ATCC 6275), *A. ochraceus* (ATCC 12066), *A. versicolor* (ATCC 11730), *A. flavus* (ATCC 9170), *A. terreus* (ATCC 16792), *Alternaria alternata* (ATCC 13963), *Penicillium ochrochloron* (ATCC 9112), *P. funiculosum* (ATCC 10509), *Cladosporium cladosporioides* (ATCC 13276), *Trichoderma viride* (IAM 5061), *Fusarium tricinctum* (CBS 514478) and *Phomopsis helianthi* (ATCC 201540). Among tested species were dermatomycetes (*Trichophyton mentagrophytes*, *Epidermophyton floccosum*, *Microsporum canis*), which are obtained directly from patients at the Centre for Preventive Medicine, VMA, Belgrade. The organisms were obtained from the Mycotheca of the Mycological Laboratory, Department of Plant Physiology, Institute for Biological Research “Dr. Siniša Stanković”, Belgrade. The fungi were maintained on potato dextrose agar (PDA) and malt agar (MA). The cultures were stored at +4 °C and subcultured once a month. In order to investigate the antifungal activity, a modified mycelial growth test with malt agar was used. The minimal inhibitory concentration (MIC) of the investigated essential oil necessary for complete inhibition of mycelial growth of the fungal strain was determined. Different concentrations of the tested essential oils were diluted in Petri dishes with malt agar (MA). All experiments were performed in triplicate. Petri dishes with ethanol were used as the control. The compound was added into molten malt agar (MA) and poured into Petri dishes. The tested fungi were inoculated at the centre of the plates.¹³ The plates were incubated for

three weeks at room temperature. After this period, the *MIC* was determined. Commercially available bifonazole, Srbolek, Belgrade, was used as the positive control.

RESULTS AND DISCUSSION

The yield of essential oil isolated by hydrodistillation of the needles with twigs of *P. menziesii* was found to be 0.67 % (w/w) based on fresh material.

The constituents identified by GC and GC/MS analysis and the area percentages are summarized in Table I. The quantitative composition of oil was analyzed by GC (FID) by internal normalization assuming an identical mass response factor for all compounds. In this study, only those components present in the oils in amounts higher than 0.1 % were taken into consideration.

TABLE I. Chemical composition of *Pseudotsuga menziesii* essential oil

Compound	<i>RI</i> ^a	Content, %
Santene	888	5.45
Tricyclene	926	2.94
α -Pinene	939	11.65
Camphene	953	29.82
β -Pinene	980	2.73
Limonene	1031	4.51
Citronellal	1151	0.94
Bornyl acetate	1285	34.65
Citronellol acetate	1354	0.21
Myrtanol acetate	1381	1.36
Total		94.26

^aRetention index on HP-5MS and according to *n*-paraffins

Monoterpene hydrocarbons were the major constituents of the oil. In addition to bornyl acetate (34.65 %), which was the major monoterpene, camphene (29.82 %), α -pinene (11.65 %), santene (5.45 %) and limonene (4.52 %) were present in quite high amounts. Most of the components identified in the Douglas fir oil were previously reported as being present in other conifers. Bornyl acetate was also the main constituent of the essential oil of *P. menziesii* from Slovakia¹⁰ and the Rocky Mountains (USA).¹¹ The essential oil from Bulgaria contained β -pinene (24.4 %), sabinene (22.2 %) and α -terpinolene (18.8 %).⁵ The main constituents of the essential oil from Austrian Douglas fir were β -pinene and sabinene.⁹

The essential oil showed significant antifungal potential against the various tested micro-organisms (Table II). The minimum inhibitory concentration (*MIC*) of the oil against *Phomopsis helianthi* was 1.5 $\mu\text{L mL}^{-1}$. The highest *MIC* (6 $\mu\text{L mL}^{-1}$) of the oil was against *Penicillium ochrochloron*, *Penicillium funiculosum* and *Microsporium canis*. The commercial fungicide, bifonazole, showed lower antifungal activity than the *P. menziesii* oil, with an *MIC* of 8.0–15.0 $\mu\text{L mL}^{-1}$. Based on the obtained results, it can be concluded that, compared to the com-

mercial fungicide, the investigated essential oil demonstrated higher potential against various pathogenic fungi.

TABLE II. Minimal inhibition concentration ($\mu\text{L mL}^{-1}$) of *Pseudosuga menziesii* essential oil and bifonazole

Fungi	Oil	Bifonazole ^a
<i>Alternaria alternata</i>	2.7±0.6	9.6±0.6
<i>Aspergillus niger</i>	3.87±0.3	9.6±0.6
<i>Aspergillus ochraceus</i>	3.87± 0.3	9.3±1.1
<i>Aspergillus versicolor</i>	3.7±0.6	9.6±0.6
<i>Aspergillus flavus</i>	3.7±0.3	9.3±1.1
<i>Aspergillus terreus</i>	3.7±0.6	10±0
<i>Cladosporium cladosporioides</i>	3.0±0	9.6±0.6
<i>Fusarium tricinctum</i>	3.0±0	9.6±0.6
<i>Penicillium ochrochloron</i>	6.0±1	14.3±1.2
<i>Penicillium funiculosum</i>	6.0±1	14.3±1.2
<i>Phomopsis helianthi</i>	1.5±0.5	7.6±0.6
<i>Trichoderma viride</i>	3.7±0.6	14.7±0.6
<i>Trichophyton mentagrophytes</i>	2.7±0.6	10±0
<i>Microsporum canis</i>	6.0±0	14.7±0.6
<i>Epidermophyton floccosum</i>	3.7±0.6	9.6±0.6

^aPositive control, commercial preparation containing 1.0 % (w/v) of bifonazole in ethanol

Acknowledgments. This research was supported by a grant from the Ministry of Science and Technological Development of the Republic of Serbia (Project 142053).

ИЗВОД

ХЕМИЈСКИ САСТАВ И АНТИФУНГАЛНА АКТИВНОСТ ЕТАРСКОГ УЉА ДАГЛАСОВЕ ЈЕЛЕ (*Pseudosuga Menziesii* Mirb. Franco) ИЗ СРБИЈЕ

ВЕЛЕ ТЕШЕВИЋ¹, СЛОБОДАН МИЛОСАВЉЕВИЋ¹, ВЛАТКА ВАЈС², ИРИС ЂОРЂЕВИЋ³,
МАРИНА СОКОВИЋ⁴, ВЕРА ЛАВАДИНОВИЋ⁵ и МИРОСЛАВ НОВАКОВИЋ²

¹Хемијски факултет, Универзитет у Београду, Студентски тирг 16, 11000 Београд, ²Институт за хемију, технологију и металургију, Универзитет у Београду, Њеђошева 12, 11000 Београд, ³Факултет ветеринарске медицине, Универзитет у Београду, Булевар ослобођења 18, 11000 Београд, ⁴Институт за биолошка истраживања "С. Станковић", Универзитет у Београду, Булевар десетог Стефана 142, 11000 Београд и ⁵Институт за шумарство, Кнеза Вишеслава 3, 11030 Београд

Хемијски састав етарског уља младих иглица са границима дуглазије (*Pseudosuga menziesii* Mirb. Franco) добијеног дестилацијом воденом паром, анализиран је гасном хроматографијом (GC) и комбинацијом гасне хроматографије и масене спектрометрије (GC/MS). Идентификовано је десет једињења укупне заступљености 94,26 %. Као главне компоненте су нађени: борнил-ацетат (34,65 %), камфен (29,82 %), α -пинен (11,65 %) и сантен (5,45 %). Поред тога, етарско уље је тестирано на антифунгалну активност. Етарско уље показује много бољу антифунгалну активност од комерцијалног фунгицидног агенса бифоназола. Минимална инхибиторна концентрација етарског уља дуглазије је у опсегу од 0,6 до 1,4 $\mu\text{L mL}^{-1}$. Најосетљивији на тестирано уље је био сој *Phomopsis helianthi*, док сојеви *Penicillium* и *Microsporum canis* показују највећу резистентност.

(Примљено 25. фебруара, ревидирано 8. априла 2009)

REFERENCES

1. D. E. Moerman, *Native American Ethnobotany*, Timber Press, Portland, OR, 1998
2. J. Zou, R. G. Cates, *J. Chem. Ecol.* **21** (1995) 387
3. J. Zou, R. G. Cates, *J. Chem. Ecol.* **23** (1997) 2313
4. J. C. Chalchat, R. Ph. Garry, P. Bastide, F. Fabre, R. Malhuret. *Plant Med. Phytother.* **25** (1991) 184
5. L. Jirovetz, G. Buchbauer, A. Stoyanova, S. Metodiev, *Sci. Pharm.* **68** (2000) 323
6. W. H. Johnston, J. J. Karchesy, G. H. Constantine, A. M. Craig, *Phytother. Res.* **15** (2001) 586
7. L. Jirovetz, C. Puschmann, A. Stojanova, S. Metodiev, G. Buchbauer, *Flavour Fragr. J.* **15** (2000) 434
8. A. Stoyanova, S. Metodiev, L. Jirovetz, G. Buchbauer, *Recent Res. Dev. Agric. Food Chem.* **5** (2001) 149
9. G. Buchbauer, L. Jirovetz, M. Wasicky, A. Nikiforov, *J. Agric. Food Chem.* **42** (1994) 2852
10. J. Supuka, F. Berta, *Ekologia* **17** (1998) 102
11. E. von Rudloff, *Can. J. Bot.* **50** (1972) 1025
12. T. Sakai, H. Maarse, R. Kepner, W. G. Jennings, W. M. Longhurst, *J. Agric. Food Chem.* **15** (1967) 1070
13. H. Hanel, W. Raether, *Mycoses* **31** (1988) 154.



J. Serb. Chem. Soc. 74 (10) 1041–1049 (2009)
JSCS–3898

New S-alkylated 1,2,4-triazoles incorporating diphenyl sulfone moieties with potential antibacterial activity

STEFANIA F. BARBUCEANU^{1*}, GABRIELA L. ALMAJAN¹, IOANA SARAMEȚ¹,
CONSTANTIN DRAGHICI², RADU SOCOTEANU³ and FLORICA BARBUCEANU⁴

¹Carol Davila University of Medicine and Pharmacy, Faculty of Pharmacy, Organic Chemistry Department, Traian Vuia Street 6, 020956, Bucharest, ²C. D. Nenișescu Institute of Organic Chemistry, Romanian Academy, Splaiul Independenței 202B, 060023, Bucharest, ³I. G. Murgulescu Institute of Physical Chemistry, Romanian Academy, Splaiul Independenței 202, 77208, Bucharest and ⁴Institute for Diagnosis and Animal Health, Dr. Staicovici Street 63, 050557, Bucharest, Romania

(Received 29 January, revised 22 April 2009)

Abstract: Alkylation of the 5-{4-[(4-bromophenyl)sulfonyl]phenyl}-4-(3/4-methylphenyl)-2,4-dihydro-3H-1,2,4-triazole-3-thiones **3a,b** with various alkylation agents, *i.e.*, ethyl bromide, phenacyl bromide and ethyl chloroacetate, afforded the S-substituted 1,2,4-triazoles **4-6a,b**. The structures of these new compounds were elucidated by elemental analysis and IR, UV, ¹H-NMR, ¹³C-NMR and MS spectroscopy. The newly synthesized products were tested for their antibacterial effects.

Keywords: alkylation; 1,2,4-triazole-3-thione; antibacterial activity.

INTRODUCTION

A large number of bioactive molecules contain a functionalized 1,2,4-triazole nucleus. Various compounds containing the 1,2,4-triazole ring are well known as drugs. For example, fluconazole, itraconazole and voriconazole are used as antimicrobial drugs;¹ ribavirin has antiviral action,² while vorozole, letrozole and anastrozole are non-steroidal drugs used for the treatment of cancer.^{3,4}

In addition, various 1,2,4-triazoles are associated with different biological activities. Among 1,2,4-triazole derivatives, mercapto- and thione-substituted 1,2,4-triazole ring systems have been studied and, to date, a variety of antibacterial, antifungal,^{5–7} antitubercular,^{8,9} anti-inflammatory, analgesic,^{10,11} antitumoral,^{12,13} antiviral¹⁴ and anticonvulsant¹⁵ properties have been reported for a large number of these compounds.

* Corresponding author. E-mail: stefaniafelicia_barbuceanu@yahoo.com
doi: 10.2298/JSC0910041B

Furthermore, diphenyl sulfone derivatives were also found to possess anti-bacterial activity.^{16,17}

The incorporation of these two moieties into a single molecule and alkylation of the –SH group can change the activity of the obtained novel compounds.

Prompted by the observed biological activities of the above-mentioned compounds and in continuation of ongoing research on the synthesis of heterocyclic compounds containing nitrogen and sulfur with expected biological activity,^{18–21} the synthesis and characterization of several *S*-alkylated 1,2,4-triazoles are described in this report. All the newly synthesized compounds were characterized by IR, UV-Vis, ¹H- and ¹³C-NMR spectroscopy. In addition, the structure of compounds **4a,b**, **5b** and **6b** were confirmed by mass spectrometry. These new compounds were investigated for their antimicrobial activity.

EXPERIMENTAL

Materials, methods and instruments

Commercially available chemicals and solvents were used as received from Sigma-Aldrich and Merck. The melting points of the new compounds were determined with a Boetius apparatus and are uncorrected. The IR spectra (in KBr pellets) were recorded on a Vertex 70 Bruker spectrometer and the wave numbers are given in cm⁻¹. The NMR spectra were registered on a Varian Gemini 300 BB spectrometer working at 300 MHz for a ¹H and 75 MHz for ¹³C in DMSO-*d*₆ or CDCl₃ (10/1, v/v). All chemical shifts are reported in δ (ppm) using TMS as the internal standard. The mass spectrum of compound **4a** was acquired with a hybrid quadrupole – time of flight (QqTOF) high resolution mass spectrometer model API QStar Pulsar produced by Applied Biosystems/SCIEX. The instrument was operated in the positive ions mode, using an atmospheric pressure pneumatically-assisted electrospray ionization interface (ESI, AB model Turboionspray). The voltage of the mass spectrometer (MS) source was set at 5000 V. Molecular ions were detected in full scan over an adequate mass range. Stock solutions were prepared at 1 mg/ml in DMSO. The sample solution (2 μ g/ml in water/methanol 1/1, v/v) was introduced by direct infusion at a flow rate of 20 μ l/min into the MS interface by means of a built-in Harvard syringe pump. The mass spectra of the compounds **4b**, **5b** and **6b** were registered using a Varian 1200 L/MS/MS triple quadrupole mass spectrometer coupled with a high performance liquid chromatograph operating with a Varian ProStar 240 pump and a Varian ProStar 410 automatic injector. An atmospheric pressure chemical ionization interface (APCI) was used in order to obtain the ions. The liquid chromatography was performed on a Hypersil Gold (Thermo) column with a pre-column; the mobile phase was 30 % water and 70 % methanol. The UV-Vis spectra were measurement on a SPECORD 40 Analytik, Jena, in methanolic solution (2.5 \times 10⁻⁵ mol/l). The elemental analyses were performed with ECS 40-10, COSTEH instrument.

General procedure for the preparation of new S-alkylated 1,2,4-triazoles

To a stirred solution of 1,2,4-triazole-3-thione **3a,b** (1.0 mmol) and sodium ethoxide (1.0 mmol of sodium dissolved in 10 mL ethanol) was added the alkylation agent (1.0 mmol). The reaction mixture was stirred at room temperature for 12 h, and then poured into ice water. The crude product was filtered off, washed with water and recrystallized from ethanol.

Biological activity

The compounds were tested for their *in vitro* growth inhibitory activity against the following Gram-negative bacteria: *Acinetobacter baumannii* (Ab) ATCC 19606; *Citrobacter freundii* (Cf) ATCC 8090, *Escherichia coli* (Ec) ATCC 11775 and *Pseudomonas aeruginosa* (Pa) ATCC 9027, and the following Gram-positive bacteria: *Enterococcus faecalis* (Ef) ATCC 19433, *Staphylococcus aureus* (Sa) ATCC 12600, *Staphylococcus epidermidis* (Se) ATCC 14990 and *Bacillus cereus* (Bc) ATCC 14579, using the paper disk diffusion method.²² Suspensions in sterile peptone water from 24 h cultures of micro-organisms were adjusted to 0.5 McFarland. Mueller-Hinton Petri dishes of 90 mm diameter were inoculated using these suspensions. Paper disks (5 mm in diameter) containing 10 μ L of the to be tested substance (at a concentration of 2048 μ g/mL in DMSO) were placed in a circular pattern in each inoculated plate. The plates were incubated at 37 °C for 18–24 h. The inhibitory activity was measured (in mm) as the diameter of the observed inhibition zones. The tests were repeated to confirm the findings and the average of the readings was taken into consideration. Discs with only DMSO were used as the control and ampicillin (10 μ g/50 μ L) served as the control drug.

RESULTS AND DISCUSSIONS

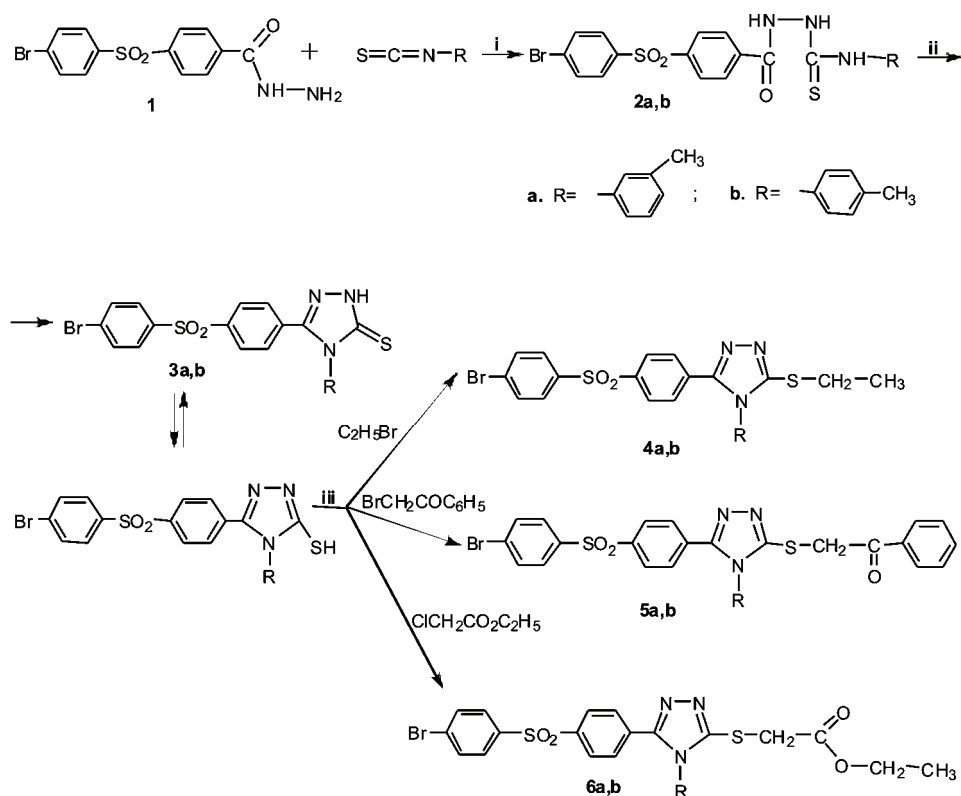
Chemistry

The key intermediates used in the synthesis of the S-alkylated 1,2,4-triazoles, the 5-{4-[(4-bromophenyl)sulfonyl]phenyl}-4-(3/4-methylphenyl)-2,4-dihydro-3H-1,2,4-triazole-3-thiones **3a** and **3b**,^{23–25} were prepared starting from 4-[(4-bromophenyl)sulfonyl]benzoic acid hydrazide **1**.²⁶ The reaction of **1** with 3- or 4-methylphenyl isothiocyanates in refluxing ethanol gave the *N*¹-{4-[(4-bromophenyl)sulfonyl]benzoyl}-*N*⁴-(3/4-methylphenyl)thiosemicarbazides (**2a,b**). 5-{4-[(4-Bromophenyl)sulfonyl]phenyl}-4-(3/4-methylphenyl)-2,4-dihydro-3H-1,2,4-triazole-3-thiones (**3a,b**) were synthesized by treating the corresponding thiosemicarbazides **2a,b** with 8 % NaOH.^{23,24,27} In the present study, the reaction of the 1,2,4-triazoles **3a,b** with ethyl bromide, phenacyl bromide or ethyl chloroacetate in presence of absolute ethanol gave the new S-alkylated triazoles **4–6a,b**.

The synthetic route of the compounds is outlined in Scheme 1.

Analytical and spectral data of the newly prepared compounds

3-{4-[(4-Bromophenyl)sulfonyl]phenyl}-5-(ethylthio)-4-(3-methylphenyl)-4H-1,2,4-triazole (**4a**). Yield: 59 %; m.p. 168–170 °C. Anal. Calcd. for C₂₃H₂₀BrN₃O₂S₂ (514.46 g/mol): C, 53.70; H, 3.92; S, 12.47. Found: C, 53.79; H, 3.88; S, 12.41. IR (KBr, cm⁻¹): 3084, 3061 (C–H stretching of aromatic ring), 2972, 2929, 2868 (CH₃, CH₂ stretching), 1601 (C=N stretching of triazole ring), 1572, 1460 (C=C-stretching of aromatic ring), 1326, 1160 (SO₂ stretching), 576 (C–Br). ¹H-NMR (300 MHz, CDCl₃, δ / ppm): 7.98 (1H, *br d*, aromatic, *J* = 7.2 Hz), 7.79 (2H, *d*, aromatic, *J* = 8.5 Hz), 7.75 (2H, *d*, aromatic, *J* = 8.5 Hz), 7.62 (4H, *d*, aromatic, *J* = 8.5 Hz), 7.30–7.40 (2H, *m*, aromatic), 7.00 (1H, *br s*, aromatic), 3.29 (2H, *q*, –SCH₂CH₃, *J* = 7.3 Hz), 2.40 (3H, *s*, –CH₃); 1.41 (3H, *t*, –SCH₂CH₃, *J* = 7.3 Hz). ¹³C-NMR (75 MHz, CDCl₃, δ / ppm): 154.35 (C₃),



i: C₂H₅OH, reflux; ii: NaOH 8 %, reflux; iii: Na+C₂H₅OH

Scheme 1. The synthetic route of the title compounds.

152.87 (C₅), 141.95, 140.69, 140.51, 134.05, 132.66, 131.93, 131.09, 129.97, 129.25, 128.47, 128.31, 127.79, 127.70, 124.34 (aromatic ring), 26.95 (–SCH₂CH₃), 21.17 (–CH₃), 14.69 (–SCH₂CH₃). MS (ESI/QTOF, *m/z*): 514.0223 [M+H]⁺, 516.0165 [M+H]⁺. UV–Vis (CH₃OH) (λ_{max} / nm (log ε)): 207 (4.69), 249 (4.36), 288 (4.29).

3-{4-[(4-Bromophenyl)sulfonyl]phenyl}-5-(ethylthio)-4-(4-methylphenyl)-4H-1,2,4-triazole (**4b**). Yield: 62 %; m.p. 171–173 °C. Anal. Calcd. for C₂₃H₂₀BrN₃O₂S₂ (514.46 g/mol): C, 53.70; H, 3.92; S, 12.47. Found: C, 53.62; H, 3.85; S, 12.42. IR (KBr, cm⁻¹): 3084, 3057 (C–H stretching of aromatic ring); 2972, 2929, 2868 (CH₃, CH₂ stretching), 1599 (C=N stretching of triazole ring), 1572, 1514 (C=C-stretching of aromatic ring), 1326, 1160 (SO₂ stretching), 574 (C–Br). ¹H-NMR (300 MHz, CDCl₃, δ / ppm): 7.81 (2H, *d*, aromatic, *J* = 8.4 Hz), 7.76 (2H, *d*, aromatic, *J* = 8.4 Hz), 7.63 (2H, *d*, aromatic, *J* = 8.4 Hz), 7.58 (2H, *d*, aromatic, *J* = 8.4 Hz), 7.33 (2H, *d*, aromatic, *J* = 8.2 Hz), 7.08 (2H, *d*, aromatic, *J* = 8.2 Hz), 3.29 (2H, *q*, –SCH₂CH₃, *J* = 7.3 Hz), 2.45 (3H, *s*, –CH₃),

1.42 (3H, *t*, $-\text{SCH}_2\text{CH}_3$, $J = 7.3$ Hz). ^{13}C -NMR (75 MHz, CDCl_3 , δ / ppm): 154.54 (C_3), 152.88 (C_5), 141.65, 140.81, 140.74, 140.08, 132.66, 131.10, 130.87, 129.22, 128.49, 128.03, 127.78, 126.87 (aromatic ring), 26.78 ($-\text{SCH}_2\text{CH}_3$), 21.32 ($-\text{CH}_3$), 14.66 ($-\text{SCH}_2\text{CH}_3$). MS (APCI, m/z): 514 $[\text{M}+\text{H}]^+$, 516 $[\text{M}+\text{H}]^+$. UV-Vis (CH_3OH) (λ_{max} / nm (log ϵ)): 206 (4.66), 249 (4.35), 287 (4.25).

2- $\{[5-(4-((4\text{-Bromophenyl)sulfonyl})\text{phenyl})-4-(3\text{-methylphenyl})-4\text{H}-1,2,4\text{-triazol-3-yl}] \text{-thio}\}$ -1-phenylethanone (**5a**). Yield: 81 %; m.p. 189–191 °C. Anal. Calcd. for $\text{C}_{29}\text{H}_{22}\text{BrN}_3\text{O}_3\text{S}_2$ (604.54 g/mol): C, 57.62; H, 3.67; S, 10.61. Found: C, 57.70; H, 3.59; S, 10.56; IR (KBr, cm^{-1}): 3084, 3062 (C–H stretching of aromatic ring), 2953, 2922, 2852 (CH_3 , CH_2 stretching), 1681 (C=O stretching), 1598 (C=N stretching of triazole ring), 1573, 1490 (C=C-stretching of aromatic ring), 1324, 1160 (SO_2 stretching), 577 (C–Br). ^1H -NMR (300 MHz, CDCl_3 , δ / ppm): 8.07 (2H, *dd*, aromatic, $J = 7.9$ Hz; 1.5 Hz), 7.82 (2H, *d*, aromatic, $J = 8.5$ Hz), 7.76 (2H, *d*, aromatic, $J = 8.6$ Hz), 7.64 (2H, *d*, aromatic, $J = 8.6$ Hz), 7.62 (2H, *d*, aromatic, $J = 8.5$ Hz), 7.61 (1H, *br t*, aromatic, $J = 7.9$ Hz), 7.50 (2H, *t*, aromatic, $J = 7.9$ Hz), 7.41 (1H, *t*, aromatic, $J = 7.9$ Hz), 7.36 (1H, *br d*, aromatic, $J = 7.9$ Hz), 7.05 (2H, *m*, aromatic), 4.99 (2H, *s*; $-\text{SCH}_2\text{CO}-$), 2.41 (3H, *s*, $-\text{CH}_3$). ^{13}C -NMR (75 MHz, CDCl_3 , δ / ppm): 192.87 (C=O), 153.72 (C_3), 153.15 (C_5), 142.14, 140.94, 135.20, 133.88, 133.50, 132.71, 131.60, 131.40, 130.18, 129.28, 129.08, 129.18, 128.85, 128.72, 128.55, 127.85, 127.60, 124.28 (aromatic ring), 41.02 ($-\text{SCH}_2\text{CO}-$), 21.24 ($-\text{CH}_3$). UV-Vis (CH_3OH) (λ_{max} / nm (log ϵ)): 206 (4.61), 248 (4.40), 285 (4.21).

2- $\{[5-(4-((4\text{-Bromophenyl)sulfonyl})\text{phenyl})-4-(4\text{-methylphenyl})-4\text{H}-1,2,4\text{-triazol-3-yl}] \text{-thio}\}$ -1-phenylethanone (**5b**). Yield: 72 %; m.p. 224–226 °C. Anal. Calcd. for $\text{C}_{29}\text{H}_{22}\text{BrN}_3\text{O}_3\text{S}_2$ (604.54 g/mol): C, 57.62; H, 3.67; S, 10.61. Found: C, 57.72; H, 3.62; S, 10.58. IR (KBr, cm^{-1}): 3063 (C–H stretching of aromatic ring), 2960, 2922, 8264 (CH_3 , CH_2 stretching), 1681 (C=O stretching), 1597 (C=N stretching of triazole ring), 1573, 1513 (C=C-stretching of aromatic ring); 1323, 1160 (SO_2 stretching), 576 (C–Br). ^1H -NMR (300 MHz, CDCl_3 , δ / ppm): 8.04 (2H, *br d*, aromatic, $J = 7.9$ Hz), 7.82 (2H, *d*, aromatic, $J = 8.5$ Hz), 7.76 (2H, *d*, aromatic, $J = 8.5$ Hz), 7.63 (2H, *d*, aromatic, $J = 8.5$ Hz), 7.60 (1H, *br t*, aromatic, $J = 7.9$ Hz), 7.58 (2H, *d*, aromatic, $J = 8.5$ Hz), 7.49 (2H, *br t*, aromatic, $J = 7.9$ Hz), 7.32 (2H, *d*, aromatic, $J = 8.2$ Hz), 7.13 (2H, *d*, aromatic, $J = 8.2$ Hz), 4.98 (2H, *s*, $-\text{SCH}_2\text{CO}-$), 2.46 (3H, *s*, $-\text{CH}_3$). ^{13}C -NMR (75 MHz, CDCl_3 , δ / ppm): 192.96 (C=O), 153.92 (C_3), 153.24 (C_5), 141.94, 141.15, 141.10, 140.15, 135.40, 134.07, 132.78, 131.54, 131.14, 129.34, 129.24, 129.20, 128.93, 128.61, 127.92, 126.92 (aromatic ring), 41.29 ($-\text{SCH}_2\text{CO}-$), 21.42 ($-\text{CH}_3$). MS (APCI, m/z): 604 $[\text{M}+\text{H}]^+$, 606 $[\text{M}+\text{H}]^+$. UV-Vis (CH_3OH) (λ_{max} / nm (log ϵ)): 205 (4.68), 248 (4.42), 286 (4.21).

Ethyl 2- $\{[5-(4-((4\text{-bromophenyl)sulfonyl})\text{phenyl})-4-(3\text{-methylphenyl})-4\text{H}-1,2,4\text{-triazol-3-yl}] \text{-thio}\}$ acetate (**6a**). Yield: 87 %; m.p. 169–170 °C. Anal. Calcd. for

$C_{25}H_{22}BrN_3O_4S_2$ (572.50 g/mol): C, 52.45; H, 3.87; S, 11.20; Found: C, 52.50; H, 3.82; S, 11.17. IR (KBr, cm^{-1}): 3080 (C–H stretching of aromatic ring), 2981, 2929, 2868 (CH₃, CH₂ stretching), 1728 (–C=O stretching of –COOH group), 1599 (C=N stretching of triazole ring), 1572, 1490 (C=C stretching of aromatic ring); 1322, 1160 (SO₂ stretching), 578 (C–Br). ¹H-NMR (CDCl₃, δ / ppm): 7.82 (2H, *d*, aromatic, *J* = 8.6 Hz), 7.76 (2H, *d*, aromatic, *J* = 8.6 Hz), 7.63 (2H, *d*, aromatic, *J* = 8.6 Hz), 7.58 (2H, *d*, aromatic, *J* = 8.6 Hz), 7.06 (2H, *m*, aromatic), 7.38 (2H, *m*, aromatic), 4.12 (2H, *s*, –SCH₂COO–), 4.22 (2H, *q*, –COOCH₂CH₃, *J* = 7.1 Hz), 2.40 (3H, *s*, –CH₃), 1.28 (3H, *t*, –COOCH₂CH₃, *J* = 7.1 Hz). ¹³C-NMR (CDCl₃, δ / ppm): 167.99 (–COO), 153.20 (C₃), 153.00 (C₅), 142.13, 140.88, 140.43, 133.69, 132.70, 131.68, 131.34, 130.13, 129.28, 128.74, 128.53, 127.83, 127.62, 124.29 (aromatic ring), 62.01 (–COOCH₂CH₃), 34.57 (–SCH₂COO–), 21.21 (–CH₃), 14.06 (–COOCH₂CH₃). UV–Vis (CH₃OH) (λ_{max} / nm (log ϵ)): 206 (4.68), 249 (4.33), 285 (4.32).

Ethyl 2-[[5-(4-((4-bromophenyl)sulfonyl)phenyl)-4-(4-methylphenyl)-4H-1,2,4-triazol-3-yl]thio]acetate (6b). Yield: 67 %; m.p. 209–211 °C. Anal. Calcd. for $C_{25}H_{22}BrN_3O_4S_2$ (572.50 g/mol): C, 52.45; H, 3.87; S, 11.20. Found: C, 52.55; H, 3.81; S, 11.25. IR (KBr, cm^{-1}): 3084 (C–H stretching of aromatic ring), 2987, 2929, 2868 (CH₃, CH₂ stretching), 1743 (–C=O stretching of –COOH group), 1599 (C=N stretching of triazole ring), 1572, 1513 (C=C stretching of aromatic ring), 1323, 1161 (SO₂ stretching), 576 (C–Br). ¹H-NMR (CDCl₃ + DMSO-*d*₆ (10/1, v/v), δ / ppm): 7.83 (2H, *d*, aromatic, *J* = 8.7 Hz), 7.77 (2H, *d*, aromatic, *J* = 8.6 Hz), 7.64 (2H, *d*, aromatic, *J* = 8.6 Hz), 7.60 (2H, *d*, aromatic, *J* = 8.7 Hz), 7.34 (2H, *d*, aromatic, *J* = 8.2 Hz), 7.14 (2H, *d*, aromatic, *J* = 8.2 Hz), 4.20 (2H, *q*, –COOCH₂CH₃, *J* = 7.1 Hz), 4.08 (2H, *s*, –SCH₂COO–), 2.47 (3H, *s*, –CH₃) 1.28 (3H, *t*, –COOCH₂CH₃, *J* = 7.1 Hz). ¹³C-NMR (CDCl₃ + DMSO-*d*₆ (10/1, v/v), δ / ppm): 167.82 (–COO), 152.99 (C₃), 152.84 (C₅), 141.65, 141.25, 140.83, 140.73, 132.58, 131.33, 130.86, 129.10, 128.64, 128.35, 127.62, 126.67 (aromatic ring), 61.84 (–COOCH₂CH₃), 34.21 (–SCH₂COO–), 21.17 (–CH₃), 13.93 (–COOCH₂CH₃). MS (APCI, *m/z*): 572 [M+H]⁺, 574 [M+H]⁺. UV–Vis (CH₃OH) (λ_{max} / nm (log ϵ)): 206 (4.61), 249 (4.28), 282 (4.23).

The spectral data of all the newly synthesized compounds are in full agreement with the proposed structures.

The infrared absorption spectra of the new S-alkylated 1,2,4-triazoles **4–6a,b** confirm the alkylation reaction by the disappearance of the stretching of the NH group, which appeared at $\approx 3400\text{ cm}^{-1}$ in the spectra of the triazoles **3a,b**.^{23,24} In addition, the absence of the absorption band characteristic of the C=S group, which appeared in the spectra of the triazoles **3a,b**^{23,24} at $\approx 1240\text{ cm}^{-1}$ proved that these compounds participated in the alkylation reaction in the thiolic tautomeric form and that substitution occurred at the sulfur atom.²⁸

The C₃ and C₅ heterocyclic carbons from the new S-alkylated compounds **4–6a,b** resonated at 152.99–155.54 ppm and 152.88–153.24 ppm, respectively. The C₃ heterocyclic carbon of these new S-alkylated derivatives is more shielded than the C₃ heterocyclic carbon from 1,2,4-triazole intermediates **3a,b** ($\delta \approx 169$ ppm).^{23,24} These results indicate that the alkylation occurred at the sulfur atom²⁹ and not at the N₂ nitrogen atom. Data from the literature indicated that if the alkylation had occurred at the N₂ heterocyclic nitrogen, the C₃ heterocyclic carbon would have resonated at 167–173 ppm.³⁰

Antimicrobial activity

The potential antibacterial activity of compounds **2–6** towards eight standard strains was investigated. From the data presented in Table I, it may be seen that the thiosemicarbazides **2a** and **2b** showed the highest inhibition zone diameter against *E. coli*, *P. aeruginosa*, *S. aureus* and *S. epidermidis*, compared with the other tested compounds. Compounds **2a** and **2b** showed no inhibitory effects against *C. freundii* and *E. faecalis* and they were moderately active against *A. baumannii* and *B. cereus*. After cyclization of **2a** and **2b** forming the 1,2,4-triazoles **3a** and **3b**, it may be seen how these effects decreased and even completely disappeared in the case of some S-alkylation derivatives.

TABLE I. Antibacterial activity of the tested compounds (highly active: inhibition zone > 12 mm; moderately active: inhibition zone 9–12 mm; slightly active: inhibition zone 6–9 mm; inactive: inhibition zone < 6 mm)

Compd.	R	Inhibition zone diameter, mm							
		Gram-negative bacteria				Gram-positive bacteria			
		Ab	Cf	Ec	Pa	Ef	Sa	Se	Bc
2a	–C ₆ H ₄ –CH ₃ (<i>m</i>)	10	–	14	15	–	17	13.5	12
3a	–C ₆ H ₄ –CH ₃ (<i>m</i>)	10.5	10	11.5	13	11	12	8	16
4a	–C ₆ H ₄ –CH ₃ (<i>m</i>)	9.5	11	–	9	–	–	12	14
5a	–C ₆ H ₄ –CH ₃ (<i>m</i>)	–	15	–	10	–	–	–	13.5
6a	–C ₆ H ₄ –CH ₃ (<i>m</i>)	–	10	–	11.5	–	–	–	15
2b	–C ₆ H ₄ –CH ₃ (<i>p</i>)	8	–	16	14	–	18	11.5	10
3b	–C ₆ H ₄ –CH ₃ (<i>p</i>)	8	12	12.5	11	11	11	–	15
4b	–C ₆ H ₄ –CH ₃ (<i>p</i>)	–	12	–	–	–	–	9	12
5b	–C ₆ H ₄ –CH ₃ (<i>p</i>)	–	16	–	–	–	–	–	12.5
6b	–C ₆ H ₄ –CH ₃ (<i>p</i>)	–	–	–	–	–	–	–	13
Ampicillin	–	14	9	10	10	11	15	13	14
DMSO	–	5	5	5	5	5	5	5	5

All the tested compounds showed good inhibitory effects against *B. cereus*. Among the S-alkylated triazoles **4–6**, the most active compounds were **6a** against *B. cereus* (15 mm diameter inhibition zone) and **5b** against *C. freundii* (16 mm diameter inhibition zone). This could be explained by electropositive effect of the methyl group attached to the phenyl moiety on the heterocyclic ring, which is

overlapped the effect of the C=O group inlaid by the S-alkylation reaction and together favorably influenced the potency of the heterocyclic nuclei.

CONCLUSIONS

This study reports the synthesis of some new S-substituted 1,2,4-triazoles by alkylation, in alkaline media, of 5-{4-[(4-bromophenyl)sulfonyl]phenyl}-4-(3/4-methylphenyl)-2,4-dihydro-3H-1,2,4-triazol-3-thiones **3a,b** with various alkylation agents (ethyl bromide, phenacyl bromide and ethyl chloroacetate). The structures of new compounds were determined from spectral data and elemental analyses. The potential antibacterial effects of the synthesized compounds, compared with those of the parent triazoles and ampicillin, were investigated using different standard micro-organisms. The most active compounds were **5b** and **6a**, which exhibited promising activities against *C. freundii* and *B. cereus*. Further investigations are in progress.

ИЗВОД

НОВИ S-АЛКИЛОВАНИ 1,2,4-ТРИАЗОЛИ КОЈИ САДРЖЕ ДИФЕНИЛСУЛФОНСКЕ ГРУПЕ СА ПОТЕНЦИЈАЛНОМ АНТИБАКТЕРИЈСКОМ АКТИВНОШЋУ

STEFANIA F. BARBUCEANU¹, GABRIELA L. ALMAJAN¹, IOANA SARAMEȚ¹,
CONSTANTIN DRAGHICI², RADU SOCOTEANU³ и FLORICA BARBUCEANU⁴

¹Carol Davila University of Medicine and Pharmacy, Faculty of Pharmacy, Organic Chemistry Department, Traian Vuia Street 6, 020956, Bucharest, ²C. D. Nenițescu Institute of Organic Chemistry, Romanian Academy, Splaiul Independenței 202B, 060023, Bucharest, ³I. G. Murgulescu Institute of Physical Chemistry, Romanian Academy, Splaiul Independenței 202, 77208, Bucharest и ⁴Institute for Diagnosis and Animal Health, Dr. Staicovici Street 63, 050557, Bucharest, Romania

Алкиловањем 5-{4-[(4-бромофенил)сулфони]фенил}-4-(3/4-метилфенил)-2,4-дихидро-3H-1,2,4-триазол-3-тиона (**3a,b**) алкилујућим реагенсима као што су етил-бромид, фенацил-бромид и етил-хлорацетат добијени су S-супституисани 1,2,4-триазоли **4-6a,b**. Структура ових нових једињења потврђена је елементалном анализом као и IR, UV, ¹H-NMR, ¹³C-NMR и MS спектрима. Испитивана је и антибактеријска активност ових једињења.

(Примљено 29. јануара, ревидирано 22. априла 2009)

REFERENCES

1. R. A. Fromtling, *Clin. Microbiol. Rev.* **1** (1988) 187
2. H. H. Balfour Jr., *N. Engl. J. Med.* **340** (1999) 1255
3. M. Clemons, R. E. Coleman, S. Verma, *Cancer Treat. Rev.* **30** (2004) 325
4. M. Serdar, N. Gümrukçüoğlu, Ş. Alpay Karaoğlu, N. Demirbaş, *Turk. J. Chem.* **31** (2007) 315
5. A. A. Siddiqui, A. Arora, N. Siddiqui, A. Misra, *Indian J. Chem. Sect. B* **44** (2005) 838
6. O. I. Abdel-Salam, S. F. Mohamed, *J. Chin. Chem. Soc.* **52** (2005) 1157
7. I. A. Shehata, *Saudi Pharm. J.* **11** (2003) 87
8. I. Mir, M. T. Siddiqui, *Tetrahedron* **26** (1970) 5235
9. I. Küçükgüzel, S. G. Küçükgüzel, S. Rollas, M. Kiraz, *Bioorg. Med. Chem. Lett.* **11** (2001) 1703

10. Y. Dündar, B. Çakir, E. Küpeli, M. F. Şahin, N. Noyanalpan, *Turk. J. Chem.* **31** (2007) 301
11. M. Amir, S. Kumar, *Acta Pharm.* **57** (2007) 31
12. H. N. Dogan, A. Duran, S. Rollas, *Indian J. Chem. Sect. B.* **44** (2005) 2301
13. A. Duran, H. N. Dogan, S. Rollas, *Il Farmaco* **57** (2002) 559
14. M. T. Abdel-Aal, W. A. El-Sayed, A. H. Abdel Aleem, E. S. H. El-Ashry, *Pharmazie* **58** (2003) 788
15. J. M. Kane, M. A. Staeger, C. R. Dalton, F. P. Miller, M. W. Dudley, A. M. L. Ogden, J. H. Kehne, H. J. Ketteler, T. C. McCloskey, Y. Senyah, P. A. Chmielewski, J. A. Miller, *J. Med. Chem.* **37** (1994) 125
16. E. F. Elslager, Z. B. Gavrilis, A. A. Phillips, D. F. Worth, *J. Med. Chem.* **12** (1969) 357
17. R. Wolf, H. Matz, E. Orion, B. Tuzun, Y. Tuzun, *Dermatol. Online J.* **8** (2002) 2
18. Ş.-F. Bărbuceanu, G. L. Almăjan, I. Şaramet, B. Drăghici, *Rev. Chim.* **58** (2007) 945
19. Ş.-F. Bărbuceanu, G. L. Almăjan, I. Şaramet, B. Drăghici, *Rev. Chim.* **57** (2006) 1253
20. Ş. Bărbuceanu, L. Almăjan, I. Şaramet, B. Drăghici, *Rev. Chim.* **56** (2005) 1270
21. G. L. Almăjan, Ş. F. Bărbuceanu, I. Şaramet, C. Drăghici, *Rev. Chim.* **56** (2005) 1182
22. E. J. Stokes, P. M. Waterworth, in *Association of Clinical Pathologists Broadsheet*, BMJ Publishing Group, BMA House, London, 1972, p. 55
23. Ş.-F. Bărbuceanu, G. L. Almăjan, I. Şaramet, C. Drăghici, *Rev. Chim.* **57** (2006) 355
24. I. Şaramet, G.-L. Almăjan, Ş. Bărbuceanu, C. Drăghici, M. D. Banciu, *Rev. Roum. Chim.* **50** (2005) 19
25. G. L. Almăjan, A. Innocenti, L. Puccetti, G. Manole, Ş. Barbuceanu, I. Şaramet, A. Scoz-zafava, C. T. Supuran, *Bioorg. Med. Chem. Lett.* **15** (2005) 2347
26. A. Mavrodin, V. Zotta, M. Stoenescu, D. Oţeleanu, *Pharm. Zentralhalle Dtschl.* **95** (1956) 353
27. I. Şaramet, C. Drăghici, C. Bărcuţean, V. Rădulescu, T. Loloiu, M. D. Banciu, *Heterocyc. Commun.* **7** (2001) 369
28. H. H. Fahmy, A. El-Masry, S. H. Ali Abdelwahed, *Arch. Pharm. Res.* **24** (2001) 27
29. R. M. Shaker, A. F. Mahmoud, F. F. Abdel-Latif, *Phosphorus Sulfur Silicon Relat. Elem.* **180** (2005) 397
30. O. A. Al-Deeb, M. A. Al-Omar, N. R. El-Brollosy, E. E. Habib, T. M. Ibrahim, *Arzneim. Forsch./Drug Res.* **56** (2006) 40.



J. Serb. Chem. Soc. 74 (10) 1051–1061 (2009)
JSCS–3899

The influence of dispersive interactions on the binding affinities of ligands with an arylpiperazine moiety to the dopamine D2 receptor

MARIO V. ZLATOVIĆ^{1*#}, VLADIMIR V. ŠUKALOVIĆ^{2#}, GORAN M. ROGLIĆ^{1#},
SLAĐANA V. KOSTIĆ-RAJAČIĆ^{2#} and DEANA B. ANDRIĆ^{1#}

¹Faculty of Chemistry, University of Belgrade, P.O. Box 51, 11158 Belgrade and ²ICTM,
Department of Chemistry, University of Belgrade, P.O. Box 473, 11001 Belgrade, Serbia

(Received 17 February, revised 21 April 2009)

Abstract: Several isosteric 1,3-dihydro-5-[2-(4-aryl-1-piperazinyl)ethyl]-2H-benzimidazole-2-thiones were used to investigate the interactions of different ligands with the binding site of the D2 receptor. Due to limitations of the simulation methods, docking analysis failed to show precisely the interactions that influence the binding affinity of the ligands. It is presumed that dispersive forces or more precisely edge-to-face interactions play an important role in the binding process, especially for the lipophilic part of the ligands. In order to confirm this hypothesis, *ab initio* calculations were applied on a model system in order to find the stabilization energies of potential edge-to-face interactions and then to correlate them with the ligand affinity. The obtained results indicate that there is a significant correlation between the strength of dispersive interactions and ligand affinity. It was shown that for the calculation of stabilization energies of modeled receptor–ligand complexes the Becke “half-and-half” hybrid DFT method can be used, thus speeding up the usually long calculation time and reducing the required computer strength.

Keywords: dispersive interactions; hybrid DFT; ligand affinity; correlation; D2.

INTRODUCTION

Dopaminergic systems have been the focus of much research over the past 30 years, mainly because several pathological conditions, such as Parkinson’s disease, schizophrenia, Tourette’s syndrome and hyperprolactinemia, have been linked to a dysregulation of dopaminergic transmission. Dopamine (DA) receptor antagonists have been developed to block hallucinations and delusions that occur in schizophrenic patients, whereas DA receptor agonists are effective in alleviating the hypokinesia of Parkinson’s disease. However, blockage of DA receptors

* Corresponding author. E-mail: mario@chem.bg.ac.rs

Serbian Chemical Society member.

doi: 10.2298/JSC0910051Z

can induce extrapyramidal effects similar to those resulting from DA depletion and high doses of DA agonists can cause psychoses. The therapies of disorders resulting from DA imbalances are thus associated with severe side effects.¹

The development of new, selective dopaminergic ligands devoid of adverse effects has become a challenging field of research.

The main feature of many substances that exhibit significant dopamine D2 receptor affinity is the presence of the arylpiperazine moiety.¹ The focus of our research was on the lipophilic part of 1,3-dihydro-5-[2-(4-aryl-1-piperazinyl)-ethyl]-2*H*-benzimidazole-2-thiones ligands, changing it in order to study the effects of different substituents on the activity of the ligand (Table I). Seven ligands were synthesized and their dopamine D2 receptor affinity tested. Only two ligands (**3** and **4**) showed a substantial increase in biological activity, while the others demonstrated no or only a small increase in activity or were inactive when compared to ligand **1**.

TABLE I. Structure of the synthesized ligands and their activities² towards the dopamine D2 receptor

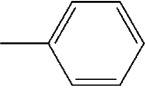
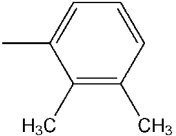
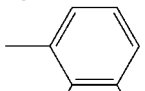
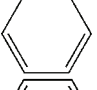
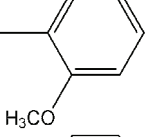
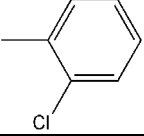
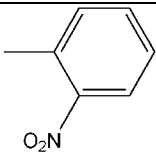
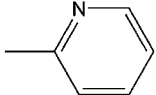
No.	R	D ₂ K _i ±SEM / nM
1		15.7±2.0
2		15.8±2.3
3		3.4±0.4
4		1.7±0.4
5		20.7±2.2
		

TABLE I. Continued

No.	R	D ₂ K _i ±SEM / nM
6		11.79±0.9
7		128

Earlier studies of the D2 receptor set up the criteria that a salt bridge to the carbonyl group of aspartate on TM3 and two hydrogen bonds to the serines (Ser 122, 141) on TM5 are essential for D2 activation.³ However, these criteria alone were incapable of explaining differences in affinity between ligands possessing all these interactions. It was later concluded that more complex decisive factors for ligand binding must exist, including additional interactions.⁴

To investigate the interactions that are responsible for receptor–ligand complex formation, methods of computational chemistry, namely docking analysis and molecular properties calculations for ligands (ClogP and electrostatic isopotential) were employed.⁵ Docking results showed that a short salt bridge to Asp 86 (TM3) together with multiple hydrogen bond formation to the serines on TM5 were present in all structures. Since the docked ligands showed different affinity towards the D2 receptor, it was obvious that there must be one or more additional interactions that determine ligand affinity. Based on docking structures and on ligand properties, a hypothesis was postulated that variations in affinity may originate from different distributions of edge-to-face (ETF) interactions in the docked structures. These interactions control the crystal structure of aromatic molecules, the stability of biological systems and molecular recognition processes.⁶ In ETF interactions, a partially positive hydrogen atom on one aromatic ring interacts with a partially negatively charged region on the second ring, hence the name edge-to-face (Fig. 1).⁷ The orientation of the amino acid residues of the ligands and re-

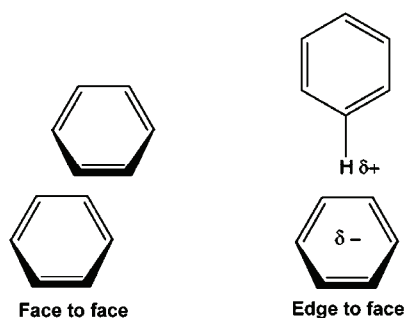


Fig. 1. Possible orientations for benzene aromatic rings. π - π stacking interaction parallel, (face-to-face) and T-shaped (edge-to-face).⁶

ceptor in results of docking simulations and calculated electrostatic isopotential maps strongly support the theory concerning ETF interactions as additional interactions and a decisive factor determining differences in ligand affinity.⁸

Observation of all interactions contributing to receptor–ligand complex formation is important when computer based methods are employed to model or explain such assemblies. Neglecting one type of interaction, such as, for instance, edge-to-face interactions, may lead to a series of wrong conclusions. However, research of structures possessing a large number of atoms, such as a dopamine D2 receptor–ligand complex, is usually limited to the methods of molecular mechanics, because only those kinds of calculations can be performed employing computer equipment with a reasonable processing power in a reasonable time. However, molecular mechanics force fields (even advanced class II ones, such as CFF)⁹ cannot guarantee that all of the influencing forces are taken into account. Dispersive forces, such as edge-to-face interactions fall well beyond the computing capabilities of MM force fields. Due to this, aromatic–aromatic interactions (namely ETF interactions) cannot be investigated without employing more precise, *ab initio* methods. Unfortunately, the use of these methods is limited to smaller molecules because of high demands for computational resources. Hence, for the application of *ab initio* calculations in research of large molecules, smaller model systems need to be postulated.

According to docking analysis, the ETF interaction between the N-aryl part of a ligand and the three aromatic amino acids (Tyr 216, Trp 182 and Phe 178) plays a significant role in receptor–ligand complex formation (Fig. 2). This conclusion is based on indirect evidence, namely on the values of the angles, distances and on mutual orientation of the corresponding amino acids and ligands, as well as on the calculated electrostatic potential.

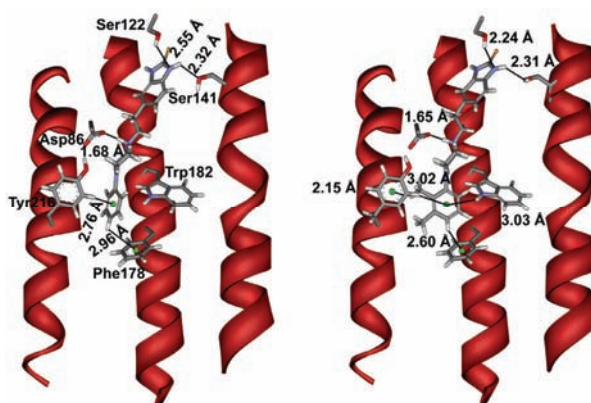


Fig. 2. Structures of benzimidazole-2-thione ligands **1** (left) and **2** (right) docked at the D2 receptor model. The orientation and distances between ligand and the lipophilic part of the binding site suggest that ETF interactions may be responsible for ligand affinity.

In order to present further evidence that will uphold the hypothesis concerning ETF interactions, a simplified binding site model system of dopamine D2 receptor–ligand ETF interactions was constructed and subjected to *ab initio* calculations in order to determine if the complex stabilization energy could be correlated to ligand affinity.

To utilize *ab initio* methods in the research of receptor–ligand interactions, several approximations had to be made, taking into account given the computer resources and the available (or reasonable) time. Thus the system had to be made smaller and the calculations more efficient. To simplify the system, our effort was concentrated on key amino acid residues and the part of the ligand that was held responsible for edge-to-face interactions. Ethylbenzene was used instead of phenylalanine, 3-ethyl-1*H*-indole instead of tryptophan and 4-ethylphenol was used to replace tyrosine. This kind of simplifications did not influence the properties of the aromatic moieties and gave a smaller and more compact model system to work on. In a similar way, the ligand molecule was shortened to arylpiperazine (Fig. 3).

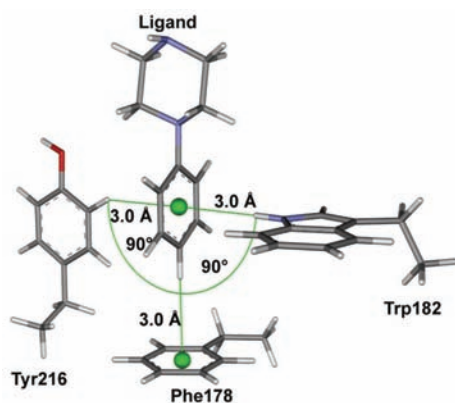


Fig. 3. Model system used in the present calculations mimics the hydrophobic pocket in the D2 receptor formed by 3-ethyl-*H*-indole (representative of Trp 182), ethylbenzene (representative of Phe 178) and 4-ethylphenol (representative of Tyr 216).

The initial receptor ligand position in this model system was taken directly from the results of docking analysis. These results positioned the arylpiperazine ligand moiety at distances of up to 3.00 Å to the receptor amino acid residues Tyr 216, Trp 182 and Phe 178 (Fig. 2). Based on these results, a model was constructed in which the ligand moiety was positioned perpendicular at 3.00 Å from each amino acid residue (Fig. 3). The same tetramer model was constructed for each ligand and subjected to *ab initio* DFT BH&H (Becke half & half) and MP2 calculations to determine the stabilization energy as described further. It is known that density function theory (DFT) calculations can not take into the account the existence and strength of dispersive forces such as ETF interactions but the BH&H hybrid DFT method was shown earlier to give rather correct results when applied on similar systems.^{10,11} The obtained results were correlated to ligand affinity but failed to show any significant correlation.

It was obvious that the docking analysis had failed to predict the exact distances between the ligand and the amino acid residues, mainly due to the fact that the employed molecular mechanics force field could not take into account the existing ETF interactions. To establish the optimal amino acid residue–ligand distance, a more complex approach was required.

First, the tetramer model system had to be further disassembled. As shown earlier, the energy of a complex system can be obtained by summing the energy of the system parts calculated separately.¹² Bearing this in mind, the system was treated as three separate dimers, each formed by ligand and one of the amino acid residues responsible for ETF interactions. The results calculated in this manner did not show significant differences, since the difference in the stabilization energy for ligand **1** calculated using the BH&H method for the tetramer and as a sum of each dimer separately was 0.59 kJ/mol (less than 1.5 % difference).

In order to swiftly determine the stabilization energy of the complex, the BH&H DFT *ab initio* method was used together with the 6-31g+* basis set. In this way, the calculation time was significantly reduced with no major loss in the quality of the result, compared to that obtained by the MP2 method.

Each ligand–amino acid residue pair was subjected to further *ab initio* calculations in which the distance was varied between 1.75 and 3.50 Å in order to establish the optimal value. The results are shown in Table II and Fig. 4. The optimal distance varies between 2.25 and 2.50 Å, depending on both the ligand and the amino acid residue. This result supports the docking analysis results, placing the ligand at an average distance of 3.00 Å from the amino acid residues. If Fig. 4 is taken into account, it can be seen that the difference in stabilization energy between 2.25 or 2.50 and 3.00 Å are noteworthy and that this is the main reason why docking analysis alone cannot be used to explain the fine differences between the investigated ligands. Finally, all the stabilization energies at the optimal distances were summed to obtain the stabilization energy of the system. These results were again correlated with the ligand affinity and the results are shown in Table III.

TABLE II. Calculated optimal distances to the corresponding amino acid residues

Ligand	Calculated optimal distance (Å) from		
	Phe178	Trp182	Tyr216
1	2.25	2.25	2.50
2	2.50	2.25	2.50
3	2.50	2.25	2.50
4	2.25	2.25	2.50
5	2.25	2.25	2.50
6	2.25	2.25	2.50
7	2.25	2.25	2.50

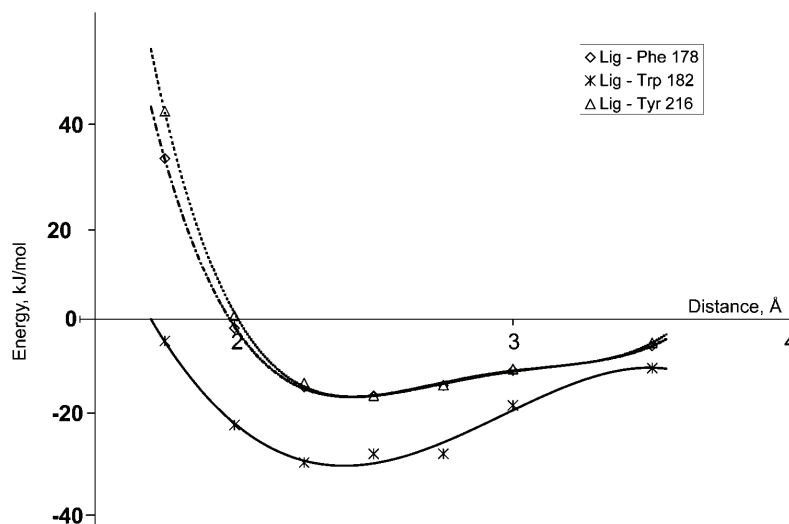


Figure 4. Calculated optimal distances between receptor amino acid residues and ligand 4.

In order to verify these results, one *ab initio* MP2 calculation was performed using the same basis set and the obtained results were similar to those obtained with BH&H DFT calculations (Table III).

TABLE III. Stabilization energies for various ligands calculated using the MP2 and BH&H method

Ligand	Stabilization energy, kJ/mol	
	MP2	BH&H
1	-38.07	-56.48
2	-38.49	-56.90
3	-42.68	-60.67
4	-30.12	-53.97
5	-30.12	-51.88
6	-38.49	-56.07
7	-26.36	-45.19

EXPERIMENTAL

Docking analysis

Ligand docking of the ligands in Table I was performed by simulated annealing using the Affinity module from InsightII in the SGI Octane2 workstation.¹³ All ligands were docked in the protonated form (protonated N-1 nitrogen on the piperazine part), using the CFF91 force field. Docking was performed using the dopamine D2 model and the binding site published earlier.⁸ During the docking procedure, the amino acid residues within the binding site were flexible, while the other amino acid residues of the protein were constrained. The initial position of the ligand in the binding site was arbitrary, with respect to the arylpiperazine part facing TM6 and TM7 (*i.e.*, Tyr 216, Try 182 and Phe 178), while the protonated nitrogen on the piperazine part was kept in close proximity to Asp86. After the initial placement of the ligand,

no further constraints were applied. A docking procedure based on the Monte Carlo methodology was performed and the obtained structures were finally optimized in order to remove steric strain, with a gradient limit of 0.0042 kJ/mol or 4000 optimization steps.¹⁴

The results were visualized using DS Visualizer, version 1.7, and the obtained images were rendered using PovRay Raytracer, version 3.6.¹⁵ Structures and affinities of the investigated ligands are given in Table I and the docking results are shown in Fig. 2.

Ab initio calculations

Gaussian 03W¹⁶ was used to carry out the calculations of the energy contribution of the chosen ligand–receptor assembly. All structures were subjected to geometry optimization using the HF method and the 6-31g+* basis set until the energy minima were attained. The mutual orientation of the interacting groups were taken from the results of docking analysis and later adjusted as required. The stabilization energies of the paired structures were calculated as the difference between the dimer and the separate molecular entities using the BH&H DFT and MP2 method, with the 6-31g+* basis set. All the reported energies were corrected for the basis set superposition error using the counterpoise method of Boys and Bernardi.¹⁷

RESULTS AND DISCUSSION

At present, it is well known that for the binding of ligands with the arylpiperazine moiety, the formation of a salt bridge between the protonated N-1 nitrogen of arylpiperazine and the negatively charged Asp 86 is required.⁴ This interaction guides the ligand towards its binding site, most probably by a zipper-like mechanism,¹⁷ leading to interactions with key residues in the receptor binding site. For substituted arylpiperazines, both hydrophobic and/or H-bonding interactions of the substituent with amino acid residues from TM6 and TM7 also play an important role in the binding.

Docking results confirmed that all the investigated ligands, can form a short salt bridge with Asp 86, within range of 1.68 to 1.80 Å,^{2,7} and fit inside the proposed hydrophobic pocket formed by amino acid residues on TM6 and TM7. Since all the investigated ligands form a short salt bridge with Asp 86, and have the same benzimidazole part of the ligand, it can be concluded that the differences in ligand affinity must arise from the number of proposed ETF interactions that the ligand can form with Tyr 216, Trp 182 and Phe 178 (Fig. 1).

BH&H Calculation of the stabilization energy for the receptor–ligand model system, designed to take into account only these ETF interactions, produced the following results:

– Although ligand **7** can fit into the hydrophobic pocket of the receptor, formed by Tyr 216, Trp 182 and Phe 178, the reason for its low affinity lies the fact that the introduction of a N atom into the aromatic part of the molecule decreases the ETF interactions, due to the withdrawal of electrons from the center of the aromatic ring. The calculated stabilization energy for this ligand showed destabilization by 11.72 kJ/mol compared to ligand **1**.

– Ligands **2**, **5** and **6** have a similar affinity or show a minimal increase in affinity compared to ligand **1**. They can form the same type and number of ETF

interactions as ligand **1**. The calculated energies for these ligands varied in range from -0.50 to 0.50 kJ/mol compared to ligand **1**, with the exception of ligand **5**, which showed destabilization by 4.60 kJ/mol. Such an amount of destabilization energy would usually lead to a significant loss of affinity, but ligand **5** showed a relatively small difference in affinity compared to ligand **1**. The reason for this unusual behavior could be that ETF interactions in ligand **5**, containing a halogen atom, could involve interactions with halogen atom itself instead of hydrogen. Although the measurements and crystal data analyzed so far confirm, without doubt, increased dispersion forces with the halogen atom present as a vicinal substituent in the aromatic ring, the real nature of the $C-X\cdots\pi$ interactions are still not completely resolved and this question is still open for discussion.¹⁹ If this is the case, the geometry of the studied model system should be altered in order to take account of this possibility.

– Although they can form the same number of multiple ETF interactions as ligands **2**, **5** and **6**, ligands **3** and **4** show increased affinity compared with ligand **1**. Increased affinity of ligand **3** is a consequence of the enlarged aromatic surface with a stronger and larger electrostatic potential when compared to **1**. This leads, as expected, to stronger dispersive ETF interactions with Tyr 216 and Trp 182. Hence, as expected, the calculated stabilization energy for this ligand was larger by -4.19 kJ/mol than that of ligand **1**. On the other hand, ligand **4** displayed a decrease in stabilization energy calculated by these methods (2.51 kJ/mol less than **1**), but this is followed by a strong increase in affinity. It is obvious that, in this case, something else in addition to dispersive ETF interactions is responsible for the affinity increase, which was not taken into account. From the structure of the ligand and the binding site of the protein, it can be seen that it is very likely that the methoxy group acts as a hydrogen acceptor for one of the possible hydrogen donors in the vicinity of Tyr 216 or Trp 182. This hydrogen bond is an interaction much stronger than the dispersive ETF interactions considered herein and is a key interaction for the binding of this ligand into this part of the binding site.

CONCLUSIONS

From the results presented herein, it is obvious that there is a significant correlation between the strength of the calculated stabilization energies (and thus with ETF interactions) and affinity of the ligands. This finding supports the hypothesis about the importance of ETF interactions for the affinity of arylpiperazine-type ligands. Ligand **4** was excluded from the present calculations as there are reasons for believing that most important interaction responsible for its affinity is not a dispersive ETF interaction, calculated in this study, but a hydrogen bond. In this case, it can easily be seen that the correlation coefficient of affinities and stabilization energies calculated using BH&H is 0.81 , and 0.91 for MP2, and r^2 is 65.5 and 82.0 %, respectively. Such high values identify a strong correlation

between the strength (and number) of edge-to-face interactions and the affinity of a ligand in this case.

Moreover, it can be seen that both the employed methods, although very different in their demands for computer time and resources, gave results with acceptable accuracy. This indicates that the BH&H method may be used in addressing the calculation of ETF stabilization energy in similar systems. The use of the BH&H method is recommended due to the fact that this method is, on average, 100 % faster than the MP2 method (2 h vs. 58 min for the pair ligand 4-Phe 178 on a reference PC system*).

Although several different interactions are responsible for the binding of the investigated ligands to the dopamine D2 receptor, it is obvious that neglecting weaker interactions can lead one astray. Investigation of large systems can sometimes proceed with difficulties due to their size and limitations in time, space and instrumental strength. In such cases, it is always wise to study ligand-receptor interactions separately and then to combine these results to give the final picture. In view of the fact that aromatic interactions are responsible for many important interactions and phenomena in chemistry and biology, a better understanding of these forces could lead to advancements in medicinal chemistry research.

Acknowledgment. This work was supported by Grant No. 142009 from the Ministry of Science and Technological Development of the Republic of Serbia.

ИЗВОД

УТИЦАЈ ДИСПЕРЗИВНИХ ИНТЕРАКЦИЈА НА АФИНИТЕТ ВЕЗИВАЊА ЛИГАНАДА СА АРИЛПИПЕРАЗИНСКОМ ФУНКЦИЈОМ ЗА ДОПАМИНСКИ D2 РЕЦЕПТОР

МАРИО В. ЗЛАТОВИЋ¹, ВЛАДИМИР В. ШУКАЛОВИЋ², ГОРАН М. РОГЛИЋ¹,
СЛАЂАНА В. КОСТИЋ-РАЈАЧИЋ² и ДЕАНА Б. АНДРИЋ¹

¹Хемијски факултет, Универзитет у Београду, б. бр. 51, 11158 Београд и ²ИХТМ-Центар за хемију, Универзитет у Београду, б. бр. 473, 11001 Београд

Неколико изостерних 1,3-дихидро-5-[2-(4-арил-1-пиперазинил)етил]-2H-бензимидазол-2-тиона је коришћено да би се испитале интеракције различитих лиганада са везивним местом допаминског D2 рецептора. Због ограничења метода коришћених за симулацију везивања, анализа ових резултата није могла да покаже прецизније које интеракције утичу на афинитет везивања лиганада. Претпостављено је да дисперзивне силе, или прецизније, тзв. *edge-to-face* интеракције, играју значајну улогу у процесу везивања, нарочито у липофилном делу лиганда. Да би се потврдила ова хипотеза применом *ab initio* израчунавања на модел систем, покушано је израчунавање стабилизационе енергије ових интеракција и њено довођење у везу са афинитетом лиганада. Добијени резултати указују да постоји значајна корелација између јачине дисперзивних интеракција и афинитета лиганда. Показано је да се при израчунавању стабилизационе енергије моделованих комплекса лиганд-рецептор може употребити Веске-ова „*half-and-half*” хибридна DFT метода, што значајно смањује време потребно за израчунавања и потребне рачунарске ресурсе.

(Примљено 17. фебруара, ревидирано 21 априла 2009)

* Intel® Pentium® Core™2Quad CPU processor 2.4 GHz, 4 GB RAM memory.

REFERENCES

1. C. Missale, S. R. Nash, S. W. Robinson, M. Jaber, M. G. Caron, *Physiol. Rev.* **78** (1998) 189
2. V. Šukalović, M. Zlatović, D. Andrić, G. Roglić, S. Kostić-Rajačić, V. Šoškić, *Arch. Pharm. Pharm. Med. Chem.* **337** (2004) 502
3. L. Shi, J. Javitch, *Annu. Rev. Pharmacol. Toxicol.* **42** (2002) 437
4. M. Y. S. Kalani, N. Vaidehi, S. E. Hall, R. J. Trabanino, P. L. Freddolino, M. A. Kalani, W. B. Floriano, V. W. T. Kam, W. A. Goddard, *Proc. Natl. Acad. USA* **101** (2004) 3815
5. M. V. Zlatović, V. V. Šukalović, C. Schneider, G. M. Roglić, *Bioorg. Med. Chem.* **14** (2006) 2994
6. A. K. Tewari, R. Dubey, *Bioorg. Med. Chem.* **16** (2008) 126
7. A. V. Muchldorf, D. V. Engen, J. C. Warner, A. D. Hamilton, *J. Am. Chem. Soc.* **110** (1988) 6561
8. V. Šukalović, M. Zlatović, D. Andrić, G. Roglić, S. Kostić-Rajačić, V. Šoškić, *Arzneim. Forsch./Drug Res.* **55** (2005) 145
9. *Insight II, Binding Site Analysis, Affinity, Discover, and WebLab Viewer are molecular modeling software*, corresponding modules and visualization software from Accelrys, Inc., San Diego, CA, <http://www.accelrys.com> (accessed 15 April, 2009)
10. M. P. Waller, A. Robertazzi, J. A. Platts, D. E. Hibbs, P. A. Williams, *J. Comput. Chem.* **27** (2006) 491
11. V. V. Šukalović, M. V. Zlatović, G. M. Roglić, S. V. Kostić-Rajačić, D. B. Andrić, *Acta Chim. Slov.* **56** (2009) 270
12. J. Vondrášek, L. Bendová, V. Klusák, P. Hobza, *J. Am. Chem. Soc.* **127** (2005) 2615
13. Silicon Graphics, Inc., CA, <http://www.sgi.com/> (accessed 15 April, 2009)
14. M. V. Zlatović, V. V. Šukalović, S. V. Kostić-Rajačić, D. B. Andrić, G. M. Roglić, *J. Serb. Chem. Soc.* **71** (2006) 1125
15. *PovRay Persistence of Vision Raytrace*, PovRay team, <http://www.povray.org> (accessed 15 April, 2009)
16. M. J. Frisch, G. W. Trucks, H. B. Schlegel, G. E. Scuseria, M. A. Robb, J. R. Cheeseman, J. A. Montgomery, Jr., T. Vreven, K. N. Kudin, J. C. Burant, J. M. Millam, S. S. Iyengar, J. Tomasi, V. Barone, B. Mennucci, M. Cossi, G. Scalmani, N. Rega, G. A. Petersson, H. Nakatsuji, M. Hada, M. Ehara, K. Toyota, R. Fukuda, J. Hasegawa, M. Ishida, T. Nakajima, Y. Honda, O. Kitao, H. Nakai, M. Klene, X. Li, J. E. Knox, Hratchian, H. P.; J. B. Cross, V. Bakken, C. Adamo, J. Jaramillo, R. Gomperts, R. E. Stratmann, O. Yazyev, A. J. Austin, R. Cammi, C. Pomelli, J. W. Ochterski, P. Y. Ayala, K. Morokuma, G. A. Voth, P. Salvador, J. J. Dannenberg, V. G. Zakrzewski, S. Dapprich, A. D. Daniels, M. C. Strain, O. Farkas, D. K. Malick, A. D. Rabuck, K. Raghavachari, J. B. Foresman, J. V. Ortiz, Q. Cui, A. G. Baboul, S. Clifford, J. Cioslowski, B. B. Stefanov, G. Liu, A. Liashenko, P. Piskorz, I. Komaromi, R. L. Martin, D. J. Fox, T. Keith, M. A. Al-Laham, C. Y. Peng, A. Nanayakkara, M. Challacombe, P. M. W. Gill, B. Johnson, W. Chen, M. W. Wong, C. Gonzalez, J. A. Pople, *Gaussian 03, Revision E.01*, Gaussian, Inc., Wallingford, CT, 2004.
17. S. F. Boys, F. Bernardi, *Mol. Phys.* **19** (1970) 553
18. A. S. Burgen, G. C. Roberts, J. Feeney, *Nature* **253** (1975) 753
19. C. D. Tatko, M. L. Waters, *Org. Lett.* **6** (2004) 3969.



Antioxidant status of atorvastatin in hypercholesterolemic patients

MOHAMMAD A. NASAR¹, ABDALLA JARRARI¹, MOHAMMAD A. NASEER²,
TARANNUM F. SUBHANI³, BEENA V. SHETTY³ and FAIYAZ SHAKEEL^{4*}

¹Department of Biochemistry, Faculty of Medicine, Al-Arab Medical University, Benghazi, Libya, ²Department of Pharmaceutical Chemistry, Faculty of Pharmacy, Jamia Hamdard, New Delhi, India, ³Department of Biochemistry, Kasturba Medical College, Manipal University, Mangalore, India and ⁴Department of Pharmaceutics, Faculty of Pharmacy, Al-Arab Medical University, Benghazi, Libya

(Received 26 February, revised 7 May 2009)

Abstract: This study was an attempt to establish the extent of increased oxidative stress in hypercholesterolemic patients and to evaluate the effect of atorvastatin on the oxidative stress and antioxidant status. Blood samples of 15 subjects (age and sex matched) from three groups: group I (healthy subjects), group II (hypercholesterolemic patients with atorvastatin treatment) and group III (hypercholesterolemic patients without any hypolipidemic drug) were taken and centrifuged to separate the plasma, which was used for the determination of vitamin E. The separated cells were washed thrice with 0.90 % w/v cold normal saline and used for the assay of the percentage hemolysis of the RBCs, and the determination of malondialdehyde, superoxide dismutase and hemoglobin. The levels of oxidative stress were higher in the hypercholesterolemic in comparison to the control and atorvastatin group. The levels of antioxidants were higher in the atorvastatin group than in the hypercholesterolemic one but were lower than the controls. From these findings, it was concluded that there is an increase in oxidative stress in hypercholesterolemia but it decreased significantly after 2 months of atorvastatin therapy and antioxidant status also improves in patients taking atorvastatin.

Keywords: atorvastatin; oxidative stress; antioxidant effects; hypercholesterolemic patients.

INTRODUCTION

Statins, such as atorvastatin, significantly reduce cholesterol synthesis through inhibition of 3-hydroxy-3-methylglutaryl-CoA (HMG-CoA) reductase and are widely prescribed for hyperlipidemia to reduce the risk of atherosclerotic com-

* Corresponding author. E-mail: faiyazs@fastmail.fm
doi: 10.2298/JSC0910063N

plications.¹ Their efficacy in reducing cardiovascular morbidity and mortality was demonstrated in large intervention trials.¹ However, debate continues as to whether the beneficial effects of statins can be ascribed purely to their ability to reduce cholesterol or whether additional actions, independent of lowering cholesterol, play a significant role.¹⁻³ Studies showed that oxidized low density lipoprotein (LDL) is a major correlate of oxidative stress in hypercholesterolemic patients and that statins may reduce oxidative stress by reducing enhanced plasma levels of LDL, which are more susceptible to peroxidation in hypercholesterolemia, and change the LDL structure, making them more resistant to peroxidation.^{1,4,5} Some studies further showed that statins may also inhibit NAD(P)H oxidase, thus decreasing the generation of reactive oxygen species (ROS), thereby adding or synergizing the biological effects of antioxidants.^{4,6} Some studies also showed that statins or their metabolites may act as antioxidants, directly or indirectly by removing “aged LDL”, which is more prone to oxidation, from the circulation.⁷ Based on these findings, it is evident that among their properties, statins also possess antioxidant activities.^{8,9} Therefore, the aim of the present investigation was to evaluate the scientific evidence of atorvastatin having such an effect and its possible clinical relevance. The antioxidant effects of statins contribute to the inhibition of atherogenesis, stabilization of atherosclerotic plaque, inhibition of myocardial hypertrophy and remodeling and modulation of vascular tone.⁶ Based on these arguments, which formed the backbone of this study, an attempt was made to determine whether there really is increased oxidative stress in hypercholesterolemics and if it is relatively decreased following atorvastatin therapy when compared to normal individuals.

In this study, the levels of malondialdehyde (MDA), percentage hemolysis and superoxide dismutase (SOD) in red blood cells and vitamin E in plasma were measured. Red blood cells were chosen as they are well known to be subject to increased hazards of free radical damage. Moreover, these cells have a finite life span in circulation and their sequestration and disposal by macrophages may be related to the extent of peroxidative damage of their membrane lipids, cytoskeletal proteins and enzymes.

EXPERIMENTAL

Study population

This study was conducted on 3 groups each of 15 subjects in the age group 40–70 years. Both male and female subjects were taken in all groups.

Group I consisted of 15 healthy subjects (8 males and 7 females) in the age range 40–70 years having a normal lipid profile (control group).

Group II consisted of 15 patients (8 males and 7 females) who had already been diagnosed as hypercholesterolemic and who had been treated with HMG–CoA reductase inhibitors (atorvastatin) for a minimum of 2 months at a minimum dosage of 10 mg/day of atorvastatin. Treatment with atorvastatin was given only in this group in order to compare the results with control and hypercholesterolemic group without administration of any hypolipidemic drug.

Group III consisted of 15 (8 males and 7 females) recently diagnosed hypercholesterolemic patients who were not taking any lipid lowering agent (hypercholesterolemic group).

Selection of cases

The test groups II and III for this study, consisting of 15 individuals in each group, were taken from the following hospitals: 1) the K. M. C. Hospital, Ambedkar Circle; 2) the K. M. C. Hospital, Attavar; 3) the Yenepoya Hospital, Kodialbail; 4) the A. J. Institute of Medical Sciences, Kuntikana; 5) the City Hospital, Kadri; 6) the Ullal General Hospital, Kudroli and 7) the Dr. Uday Nayak Clinic, Bejai, all in Mangalore, India.

While choosing the subjects for the test and control groups, care was taken to eliminate those with habits such as smoking, tobacco chewing, and alcohol consumption, as well as those with a history of chronic inflammatory disease such as tuberculosis, rheumatoid arthritis, diabetes mellitus and malignancy, all of which play a vital role in contributing to oxidative stress injury. Approval to perform these studies on human subjects was obtained from the Institutional Clinical Ethics Committee of the Kasturba Medical College, Mangalore, India, and their guidelines were followed throughout the studies.

Sample collection

Venous blood (5.0 ml) was collected in ethylenediaminetetraacetic acid (EDTA) containers from the median cubital vein or basilic vein of each study subject under strictly aseptic conditions. The blood samples were centrifuged at 3000 rpm for 10 min within 3 h of collection. The plasma was separated and used for the determination of vitamin E. The separated cells were washed thrice with 0.90 % w/v cold normal saline, after which they were suspended in an equal volume of the same saline solution. This was then stored as a 50 % cell suspension in a refrigerator (4–5 °C) until used for the assay of:

- percentage hemolysis of RBCs at 0 and 2 h (which represented before and after incubation with hydrogen peroxide, respectively);
- malondialdehyde (MDA);
- superoxide dismutase (SOD);
- hemoglobin (Hb).

Lipid peroxidation (MDA)

Red cell lipid peroxidation was studied as thiobarbituric acid (TBA) reaction products. The method of Stocks and Dormandy was followed with certain modifications.¹⁰ The sample under test was heated with TBA at a low pH and the resulting pink chromogen, allegedly a (TBA)₂-MDA adduct, was measured spectrophotometrically at a wavelength of 535 nm.¹¹ An erythrocyte suspension (1.0 ml) was added to 8.5 ml of 0.90 % w/v normal saline and mixed well. Then 0.50 ml of 0.44 M H₂O₂ was added.

From this mixture, a 2.5 ml of aliquot was immediately taken, to which 1.0 ml of 28 % trichloroacetic acid (TCA) in 0.10 M sodium metaarsenite was added. This was mixed well and allowed to stand for 10 min, after which it was centrifuged. An aliquot (3.0 ml) of the supernatant was then taken, to which 1.0 ml of 1.0 % TBA in 50 mM NaOH was added. This was then kept in a boiling water bath for 15 min and then immediately cooled under tap water. The pink chromogen was determined spectrophotometrically at a wavelength of 535 nm. The values are expressed as nanomoles of MDA formed per dl of RBC, taking the molar extinction coefficient of the chromogen as 1.56×10^5 l/mol/cm.¹⁰

MDA (10^{-9} mol/100 ml of RBC) was determined using the equation:

$$MDA = \frac{10^{11} A_T DFV}{\epsilon}$$

where A_T is the absorbance of the test sample, DF is the dilution factor, V is the volume of the RBC suspension and ϵ is the extinction coefficient.

Oxidative hemolysis of RBCs or percentage hemolysis of RBCs

Oxidative hemolysis of the erythrocytes was measured by the method of Kartha and Krishnamurthy¹² at 0 and 2 h, *i.e.*, before and after 2 h incubation with H_2O_2 . The principle of this method is based on the fact that an accelerated form of non-enzymatic breakdown can be induced in red blood cells by exposure to H_2O_2 .¹⁰

RBC suspension (1.0 ml) was added to 8.5 ml of 0.90 % w/v of normal saline and mixed well. Then 0.50 ml of 0.44 M H_2O_2 was added and the mixture incubated at 37 °C.

Immediately, 0.50 ml aliquots each were withdrawn and put into 2 different centrifuge tubes labeled as "saline" and "water".

To the centrifuge tube labeled "saline", 4.5 ml of 0.90 % w/v of normal saline was added and centrifuged. The supernatant was then separated and its absorbance (optical density) was determined at 520 nm in a colorimeter. This represented non-hemolysed RBCs (NH) at 0 h or before incubation with H_2O_2 .

To the centrifuge tube labeled "water", 4.5 ml of distilled H_2O was added and centrifuged. The supernatant was then separated and its optical density was determined at 520 nm in a colorimeter. This represented complete hemolysis of RBCs (CH) at 0 h or before incubation with H_2O_2 .

The above procedure was again repeated after 2 h incubation with H_2O_2 at 37 °C. The centrifuge tubes labeled "saline" and "water" now represented non-hemolysed (NH) and completely hemolysed (CH) RBCs, respectively, at 2 h or after incubation with H_2O_2 .

The percentage hemolysis of RBCs at 0 and 2 h was determined using the equation:

$$\text{Hemolysis (\%)} = 100 \frac{O.D. \text{ of NH (saline)}}{O.D. \text{ of CH (water)}}$$

Vitamin E (α -tocopherol)

Plasma vitamin E was measured using the Emmorie Engel reaction, which is based on the reduction of ferric to ferrous ions by tocopherols, which then form a red complex with α, α' -dipyridyl. Tocopherol and carotenes were extracted into petroleum ether and the extinction at 450 nm was measured. A correction was made for carotenoids after adding $FeCl_3$. The reading was taken at 520 nm after 90 s.^{13,14}

Plasma (1.0 ml) was thoroughly mixed with 1.0 ml of redistilled 95 % ethanol in a 15 ml stoppered tube. Petroleum ether (3.0 ml) was then added and the tube shaken vigorously for 3 min. This was then centrifuged and 2.0 ml of the clear supernatant was transferred to a clear dry cuvette. The optical density was measured at 450 nm in a colorimeter for carotenes; petroleum ether served as the blank.

The petroleum ether was then evaporated off at room temperature and the residue dissolved in 1.0 ml of chloroform; 1.0 ml of 95 % ethanol was then added followed by 1.0 ml of 0.20 % α, α' -dipyridyl and 0.10 ml of 0.10 % $FeCl_3$. After 1.5 min, the absorbance at 520 nm was measured in a colorimeter.

The concentration of vitamin E, mg/l of plasma, was determined using the equation:

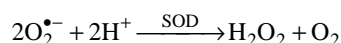
$$c = \frac{A_T - A_C}{A_S}$$

where A_T , A_C and A_S are absorbance of test, carotene and standard sample, respectively.

Superoxide dismutase (SOD)

The method of Beauchamp and Fridovich was followed for the measurement of SOD.

The enzyme superoxide dismutase catalyses the reaction:



Inhibition of the reduction of nitroblue tetrazolium (NBT) by superoxide radicals, generated by the illumination of riboflavin in the presence of oxygen was the principle of SOD determination. An electron donor, methionine, was used for the assay of superoxide dismutase.¹⁵

The hemolysate was prepared by the method of McCord and Fridovich.¹⁶ To 1.0 ml of erythrocytes (washed with 0.90 % w/v normal saline), 1.0 ml of deionized water was added to lyse the cells. To this, 0.50 ml of distilled ethanol followed by 0.30 ml of chloroform were added, mixed well and allowed to stand for 15 min. Then 0.20 ml of H_2O was added and then the mixture was centrifuged at 4 °C.

The supernatant contained the SOD activity and was used for the assay of SOD after dilution with potassium phosphate buffer (pH 7.8, 0.050 M); 0.10 ml of hemolysate was diluted with 1.9 ml of potassium phosphate buffer. This was the final diluted hemolysate that was used in the procedure given below.

Four test tubes were taken and labeled as “test”, “control”, “test blank” and “control blank”.

To the “test”, 2.9 ml of reaction mixture with NBT containing 149 mg of methionine, 4.93 ml of NBT (1 mg/ml), 0.63 ml of riboflavin (1 mg/ml) was diluted to 100 ml with potassium phosphate buffer (pH 7.8, 0.050 M) and 0.10 ml of diluted hemolysate was added. To the “test blank”, 2.9 ml of same reaction mixture without NBT and 0.10 ml of diluted hemolysate was added. To the “Control”, 2.9 ml of same reaction mixture with NBT and 0.10 ml of potassium phosphate buffer (pH 7.8, 0.050 M) was added. To the “control blank”, 2.9 ml of the same reaction mixture without NBT and 0.10 ml of potassium phosphate buffer (pH 7.8, 0.050 M) was added. Each of the above solutions was poured into a 10 ml beaker. The beakers were kept in an aluminum foil lined box fitted with a 15 W fluorescent lamp for 10 min.

The absorbance of the solutions after irradiation was measured at wavelength of 560 nm in a spectrophotometer.

One unit of SOD activity was taken as that producing a 50 % inhibition of NBT (nitroblue tetrazolium) reduction. The obtained values, expressed as units /g Hb, were calculated using the equation:

$$\text{Unit/dl SOD (x)} = 2.4 \times 10^5 \frac{C - T}{C}$$

$$\text{SOD activity (units/g Hb)} = \frac{x}{\text{Hb}} \text{ (Units/g Hb of SOD)}$$

where C and T are the absorbance of the control and test, respectively.

Estimation of hemoglobin

The hemoglobin content of the erythrocytes was determined by the cyanmethemoglobin method.¹⁷

Hemoglobin was treated with a reagent containing potassium ferricyanide, potassium cyanide and potassium dihydrogen phosphate (Drabkins Reagent). The ferricyanide oxidizes hemoglobin to methemoglobin, which is converted to cyanmethemoglobin by the cyanide. The absorbance was measured at 540 nm in a colorimeter.

RBC suspension (20 µl) was added to 4.0 ml of ferricyanide reagent and allowed to stand for 4 min. The absorbance was measured at 540 nm in a colorimeter against a reagent blank. The absorbance of the standard solution was measured by directly taking 4.0 ml of a standard cyanmethaemoglobin solution (60 mg/dl).¹⁸

Hemoglobin (g/dl) was determined using the equation:

$$\text{Hemoglobin (g/dl)} = \frac{A_T \times \text{Dilution factor} \times \text{Conc. of std. (mg/dl)}}{1000A_S}$$

where Conc. of std. is 60 mg/dl.

Statistical analysis

All the biochemical parameters were compared using the Fishers *F*-test for analysis of variance (ANOVA), except for hemolysis. The student's paired *t*-test was used for hemolysis (0 and 2 h). The statistical software SPSS (statistical package for social sciences), version 11, was used for this purpose.

RESULTS AND DISCUSSION

In this study, the products of lipid peroxidation, hemolysis of RBCs and anti-oxidant levels were compared between those having a high cholesterol level, those who had been on treatment with atorvastatin for a minimum of 2 months (minimum dosage of 10 mg/day) and those individuals of the same age group having a normal lipid profile, who were taken as controls.

Free oxygen radicals and insufficient antioxidant enzymes have been implicated in the pathogenesis of hypercholesterolemia.^{2,4,19,20} Statins have been used effectively for the treatment of hypercholesterolemia.^{2,20,21} These facts formed the basis of this study, *i.e.*, to investigate the antioxidant system and oxidative stress in hypercholesterolemic patients, as well as in patients who had been treated with atorvastatin for a minimum of 2 months.

The mean total cholesterol levels of the 3 groups are given in Table I. In patients taking atorvastatin, the mean total cholesterol was reduced after 2 months of treatment (246.66±8.54 mg/dl) as compared to the hypercholesterolemic patients (325.33±11.23 mg/dl).

RBC malondialdehyde (MDA)

As a measure of oxidative stress, MDA, the end-product of lipid peroxidation, was estimated by the TBA method. RBC MDA levels were highest in the hypercholesterolemic group (742.67±74.10 µmol/l) and lowest in control group (545.63±48.03 µmol/l). These values are statistically highly significant (*p* = 0.001)

when the hypercholesterolemic group was compared with the control group and statistically significant ($p = 0.034$) when the atorvastatin group was compared with the control group, as indicated in Table II.

TABLE I. Mean total cholesterol levels of the 3 groups, *i.e.*, control, atorvastatin and hypercholesterolemic

Group	No. of subjects	Mean total cholesterol level, mg/dl ^a
Control	15	161.25±5.43
After a minimum of 2-months- -atorvastatin therapy	15	246.66±8.54
Hypercholesterolemic	15	325.33±11.23

^aMean±SD

TABLE II. Mean RBC MDA levels of the 3 groups (control, atorvastatin and hypercholesterolemic) determined by Fisher's *F*-test

Group	No. of subjects	Mean, $\mu\text{mol/l}$	SD	<i>p</i>	Remarks
Control	15	545.63	48.03	–	–
Atorvastatin	15	590.23	39.63	0.034	S ^a
Hypercholesterolemic	15	742.67	74.10	0.001	HS ^b

^aSignificant; ^bhighly significant

The high level of MDA in the hypercholesterolemic group suggests an increase in oxidative stress in patients with hypercholesterolemia. Its relatively lower level in the atorvastatin group suggests a decrease in oxidative stress. These findings further confirm the antioxidant properties of statins such as atorvastatin.²

Percentage hemolysis of RBCs and vitamin E

The percentage hemolysis of RBCs was measured as an indicator of damage to RBC membranes as a result of oxidative stress. Amongst the antioxidants, vitamin E was chosen because, despite its low molar concentration in membranes, it effectively serves as the major lipid-soluble, chain-breaking antioxidant.²² This study showed an increased hemolysis of RBCs in the hypercholesterolemic group (4.52±1.06 %) as compared to the atorvastatin (2.48±0.67 %) and control groups (1.69±1.04 %), but in the atorvastatin group it was more than in the control but less than the hypercholesterolemic group, both before (2.48±0.67 %) and after incubation (3.52±0.81 %) with hydrogen peroxide (Table III). The values are statistically highly significant both before and after incubation with hydrogen peroxide ($p < 0.05$). This could be explained based on increased oxidative stress in the hypercholesterolemia patients and the effect of atorvastatin in reducing oxidative stress in the hypercholesterolemic patients after 2 months of treatment. The mean vitamin E levels were lower in the atorvastatin group (7.74±1.05 mg/dl) and the lowest in hypercholesterolemic group (6.28±0.68 mg/dl) as compared to the control group (9.31±1.36 mg/dl) as shown in Table IV. The values are statistically highly significant ($p < 0.05$). Studies showed that vitamin E plays a critical role

in protecting the polyunsaturated fatty acids of cell membranes against lipid peroxidation through its free-radical quenching activity at an early stage of free-radical attack, thus suppressing hemolysis.²² This has made vitamin E one of the important factors determining the susceptibility of red cells to auto-oxidation hemolysis.²² Vitamin E appeared to be highly efficient as an antioxidant and is accepted as the first line of defense against lipid peroxidation.²²⁻²⁵

TABLE III. Percentage hemolysis of RBCs before and after incubation with H₂O₂ in the 3 groups (control, atorvastatin and hypercholesterolemic). Name of the test used: Fisher's *F*-test

Group	No. of subjects	Mean	SD	<i>p</i>	Remarks
Hemolysis before incubation					
Control	15	1.69	1.04	–	–
Atorvastatin	15	2.48	0.67	0.001	HS ^a
Hypercholesterolemic	15	4.52	1.06	0.001	HS
Hemolysis after incubation					
Control	15	2.78	0.88	–	–
Atorvastatin	15	3.52	0.81	0.001	HS
Hypercholesterolemic	15	6.01	1.12	0.001	HS

^aHighly significant

The popular finding that vitamin E is inversely related to the respective tissue MDA level fits here as the MDA level in this study was found to be the highest in the hypercholesterolemic group (742.67±74.10 µmol/l) and the lowest in control group (545.63±48.03 µmol/l). The increased hemolysis of RBCs in the hypercholesterolemic group could be further documented by the decreased levels of vitamin E, which is the first line of defense against membrane damaging lipid peroxidation.²²⁻²⁵

In the atorvastatin group, the level of vitamin E was more than in the hypercholesterolemic group but less than in the control group (Table IV). The results of percentage hemolysis of RBCs were in the same order; hemolysis was the lowest in the control group, higher in the atorvastatin group and the highest in the hypercholesterolemic group. The controls had the highest level of vitamin E as they are considered to be the group with the least oxidative stress due to the normal lipid profile of their blood. It may be hypothesized that due to increased oxidative stress in the hypercholesterolemic group, the utilization of vitamin E, which is an antioxidant, might have increased. This agrees with the work of Moriel *et al.*¹⁹

TABLE IV. Plasma vitamin E levels of the 3 groups (control, atorvastatin and hypercholesterolemic). Name of the test used: Fisher's *F*-test

Group	No. of subjects	Mean, mg/dl	SD	<i>p</i>	Remarks
Control	15	9.31	1.36	–	–
Atorvastatin	15	7.74	1.05	0.001	HS ^a
Hypercholesterolemic	15	6.28	0.68	0.001	HS

^aHighly significant

Superoxide dismutase (SOD)

Superoxide dismutase was chosen in this study as it plays an important role in the removal of superoxide radicals ($O_2^{\bullet-}$) formed in red cells and because hemoglobin and SOD were shown to be in close association with red cells. In addition to this, some studies also suggested that SOD is one of the most important enzymes in the front line of defense against oxidative stress and is the most effective in protecting RBCs against damage by exogenous superoxide radicals ($O_2^{\bullet-}$), especially at higher concentrations.²⁶⁻²⁸ This study showed low levels of SOD in the hypercholesterolemic group (6.28 ± 0.69 units/mg), as shown in Table V. In the atorvastatin group, the SOD level (7.74 ± 1.05 units/mg) was more than in the hypercholesterolemic but less than in the controls. The values were statistically highly significant ($p < 0.05$). Low levels of SOD in the cellular and extracellular fluids reduce their oxygen-derived, free radical (ODFR) scavenging capacity, making the tissues more vulnerable to ODFR damage.²⁸ The low level of SOD found in hypercholesterolemic patients is indicative of increased oxidative stress in patients with hypercholesterolemia (Table V). Studies that showed that there is a reduced activity of SOD in hypercholesterolemia, which improved after 3 months of treatment with fluvastatin, further strengthens the idea of increased oxidative stress in hypercholesterolemics and reduction of oxidative stress after the use of atorvastatin, which inhibits superoxide anion production, preserves intracellular SOD and prevents ROS (reactive oxygen species) permeation into lipoproteins.^{2,26,27} Thus, it can be concluded that the trends seen in this study definitely suggest that there is an increased occurrence of oxidative stress as a result of hypercholesterolemia and that after the use of atorvastatin, the oxidative stress decreased, for which there may be two reasons. The first reason may be due to the decreased cholesterol levels and the second, due to the anti-oxidant effect of atorvastatin, as shown in many studies.

TABLE V. RBC superoxide dismutase (SOD) levels in the 3 groups (control, atorvastatin and hypercholesterolemic). Name of the test used: Fisher's *F*-test

Group	No. of subjects	Mean, units/mg	SD	<i>p</i>	Remarks
Control	15	8078.63	762.50	–	–
Atorvastatin	15	7432.69	657.92	0.001	HS ^a
Hypercholesterolemic	15	5281.79	525.19	0.001	HS

^aHighly significant

CONCLUSIONS

This study was an attempt to establish the extent of increased oxidative stress in hypercholesterolemic patients and to evaluate the effect of atorvastatin on the oxidative stress and antioxidant status after 2 months of treatment.

The levels of oxidative stress were higher in the hypercholesterolemic patients than in the control and atorvastatin groups. The levels of oxidative stress in

the atorvastatin group were lower than in the hypercholesterolemic group but higher than in the control group. The levels of antioxidants were higher in the atorvastatin group than hypercholesterolemic group but were lower than in the controls. From these findings, it can be concluded that there is an increase in oxidative stress in hypercholesterolemia but it decreases significantly after 2 months of atorvastatin therapy and there is simultaneously an improvement in the antioxidant status in patients taking atorvastatin.

ИЗВОД

АНТИОКСИДАТИВНИ СТАТУС КОД ПАЦИЈЕНАТА СА ХИПЕРХОЛЕСТЕРОЛЕМИЈОМ НА ТЕРАПИЈИ АТОРВАСТАТИНОМ

МОХАММАД А. НАСАР¹, АБДАЛЛА ЈАРАРИ¹, МОХАММАД А. НАСЕЕР², ТАРАННУМ Ф. СУБХАНИ³, БЕЕНА В. ШЕТИ³ и ФАЈАЗ ШАКЕЛ⁴

¹Department of Biochemistry, Faculty of Medicine, Al-Arab Medical University, Benghazi, Libya, ²Department of Pharmaceutical Chemistry, Faculty of Pharmacy, Jamia Hamdard, New Delhi, India, ³Department of Biochemistry, Kasturba Medical College, Manipal University, Mangalore, India u ⁴Department of Pharmaceutics, Faculty of Pharmacy, Al-Arab Medical University, Benghazi, Libya

У овој студији је проучавано повећање оксидативног стреса код пацијената са хиперхолестеролемијом и праћен је ефекат аторвастатина на оксидативни стрес и антиоксидативни статус. Анализирана је плазма људи из три групе (по 15 узорака): здрави људи, пацијенти са хиперхолестеролемијом на терапији аторвастатином и пацијенти са хиперхолестеролемијом без терапије. У плазми је одређиван витамин Е. Изоловане ћелије су испране три пута хладним физиолошким раствором и коришћене су за одређивање степена хемоллизе еритроцита и концентрације малондиалдехида, супероксид-дисмутазе и хемоглобина. Степен оксидативног стреса је био већи код пацијената без терапије него код здравих особа и пацијената на третману аторвастатином. Ниво антиоксиданаса је био већи код пацијената под терапијом, али ипак мањи него у контролној групи. На основу резултата је закључено да је оксидативни стрес повећан код пацијената са хиперхолестеролемијом, али да се значајно смањује после двомесечне терапије аторвастатином, уз побољшање антиоксидативног статуса.

(Примљено 26. фебруара, ревидирано 7. маја 2009)

REFERENCES

1. J. C. Mason, *Clin. Sci.* **105** (2003) 251
2. M. I. Yilmaz, Y. Baykal, M. Killic, A. Sonmez, F. Bulucu, A. Aydin, A. Sayal, I. H. Kocar, *Biol. Trace Elem. Res.* **98** (2004) 119
3. R. S. Rosenson, *Curr. Cardiol. Rep.* **1** (1999) 228
4. R. D. Caterina, F. Cipollone, M. Zimarino, G. Ciabattini, *Circulation* **106** (2002) 2543
5. O. Shovman, Y. Levy, B. Gilburd, Y. Shoenfeld, *Immunol. Res.* **25** (2002) 271
6. J. Beltowski, *Toxicol. Mech. Methods* **15** (2005) 61
7. R. Mira, H. Tony, H. Khetam, M. Aviram, *Lett. Drug Des. Discovery* **1** (2004) 269
8. G. D. Norata, A. Pirillo, A. L. Catapano, *Circulation* **109** (2004) 3164
9. B. Ky, A. Barke, S. Tsimikas, M. L. Wolfe, M. G. Tadesse, P. O. Szapary, J. L. Witztum, G. A. Fitz-Gerald, D. J. Rader, *J. Am. Coll. Cardiol.* **51** (2008) 1653
10. J. Stocks, T. L. Dormandy, *Br. J. Haematol.* **20** (1971) 95
11. B. Halliwell, C. Susanna, *Am. J. Clin. Nutr.* **57** (1993) 715

12. V. N. R. Kartha, S. Krishnamurthy, *J. Lipid Res.* **19** (1978) 332
13. J. G. Bieri, L. Teets, B. Belvady, E. L. Andrew, *Arch. Proc. Soc. Exp. Biol. Med.* **117** (1964) 131
14. N. W. Teitz, *Text book of clinical chemistry*, W. B. Saunders Co., London, 1986, pp. 1285–1288
15. I. Fridovich, *Ann. Rev. Biochem.* **44** (1975) 147
16. J. M. McCord, I. Fridovich, *J. Biol. Chem.* **244** (1969) 6049
17. D. L. Drabkin, J. H. Austin, *J. Biol. Chem.* **98** (1932) 719
18. O. W. Van Assendelft, W. G. Zijlstra, E. P. Van Kampen, A. H. Holtz, *Clin. Chim. Acta* **13** (1966) 521
19. P. Moriel, F. L. Plavnik, M. T. Zanella, M. C. Bertolami, D. S. Abdalla, *Biol. Res.* **33** (2000) 105
20. D. S. Ng, *Curr. Drug Targets Cardiovasc. Haematol. Disord.* **5** (2005) 165
21. G. Davi, M. Romano, A. Mezetti, A. Procopio, A. B. Bon, *Circulation* **97** (1998) 953
22. L. Packer, *Am. J. Clin. Nutr.* **53** (1991) 1050
23. H. Argani, A. Ghorbani, N. Rashtchizade, M. Rahbaninobar, *Lipids Health Dis.* **3** (2004) E6
24. S. Garibaldi, P. Fabbi, G. Bertero, P. Altieri, S. Nasti, V. Manca, G. Ghigliotti, N. Traverso, C. Brunelli, A. Barsotti, *Ital. Heart J.* **3** (2002) 49
25. E. Simon, J. L. Paul, T. Soni, A. Simon, N. Moatti, *J. Clin. Chem.* **43** (1997) 285
26. F. A. Oski, *N. Engl. J. Med.* **303** (1980) 454
27. P. Klatt, S. Lamas, *Eur. J. Biochem.* **267** (2001) 4928
28. V. K. Gupta, V. Mallika, Y. Gupta, D. K. Srivastava, *Indian J. Clin. Biochem.* **7** (1992) 3.



J. Serb. Chem. Soc. 74 (10) 1075–1084 (2009)
JSCS–3901

Template synthesis, characterization and antimicrobial activity of some new complexes with isonicotinoyl hydrazone ligands

LIVIU MITU^{1*}, NATARAJAN RAMAN², ANGELA KRIZA³,
NICOLAE STĂNICĂ⁴ and MARIANA DIANU³

¹University of Pitești, Faculty of Science, Department of Physics and Chemistry, Târgul din Vale 1, 110040, Pitești, Romania, ²Department of Chemistry, College VHNSN, Virudhunagar-626001, India, ³University of Bucharest, Faculty of Chemistry, Department of Inorganic Chemistry, Dumbrova Roșie 23, 020461, Bucharest and ⁴Romanian Academy, Institute of Physical-Chemistry "I. G. Murgulescu", Splaiul Independenței 202A, 060021, Bucharest, Romania

(Received 17 January, revised 15 April 2009)

Abstract: Complexes of Cu(II), Ni(II), Co(II) with the 9-anthraldehyde isonicotinoyl hydrazone ligand (HL¹) and the 3,5-di-*tert*-butyl-4-hydroxybenzaldehyde isonicotinoyl hydrazone ligand (H₂L²) were synthesized by the template method. The complexes were characterized by analytical analysis, IR, UV-Vis and ESR spectroscopy, magnetic measurements, conductometry and thermal analysis and the two ligands by ¹H-NMR spectroscopy. From the elemental analysis, 1:2 (metal:ligand) stoichiometry for the complexes of Cu(II), Ni(II) with the ligands HL¹ and H₂L² and 1:1 (metal:ligand) stoichiometry for the complex of Co(II) with the ligand HL¹ are proposed. The molar conductance data showed that the complexes are non-electrolytes. The magnetic susceptibility results coupled with the electronic and ESR spectra suggested a distorted octahedral geometry for the complexes Ni(II)/HL¹, Ni(II)/H₂L² and Cu(II)/H₂L², a tetrahedral stereochemistry for the complex Cu/HL¹ and a square-planar geometry for the complex Co/HL¹. The IR spectra demonstrated the bidentate coordination of the ligands HL¹ and H₂L² by the O=C amide oxygen and the azomethine nitrogen, as well as monodentate coordination of the ligand HL¹ by the azomethine nitrogen in the Cu(II) complex. The antibacterial activity of the ligands and their metallic complexes were tested against *Staphylococcus aureus*, *Escherichia coli* and *Klebsiella pneumoniae*.

Keywords: Cu(II), Ni(II) and Co(II) complexes; template synthesis; isonicotinoylhydrazone; characterization; antibacterial activity.

* Corresponding author. E-mail: ktm7ro@yahoo.com
doi: 10.2298/JSC0910075M

INTRODUCTION

Hydrazone ligands and their complexes with different transition metal ions have been thoroughly studied due to their biological activity.¹⁻³ The aroylhydrazones contain in their structure the $-\text{CO}-\text{NH}-\text{N}=\text{C}<$ group that imparts on these chelating agents fungicidal,⁴ antibacterial,⁵ antiparasital⁶ and anticancerous⁷ properties. The complexes of Ni(II), Mn(II) with 6-methylpyridine 2-carboxaldehyde isonicotinoyl hydrazone exhibit antituberculosis activity.⁸ The parameters of the chemical structure, and the physical and electronic characteristics of the ligands are determining factors in the manifestation of bioactivity. In continuation of ongoing studies⁹ on complexes with ligands of the isonicotinoylhydrazone class, the synthesis and study of new mixed-ligand complexes of Cu(II), Ni(II) and Co(II) with such ligands are presented in this paper.

EXPERIMENTAL

All the employed reagents and solvents were of AR grade and were used without further purification. The M and Cl contents were obtained by literature methods¹⁰ and C, H and N were determined with a Hewlett Packard 185 CHN-analyzer. The molar conductivity of the complexes was measured with a HACH-sens ion 5-conductivity meter using 10^{-3} M solutions in DMF. The IR spectra were recorded between $4000-400\text{ cm}^{-1}$ on a BIORAD-FT-IR 135 FTS spectrophotometer using the KBr disc technique. The electronic reflectance spectra (300–1100 nm) were obtained on a VSU-2P Zeiss-Jena spectrophotometer using MgO as the standard. The ESR spectra for the Cu(II) complexes were registered at room temperature (293 K) on a microcrystalline powder with an ART5 spectrophotometer. The magnetic moments were determined by the Faraday method at the room temperature. The ^1H - and ^{13}C -NMR spectra were recorded on a Varian Gemini 300BB instrument in DMSO- d_6 . The thermal analysis was realized with an MOM-Q-1500D derivatograph in air at a heating rate of $5\text{ }^\circ\text{C min}^{-1}$.

Synthesis

A solution of 0.0010 mol of isonicotinoylhydrazine and 0.0010 mol of aldehyde (9-anthraldehyde or 3,5-di-*tert*-butyl-4-hydroxybenzaldehyde) in 75 ml of methanol was refluxed for 5 h on a water bath. Subsequently, reaction mixture was concentrated. The precipitate was filtered and recrystallized from ethanol.

A methanolic solution of anhydrous metal chloride MCl_2 ($\text{M} = \text{Cu(II)}, \text{Co(II)}$ or Ni(II)) (0.0010 mol in 30 ml of MeOH) was added to a mixture of isonicotinoylhydrazine (0.0020 mol in 30 ml of MeOH) and aldehyde (9-anthraldehyde or 3,5-di-*tert*-butyl-4-hydroxybenzaldehyde, 0.0020 mol in 75 ml of MeOH). The reaction mixture was refluxed on a water-bath for 4 h after which a part of the solvent was removed by distillation. The precipitated complexes were filtered off, washed with MeOH and then with diethyl ether and finally dried under vacuum over anhydrous CaCl_2 .

Antibacterial activity

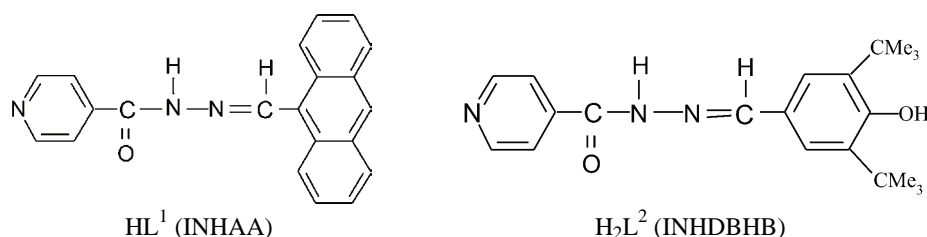
The metal complexes and the free isonicotinoylhydrazone ligands were tested for their activity against the pathogenic strains of bacteria: *Staphylococcus aureus* (Gram-(+)), *Escherichia coli* (Gram-(-)) and *Klebsiella pneumoniae* (Gram-(-)). The paper disc diffusion method¹¹ was applied using DMF as the solvent (the concentration was $125\text{ }\mu\text{g ml}^{-1}$).

RESULTS AND DISCUSSION

The obtained complexes were coloured powders, stable for a long time in the open atmosphere, insoluble in methanol, ethanol, chloroform and acetone. The complexes Co(II)/HL¹, Cu(II)/H₂L² and Ni(II)/H₂L² were soluble in DMF but Cu(II)/HL¹ and Ni(II)/HL¹ were only partly soluble in this solvent. The elemental analysis showed a stoichiometry of 1:2 (metal:ligand) for the complexes, except for the Co(II)/HL¹ complex which had a 1:1 ratio. The analytical data of the ligands and complexes are given in Table I. The presence of lattice water was confirmed by TG analysis. The low values of the molar conductivity supported a non-electrolyte nature for the metal complexes. The structural formulas corresponding to the ligands HL¹ (INHAA) and H₂L² (INHDBHB) are presented in Fig. 1.

TABLE I. Analytical and physical data of the complexes

Compound	M.p. °C	Colour	Found (Calcd.), %					μ_{eff} μ_{B}	A_{m}^{a} $\Omega^{-1} \text{cm}^2 \text{mol}^{-1}$
			M	C	H	N	Cl		
Ligand HL ¹ C ₂₁ H ₁₅ N ₃ O	271	Yellow	–	77.31 (77.53)	4.40 (4.61)	12.73 (12.92)	–	–	–
[Cu(HL ¹) ₂ Cl ₂]	254	Khaki	7.88 (8.09)	64.05 (64.24)	3.64 (3.82)	10.48 (10.70)	8.83 (9.04)	2.16	–
[Ni(HL ¹) ₂ Cl ₂]	272	Dark ochre	7.33 (7.52)	64.42 (64.63)	3.61 (3.84)	10.56 (10.77)	8.89 (9.10)	3.31	–
[Co(HL ¹)Cl ₂]	265	Light ochre	12.74 (12.95)	55.18 (55.39)	3.08 (3.29)	9.04 (9.23)	15.38 (15.60)	2.18	10.47
Ligand H ₂ L ² C ₂₁ H ₂₇ N ₃ O ₂	263	Light yellow	–	71.19 (71.38)	7.43 (7.64)	11.67 (11.89)	–	–	–
[Cu(H ₂ L ²) ₂ Cl ₂].2H ₂ O	248	Green	7.06 (7.24)	57.28 (57.49)	6.38 (6.61)	9.37 (9.58)	7.88 (8.10)	1.85	11.52
[Ni(H ₂ L ²) ₂ Cl ₂].4H ₂ O	242	Pale yellow	6.27 (6.46)	55.29 (55.52)	6.61 (6.83)	9.03 (9.25)	7.61 (7.82)	3.29	13.64

^a10⁻³ M solution in DMFFig. 1. The structural formulas of the ligands HL¹ and H₂L².¹H-NMR spectroscopy

Ligand HL¹. ¹H-NMR (300 MHz, DMSO-*d*₆, δ / ppm): 12.32 (1H, *s*, N₈-H), 9.68 (1H, *s*, C₁₀-H), 8.76 (2H, *d*, $J = 10.3$ Hz, C_{2,6}-H), 7.93 (2H, *d*, $J = 11.4$ Hz, C_{3,5}-H), 7.53–7.74 (8H, *m*, anthracene rings).

Ligand H_2L^2 . 1H -NMR (300 MHz, DMSO- d_6 , δ / ppm): 11.93 (1H, *s*, N_8 -H), 8.83 (2H, *d*, $J = 6.2$ Hz, $C_{2,6}$ -H), 8.40 (1H, *s*, C_{10} -H), 7.85 (2H, *d*, $J = 6.8$ Hz, $C_{3,5}$ -H), 1.41 (18H, *s*, $C_{13,15}$ -*t*-Bu).

The signal of the azomethine proton ($-N=CH-$) at δ 9.68 or 8.40 ppm in the 1H -NMR spectrum, as well as the peak at δ 148.38 or 149.31 ppm, assigned to the azomethine carbon in the ^{13}C -NMR spectrum, sustain the formation of the isonicotinoylhydrazone ligands.

IR spectroscopy

The characteristic frequencies for ligands HL^1 , H_2L^2 and their complexes are presented in Table II. In the IR spectrum of the 9-anthraldehyde isonicotinoyl hydrazone ligand (HL^1), the amide I band, $\nu(C=O)$, was present at 1656 cm^{-1} ,¹² and the absorption at 1597 cm^{-1} is ascribed to the $\nu(C=N)$ vibration, which is specific for the azomethine group.¹³ The low intensity band at 602 cm^{-1} corresponds to the in-plane “ β ” deformation vibration for the pyridine ring.¹⁴ The amide I valence vibration shifted to lower values in the Ni(II) and Co(II) complexes but it exhibited a positive shift in the Cu(II) complex, which support the coordination of only the $O=C$ amide oxygen to the Ni(II) and Co(II) ions.¹⁵ The absorption of the $\nu(C=N)$ azomethine group for all the complexes was situated at lower wave numbers than the value for the free ligand, consequently confirming the coordination of the azomethine nitrogen atom to the Cu(II), Ni(II) and Co(II) ions.¹⁶ The “ β ” deformation vibration corresponding to the pyridine ring did not suffer significant shifts in the spectra of complexes, suggesting that the nitrogen from the pyridine ring does not participate in the coordination.¹⁷ The coordination of the azomethine nitrogen of the HL^1 ligand to the Cu(II), Ni(II) and Co(II) ions was also proved by the $\nu(M-N)$ vibrations appearing in the range $485\text{--}419\text{ cm}^{-1}$,¹⁸ which were absent in the spectrum of the ligand. The IR spectrum of the 3,5-di-*tert*-butyl-4-hydroxybenzaldehyde isonicotinoyl hydrazone ligand (H_2L^2) had an absorption band at 3401 cm^{-1} , attributed to the $\nu(OH)$ valence vibration in the phenolic group. The amide I $\nu(C=O)$ vibration was situated at 1644 cm^{-1} and the band at 1593 cm^{-1} corresponds to the $\nu(C=N)$ vibration in the azomethine

TABLE II. Characteristic IR bands (cm^{-1}) for ligands HL^1 , H_2L^2 and their complexes

Compound	$\nu(NH)$	$\nu(C=O)$ Amide I	$\nu(C=N)$	$\delta(NH)$ Amide II	$\gamma(NH)$ Amide III	β ring pyridine in plane	$\nu(M-N)$
INHAA (HL^1)	3046	1656	1597	1552	1365	602	–
$[Cu(HL^1)_2Cl_2]$	3049	1663	1572	1554	1372	603	481
$[Ni(HL^1)_2Cl_2]$	3051	1641	1568	1517	1378	598	485
$[Co(HL^1)_2Cl_2]$	3050	1642	1583	1540	1367	601	419
INHDBHB (H_2L^2)	3019	1644	1593	1553	1359	590	–
$[Cu(H_2L^2)_2Cl_2] \cdot 2H_2O$	3043	1630	1580	1518	1366	575	498
$[Ni(H_2L^2)_2Cl_2] \cdot 4H_2O$	3041	1607	1575	1550	1364	585	476

group. The weak band at 590 cm^{-1} represents the in-plane “ β ” deformation vibration for the pyridine ring. In the spectra of the Cu(II) and Ni(II) complexes with the H_2L^2 ligand, the intense band at 3260 or 3205 cm^{-1} is attributed to the lattice water present in these complexes.¹⁹ The $\nu(\text{OH})$ valence vibration of the phenolic group appears in the spectra of the Cu(II) and Ni(II) complexes at 3392 and 3386 cm^{-1} , respectively, which reveals that the phenolic group is not deprotonated and is not coordinated to the metal ions. The amide I band and the azomethine vibration band suffered negative shifts in the spectra of the Cu(II) and Ni(II) complexes, suggesting the H_2L^2 ligand coordinated to the Cu(II) and Ni(II) ions *via* the O=C amide oxygen and azomethine nitrogen atoms. The band of the “ β ” deformation mode of the pyridine ring suffered shifts to lower values in comparison with that from the free ligand, meaning that the pyridine nitrogen did not participate in the coordination. The coordination of the H_2L^2 ligand to the Cu(II) and Ni(II) ions by the azomethine nitrogen is also supported by the $\nu(\text{M-N})$ vibration, appearing at 498 or 476 cm^{-1} , which was not found in the spectrum of the ligand.

Electronic and ESR spectra

In its electronic spectrum, the INHAA (HL^1) ligand presents an intense band at 25575 cm^{-1} , which can be assigned to a $n \rightarrow \pi^*$ transition. In the spectra of the complexes, this transition shifts to lower values, with $\Delta\nu$ 1766 – 884 cm^{-1} , indicating coordination of the ligand to the metal ions. The electronic spectrum of the INHDBHB (H_2L^2) ligand presents an absorption maximum at 27624 cm^{-1} due to a $n \rightarrow \pi^*$ transition in the C=O and C=N chromophoric groups. This transition was found in the spectra of the complexes but shifted to lower frequencies, indicating coordination of the ligand to the metal ions. Information regarding the geometry of the complexes was obtained from the electronic spectra and from the values of the magnetic moments.

The $[\text{Cu}(\text{HL}^1)_2\text{Cl}_2]$ complex presents in its reflectance spectrum a wide band at 12820 cm^{-1} characteristic of the ${}^2\text{T}_2 \rightarrow {}^2\text{E}$ transition, being specific for a Cu(II) ion in a tetrahedral environment. The value of the magnetic moment of $2.16\ \mu_{\text{B}}$ supports the proposed geometry.²⁰

The electronic spectrum of the $[\text{Ni}(\text{HL}^1)_2\text{Cl}_2]$ complex contains two absorption bands at 15948 and 10288 cm^{-1} , corresponding to the ${}^3\text{A}_{2\text{g}} \rightarrow {}^3\text{T}_{1\text{g}}(\text{F})$ (ν_2) and ${}^3\text{A}_{2\text{g}} \rightarrow {}^3\text{T}_{2\text{g}}(\text{F})$ (ν_1) transitions, respectively. These transitions suggest an octahedral stereochemistry for the Ni(II) ion, which is in accordance with the magnetic moment value of $3.31\ \mu_{\text{B}}$.²¹ The ratio ν_2/ν_1 is 1.55 , which is within the range for octahedral complexes of Ni(II). For this complex, the following parameters 10 Dq , B and β were obtained by calculation: $10\text{ Dq} = 10280\text{ cm}^{-1}$, $B = 679\text{ cm}^{-1}$, $\beta = 0.65$. The obtained value of the β parameter indicates a moderate to intense covalent character for the metal–ligands bonds.

In the reflectance spectrum of the $[\text{Co}(\text{HL}^1)\text{Cl}_2]$ complex, the two absorption bands at 21052 cm^{-1} and 16129 cm^{-1} were assigned to the ${}^2\text{A}_{1\text{g}} \rightarrow {}^2\text{E}_{\text{g}}$ and ${}^2\text{A}_{1\text{g}}$

→ ${}^2B_{2g}$, respectively. They are characteristic for square-planar stereochemistry of the Co(II) ion. The magnetic moment of $2.18 \mu_B$ supports this geometry for the low-spin Co(II).²²

The electronic spectrum of the $[Cu(H_2L^2)_2Cl_2] \cdot 2H_2O$ complex contains a wide band situated at approximately 15350 cm^{-1} . This band is characteristic for a Cu(II) ion with tetragonally distorted octahedral stereochemistry and can be assigned to the ${}^2E_g \rightarrow {}^2T_{2g}$ transition.²³ The magnetic moment of $1.85 \mu_B$ suggests a monomeric octahedral geometry.

For the $[Ni(H_2L^2)_2Cl_2] \cdot 4H_2O$ complex, two absorption bands at 15873 and 10256 cm^{-1} were registered in the electronic spectrum. These bands can be assigned to the ${}^3A_{2g} \rightarrow {}^3T_{1g}(F)$ (ν_2) and ${}^3A_{2g} \rightarrow {}^3T_{2g}(F)$ (ν_1) transitions and are specific for the Ni(II) ion in octahedral coordination, which was also confirmed by the magnetic moment of $3.29 \mu_B$. The ratio ν_2/ν_1 is 1.54 , which is within the range found for Ni(II) octahedral complexes. The absorption band associated with the ${}^3A_{2g} \rightarrow {}^3T_{1g}(P)$ (ν_3) transition is covered by the much higher intensity $n \rightarrow \pi^*$ transition characteristic of the ligand. For this complex, the following $10 Dq$, B and β parameters were determined: $10 Dq = 10256 \text{ cm}^{-1}$, $B = 671 \text{ cm}^{-1}$, $\beta = 0.66$. The value of the β parameter indicates a moderate to intense covalent character for the metal–ligands bonds.

The ESR spectrum of a polycrystalline sample of the $[Cu(HL^1)_2Cl_2]$ complex was recorded at room temperature. This complex exhibited a broad and intense slightly anisotropic signal, assigned to the Cu(II) ion in a slightly distorted tetrahedral environment.²⁴ The extremely high intensity of the ESR signal indicates a monomeric structure for the complex.

The ESR spectrum of the $[Cu(H_2L^2)_2Cl_2] \cdot 2H_2O$ complex was recorded on microcrystalline powder at room temperature. The high intensity of the signal confirms the monomeric molecular formula. An axial signal with two “ g ” values at 293 K ($g_{\parallel} = 2.1914$; $g_{\perp} = 2.0685$) was registered. The anisotropic shape of the spectrum with $g_{\parallel} > g_{\perp}$ indicates a compound with an axially distorted octahedral geometry. The g_{\parallel} and g_{\perp} values were > 2 , corresponding to an axial symmetry with all main axes disposed parallelly. The fact that $g_{\parallel} > g_{\perp} > 2.0023$ supports a ground state of the Cu(II) ion with the unpaired electron in the $d_{x^2-y^2}$ orbital and from the ESR spectrum there results an octahedral stereochemistry tetragonally distorted by elongation.²⁵ The G parameter determined with the formula $G = ((g_{\parallel} - 2)/(g_{\perp} - 2))$ was less than 4 and, consequently, there is considerable interaction in the solid state in this complex.

Thermal analysis

The thermal decomposition of the synthesized complexes was studied in the air in the range $25\text{--}700 \text{ }^\circ\text{C}$ and the results are listed in Table III.

For the Cu(II) and Ni(II) complexes with the H₂L² ligand, lattice water was lost between 80–170 °C. All complexes underwent decomposition at high temperatures ($t > 245$ °C) and the HL¹ and H₂L² ligands were eliminated in two stages. The stable residue at the final temperature (≈ 700 °C) contained CuO, NiO or Co₃O₄. The results obtained from the thermal analysis supported the molecular formulas assigned to the complexes.

The structural formulas assigned to the complexes are presented in Fig. 2.

TABLE III. Thermal analysis data of the prepared complexes

Complex	Total mass losses, %		Temperature, °C	Loss, %
	Theoretical	Experimental		
[Cu(HL ¹) ₂ Cl ₂]	89.80	89.54	250–385	39.68
			385–670	49.86
			670–700	9.89 exp./res. 10.13 calc./res.
[Ni(HL ¹) ₂ Cl ₂]	87.77	88.64	80–240	–
			240–365	49.23
			365–495	39.41
			495–700	9.72 exp./res. 9.58 calc./res.
[Co(HL ¹)Cl ₂]	82.29	82.40	257–405	67.12
			405–675	15.28
			675–700	17.42 exp./res. 17.64 calc./res.
[Cu(H ₂ L ²) ₂ Cl ₂].2H ₂ O	90.92	91.08	80–170	3.81
			170–375	32.33
			375–625	54.94
			625–700	8.91 exp./res. 9.07 calc./res.
[Ni(H ₂ L ²) ₂ Cl ₂].4H ₂ O	91.73	91.15	85–160	7.72
			160–370	65.93
			370–525	17.50
			525–700	8.06 exp./res.
				8.23 calc./res.

Antibacterial activity

The antibacterial activity of the HL¹, H₂L² ligands and of their complexes were studied on the Gram-(+) bacteria *Staphylococcus aureus* and on the Gram-(–) bacteria *Escherichia coli* and *Klebsiella pneumoniae*. The experimental data expressed as the diameter of the inhibition zone (in mm) of bacterial growth by the tested compounds are presented in Table IV.

The results show that HL¹ and H₂L² exhibited weak activity. The HL¹ ligand was slightly more active than the H₂L² ligand. Against the three bacterial agents, the Cu(II)/HL¹ complex was more active than the HL¹ ligand, while the Ni(II)/HL¹ and Co(II)/HL¹ complexes showed lower activity. The Cu(II)/H₂L² and

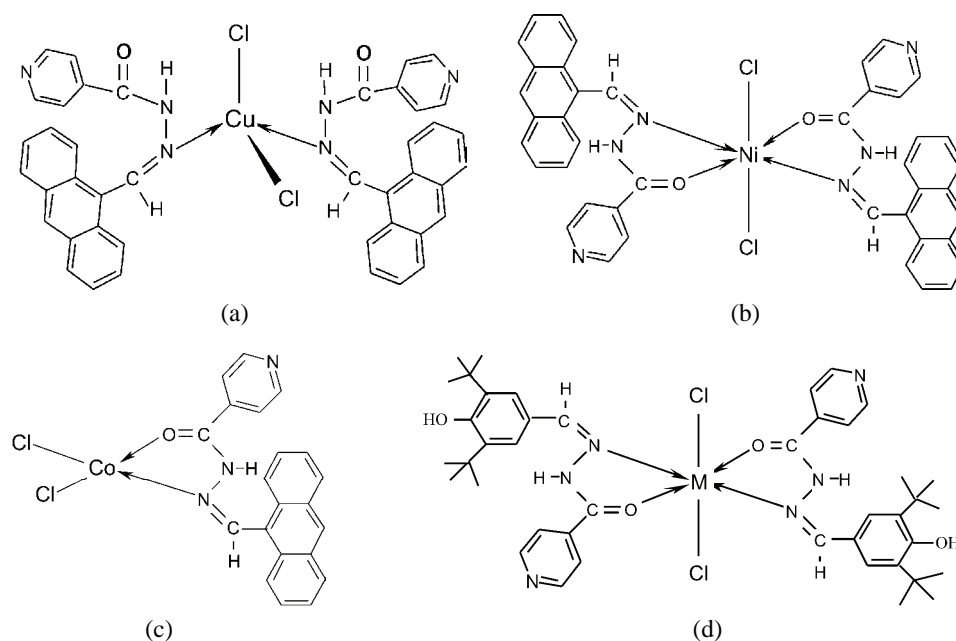


Fig. 2. The structural formulas of the complexes: a) $[\text{Cu}(\text{HL}^1)_2\text{Cl}_2]$, b) $[\text{Ni}(\text{HL}^1)_2\text{Cl}_2]$, c) $[\text{Co}(\text{HL}^1)\text{Cl}_2]$ and d) $[\text{M}(\text{H}_2\text{L}^2)_2\text{Cl}_2] \cdot x\text{H}_2\text{O}$ ($\text{M} = \text{Cu}(\text{II}): x = 2$; $\text{M} = \text{Ni}(\text{II}): x = 4$).

TABLE IV. Antibacterial activity data for 0.125 mg bacterium ml^{-1}

Compound	Inhibition zone of bacterial growth, mm		
	<i>Staphylococcus aureus</i>	<i>Escherichia coli</i>	<i>Klebsiella pneumoniae</i>
INHAA (HL^1)	6	4	5
$[\text{Cu}(\text{HL}^1)_2\text{Cl}_2]$	9	6	7
$[\text{Ni}(\text{HL}^1)_2\text{Cl}_2]$	2	3	2
$[\text{Co}(\text{HL}^1)\text{Cl}_2]$	3	2	2
INHDBHB (H_2L^2)	3	2	2
$[\text{Cu}(\text{H}_2\text{L}^2)_2\text{Cl}_2] \cdot 2\text{H}_2\text{O}$	5	6	4
$[\text{Ni}(\text{H}_2\text{L}^2)_2\text{Cl}_2] \cdot 4\text{H}_2\text{O}$	7	8	6

$\text{Ni}(\text{II})/\text{H}_2\text{L}^2$ complexes possessed a higher antibacterial activity than the free H_2L^2 ligand. The data in Table IV show that *S. aureus* was much more inhibited by the $\text{Cu}(\text{II})/\text{HL}^1$ complex, giving the opportunity for its use in medical practice. The increased activity of the chelates can be explained based on the overtone concept and the Tweedy chelation theory.²⁶ According to the overtone concept of cell permeability, the lipid membrane surrounding the cell favours the passage of only lipid-soluble materials, which means that liposolubility is an important factor controlling antimicrobial activity. On chelation, the polarity of a metal ion is greatly reduced due to overlap with the ligand orbital and the partial sharing of its

positive charge with the donor groups. In addition, it is also due to delocalization of the π -electrons over the whole chelate ring, thus enhancing the penetration of the complexes into the lipid membranes and the blocking of the metal binding sites of the enzymes of the micro-organisms.

CONCLUSIONS

The Cu(II), Ni(II) and Co(II) complexes with 9-anthraldehyde isonicotinoyl hydrazone (HL¹), as well as those of Cu(II) and Ni(II) with 3,5-di-*tert*-butyl-4-hydroxybenzaldehyde isonicotinoyl hydrazone (H₂L²) are described. They were synthesized by the template method and characterized by their analytical and spectral data. A tetrahedral geometry was assigned to the Cu(II)/HL¹ complex, a square-planar to the Co(II)/HL¹ complex and octahedral one to the Ni(II)/HL¹, Cu(II)/H₂L² and Ni(II)/H₂L² complexes. The Cu(II)/HL¹, Cu(II)/H₂L² and Ni(II)/H₂L² complexes demonstrated higher antibacterial activity than the corresponding free ligands.

ИЗВОД

ТЕМПЛАТНА СИНТЕЗА, КАРАКТЕРИЗАЦИЈА И АНТИМИКРОБНА АКТИВНОСТ НОВИХ КОМПЛЕКСА СА ИЗОНИКОТИНОИЛ-ХИДРАЗОНСКИМ ЛИГАНДИМА

LIVIU MITU¹, NATARAJAN RAMAN², ANGELA KRIZA³, NICOLAE STĂNICĂ⁴ и MARIANA DIANU³

¹University of Pitești, Faculty of Science, Department of Physics and Chemistry, Târgul din Vale 1, 110040, Pitești, Romania, ²Department of Chemistry, College VHNSN, Virudhunagar-626001, India, ³University of Bucharest, Faculty of Chemistry, Department of Inorganic Chemistry, Dumbrava Roșie 23, 020461, Bucharest u ⁴Romanian Academy, Institute of Physical Chemistry, "I. G. Murgulescu", Splaiul Independenței 202A, 060021, Bucharest, Romania

Темплатном методом синтетисани су комплекси Cu(II), Ni(II), и Co(II) са 9-антралдеhid-изоникотиноил-хидразонским (HL¹), као и 3,5'-ди-*терц*-бутил-4-хидроксибензалдеhid-изоникотиноил-хидразонским лигандом (H₂L²). Комплекси су окарактерисани аналитичким подацима, IR, UV-Vis, ESR спектрима, магнетним мерењима, кондуктометријом, термичком анализом и за два лиганда ¹H-NMR спектрима. Из елементалне анализе стехиометрија за комплексе Cu(II), Ni(II) са лигандима HL¹ и H₂L² је 1:2 (метал:лиганд), док је за комплекс Co(II) са HL¹ лигандом предложена 1:1 (метал:лиганд). Подаци моларне проводљивости указују да су комплекси неелектролити. Магнетна суспектибилност са електронским и ESR спектрима сугерише дисторговану октаедарску геометрију за комплексе Ni(II)/HL¹, Ni(II)/H₂L², Cu(II)/H₂L², тетраедарску стереохемију за комплекс Cu/HL¹ и квадратно-планарну геометрију за комплекс Co/HL¹. IR спектри показују бидентатну координацију лиганда HL¹, H₂L² преко O=C амидног кисеоника и азометинског азота, као и монодентатну координацију лиганда HL¹ помоћу азометинског азота у комплексу Cu(II). Тестирана је и нађена антибактеријска активност лиганда и њихових металних комплекса према *Staphylococcus aureus*, *Escherichia coli* и *Klebsiella pneumoniae*.

(Примљено 17. јануара, ревидирано 15. априла 2009)

REFERENCES

1. R. M. Issa, S. A. Abdel-Latif, H. A. Abdel-Salam, *Synth. React. Inorg. Met.-Org. Chem.* **31** (2001) 95
2. C. Z. Hussain, S. K. Aftab, *J. Chem. Soc. Pak.* **19** (1997) 196
3. B. N. Sivasankar, S. Gavindaragam, *Synth. React. Inorg. Met.-Org. Chem.* **25** (1995) 127
4. A. Ghaib, S. Menager, P. Verite, O. Lafont, *Farmaco* **57** (2002) 89
5. P. M. Gurubasavaraj, P. M. Veerasha, *Asian J. Chem.* **20** (2008) 2841
6. N. Nawar, N. M. Hosny, *Transition Met. Chem.* **25** (2000) 1
7. B. Zdzislaw, *Acta Pol. Pharm.* **54** (1997) 49
8. H. Kaur, S. K. Sangal, *Chim. Acta Turk.* **26** (1996) 123
9. L. Mitu, A. Kriza, M. Dianu, *Asian J. Chem.* **19** (2007) 5666
10. C. Gh. Macarovici, *Inorganic Quantitative Chemical Analysis*, Editura Academiei, Bucuresti, 1979, pp. 338, 364
11. S. K. Srivastava, K. A. Gupta, *Acta Chim. Hung.* **118** (1985) 255
12. R. S. Baligar, V. K. Revankar, *J. Serb. Chem. Soc.* **71** (2006) 1301
13. N. Raman, S. S. Ali Fathima, J. D. Raja, *J. Serb. Chem. Soc.* **73** (2008) 1063
14. B. V. Agarwala, P. S. Reddy, *Acta Chim. Hung.* **127** (1990) 269
15. V. K. Sharma, S. Srivastava, A. Srivastava, *Pol. J. Chem.* **80** (2006) 387
16. S. Tuna, E. Canpolat, M. Kaya, *Pol. J. Chem.* **80** (2006) 227
17. F. T. Greenaway, A. Pezeshk, A. Cordes, *Inorg. Chim. Acta* **93** (1984) 67
18. C. L. Peizhi, D. Xiaolan, Z. Bo, *Asian J. Chem.* **17** (2005) 969
19. T. L. Yang, W. W. Qin, *Pol. J. Chem.* **80** (2006) 1657
20. E. Canpolat, *Pol. J. Chem.* **79** (2005) 619
21. P. K. Singh, D. N. Kumar, *Spectrochim. Acta A* **64** (2006) 853
22. A. K. Singh, B. K. Puri, R. K. Rowley, *Indian J. Chem.* **27A** (1988) 430
23. R. K. Agarwal, S. Sharma, *Pol. J. Chem.* **67** (1993) 581
24. B. J. Hathaway, D. E. Billing, *Coord. Chem. Rev.* **5** (1970) 143
25. K. K. Narang, P. V. Singh, *Transition Met. Chem.* **21** (1996) 507
26. N. Raman, A. Kulandaisamy, C. Tungaraja, *Transition Met. Chem.* **29** (2004) 129.



J. Serb. Chem. Soc. 74 (10) 1085–1096 (2009)
JSCS–3902

Synthesis of ruthenium(II) carbonyl complexes with 2-monosubstituted and 1,2-disubstituted benzimidazoles

GANGA NAIK KRISHNAMURTHY^{1*} and NARASHIMAIAH SHASHIKALA²

¹Department of Chemistry, Sahyadri Science College (Autonomous), Kuvempu University, Shimoga 577 203, Karnataka and ²Department of Chemistry, Central College Campus, Bangalore University, Bangalore-560 001, Karnataka, India

(Received 16 January, revised 31 March 2009)

Abstract: The reaction of the polymeric carbonyl complex $[\text{RuCl}_2(\text{CO})_2]_x$ with 2-monosubstituted and 1,2-disubstituted benzimidazoles and 1,4-bis(benzimidazol-2-yl)benzene (L_9) in 2-methoxyethanol produces various coloured complexes of the formulae $[\text{Ru}(\text{CO})_2\text{Cl}_2(\text{L})_2] \cdot x\text{H}_2\text{O}$ ($\text{L} = 1-(o\text{-hydroxybenzyl})\text{-}2\text{-}(o\text{-hydroxyphenyl})\text{benzimidazole}$ (L_1), $1-(o\text{-hydroxyphenyl})\text{benzimidazole}$ (L_4), $1-(p\text{-hydroxyphenyl})\text{benzimidazole}$ (L_5), $1-(p\text{-chlorobenzyl})\text{-}2\text{-}p\text{-chlorophenylbenzimidazole}$ (L_7), $1\text{-}[1\text{-}(\text{dimethylamino})\text{benzyl}]\text{-}2\text{-}[1\text{-}(\text{dimethylamino})\text{phenyl}]\text{benzimidazole}$ (L_{10}), $x = 0$; $\text{L} = 2\text{-benzylbenzimidazole}$ (L_8), $1,4\text{-bis}(\text{benzimidazol-}2\text{-yl})\text{benzene}$ (L_9), $x = 2$; $\text{L} = 1-(o\text{-chlorobenzyl})\text{-}1-(o\text{-chlorophenyl})\text{benzimidazole}$ (L_6); $x = 3$), $[\text{Ru}(\text{CO})_2\text{Cl}(\text{L}_2)_3]\text{Cl} \cdot 3\text{H}_2\text{O}$ and $[\text{Ru}(\text{CO})_2(\text{L}_3)_4]\text{Cl}_2 \cdot 3\text{H}_2\text{O}$ ($\text{L}_2 = 1-(m\text{-hydroxybenzyl})\text{-}2-(m\text{-hydroxyphenyl})\text{benzimidazole}$; $\text{L}_3 = 1-(p\text{-hydroxybenzyl})\text{-}2-(p\text{-hydroxyphenyl})\text{benzimidazole}$). The complexes were characterized by elemental analysis, conductivity measurements, as well as infrared, electronic, ^1H - and ^{13}C -NMR spectral studies.

Keywords: carbonyl complexes; 2-mono and 1,2-disubstituted benzimidazoles; ruthenium(II) carbonyl complexes.

INTRODUCTION

Ruthenium exhibits dissimilar behaviour in forming complexes compared to the other platinum group metals. It exhibits variable oxidation states 0, +2, +3 and +4, as well as unusual oxidation states. Furthermore, the metal also shows different coordination numbers for the same oxidation state. The complexes of ruthenium are important due to their catalytic activity towards several reactions, such as polymerisation, photo-splitting of water, solar energy conversion,¹ hydroformylation,² isomerisation and other reactions involving organic substrates.^{3–5} Some of the complexes form adducts with dioxygen and dinitrogen and the study

* Corresponding author. E-mail: gkmaik_sahyadri@yahoo.co.in
doi: 10.2298/JSC0910085K

of the properties of such adducts was helpful in the understanding of the mechanism of oxygen metabolism and nitrogen fixation in biological systems.^{6,7}

Carbonyl complexes of ruthenium are important in the homogeneous catalysis of carbonylation and oxo reactions.⁸ Much of the knowledge concerning carbonyl complexes has come from the study of metal complexes in lower oxidation states,⁹ mainly due to the stabilization of these oxidation states by CO. Studies of carbonyl complexes of higher valent ruthenium in aqueous solutions are, however, scarce because of the hydrolytic tendency of the metal ion in aqueous solution.^{10,11} The synthesis of various carbonyl complexes by the passage of CO through a suspension of substituted N-heterocyclic complexes of ruthenium(II) was reported.¹² However, *in situ* reactions wherein CO generation occurs in a homogeneous medium are simpler and more effective. Reaction of $\text{RuCl}_3 \cdot \text{H}_2\text{O}$ with CO in acidic medium yields the octahedral species $[\text{RuCl}_5(\text{CO})]^{2-}$.¹² In view of the increased interest in oxygenation and carbonylation of ruthenium(II) complexes as new catalysts,^{13,14} the synthesis and characterization of carbonyl complexes of ruthenium(II) with various 2-monosubstituted and 1,2-disubstituted N-heterocycles are reported herein. The substituted benzimidazoles used for the synthesis of ruthenium(II) chlorocarbonyl complexes are: 1-(*o*-hydroxybenzyl)-2-(*o*-hydroxyphenyl)benzimidazole (L_1), 1-(*m*-hydroxybenzyl)-2-(*m*-hydroxyphenyl)benzimidazole (L_2), 1-(*p*-hydroxybenzyl)-2-(*p*-hydroxyphenyl)benzimidazole (L_3), 2-(*o*-hydroxyphenyl)benzimidazole (L_4), 2-(*p*-hydroxyphenyl)benzimidazole (L_5), 1-(*o*-chlorobenzyl)-1-(*o*-chlorophenyl)benzimidazole (L_6), 1-(*p*-chlorobenzyl)-2-(*p*-chlorophenyl)benzimidazole (L_7), 2-benzylbenzimidazole (L_8), 1,4-bis(benzimidazol-2-yl)benzene (L_9) and 1-[*p*-(dimethylamino)benzyl]-2-[*p*-(dimethylamino)phenyl]benzimidazole (L_{10}), Fig. 1.

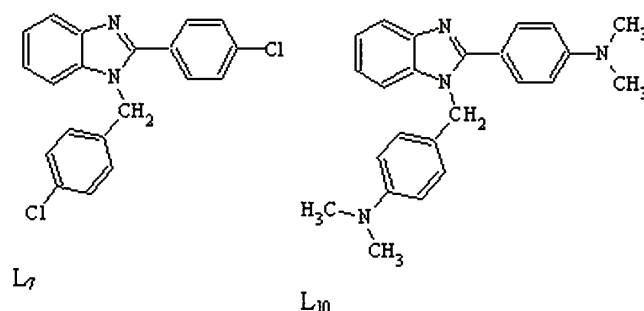


Fig. 1. Structures of the ligands 1-(*p*-chlorobenzyl)-2-(*p*-chlorophenyl)benzimidazole (L_7) and 1-[*p*-(dimethylamino)benzyl]-2-[*p*-(dimethylamino)phenyl]benzimidazole (L_{10}).

EXPERIMENTAL

Reagents

Hydrated ruthenium(II) chloride was purchased from Arora-Matthey. *o*-Phenylenediamine, salicylaldehyde, *m*-hydroxybenzaldehyde and *p*-hydroxybenzaldehyde were fine

chemicals from Merck/SD. The employed solvents were Merck chemicals, which were purified according to literature methods.¹⁵

Methods and instruments

The microanalyses of the carbon, hydrogen and nitrogen contents of the complexes were performed on a Carlo-Erba analyzer. The IR spectra (in nujol) were recorded on a Nicolet 4000D spectrophotometer. The molar conductivity measurements were made in dimethylformamide (DMF) using a digital conductivity meter-304 (SYSTRONICS) with a conventional dip type conductivity cell with a cell constant 1.00 cm⁻¹. The NMR spectra were recorded (in DMSO-*d*₆) on a Bruker WH-270 or AMX-400 MHz spectrometer using TMS as the internal standard. A Shimadzu UV-Vis-NIR Model UV-3101pc and a Hitachi-V3400 UV-visible-spectrophotometer were used for recording the electronic spectra of the solid samples as nujol-mull.

Preparation of the ligands

The ligands were prepared according to literature methods.¹⁶ A mixture of salicylaldehyde (0.20 mol) and *o*-phenylenediamine (0.10 mol) in the molar ratio of 2:1 in benzene was refluxed on a water bath for 1 h. The solution was cooled and left over night. After the evaporation of the solvent, a yellow solid separated out. This was filtered to obtain 1-(*o*-hydroxybenzyl)-2-(*o*-hydroxyphenyl)benzimidazole (L₁).

A similar procedure was followed for the preparation of the other ligands. A mixture of *m*-hydroxybenzaldehyde (0.20 mol) and *o*-phenylenediamine (0.10 mol) in benzene was refluxed for 1 h. After workup, a pale-yellow coloured compound, L₂, (yield: 90 %) was obtained.

A solution of *p*-hydroxybenzaldehyde (0.20 mol) and *o*-phenylenediamine (0.10 mol) in benzene was refluxed for 1 h. After workup, a pale-buff coloured compound, L₃, (yield: 60 %) was obtained.

To a solution of *o*-phenylenediamine (0.10 mol) in benzene (100 mL), a solution of *o*-chlorobenzaldehyde (0.20 mol) was added and the mixture was refluxed for 2 h on a steam bath. On standing over night, a yellow crystalline solid separated out, which was filtered to afford L₆ (yield: 80 %).

A solution of *o*-phenylenediamine (0.10 mol) and *p*-chlorobenzaldehyde (0.20 mol) in benzene (100 mL) was refluxed of 2 h on a steam bath. On standing over night, a yellow crystalline solid separated out, which was filtered to afford L₇ (yield: 70 %).

A mixture of *o*-phenylenediamine (0.10 mol) and *p*-(dimethylamino)benzaldehyde (0.20 mol) in benzene (100 mL) was refluxed for 2 h on a steam bath. On standing over night, a yellow crystalline solid, 1-[*p*-(dimethylamino)benzyl]-2-[*p*-(dimethylamino)phenyl]benzimidazole, (L₁₀), separated, which was recrystallized from ethanol to afford pale yellow crystals (yield: 80 %).

The ligand L₉ was prepared by refluxing *o*-phenylenediamine (20 mmol) and terephthalic acid (10 mmol) in syrupy phosphoric acid at 240 °C for 4 h. The coloured melt was poured into cold water (500 mL) under stirring, whereby a blue-green coloured precipitate was obtained. The precipitate was neutralized with 10 % aqueous sodium carbonate solution. The resulting solid was recovered by filtration and then recrystallized from ethanol to afford a pale pink-coloured compound (yield: 75 %).

Preparation of the complexes

The polymeric compound [Ru(CO)₂Cl₂]_x was prepared by reacting RuCl₃·3H₂O (1.0 mmol) with HCOOH (2.0 mmol). This was refluxed for 4–5 h, whereby the reaction mixture

turned lemon yellow. The resultant solution was cooled and evaporated slowly to obtain a yellow-coloured solid. To this, a solution of the ligand (2.0 mmol) in 2-methoxyethanol (10 mL) was added and the solution was refluxed for 4–5 h. After the evaporation of the solvent, distilled water (5.0 mL) was added, when a coloured compound separated out. The solid was filtered and washed with water and dried under vacuum (yield: 70–80 %).

RESULTS AND DISCUSSION

Synthesis and characterization

The complexes were soluble in common organic solvents. The molar conductance values of the complexes (Table I) in nitrobenzene indicated the uni-univalent and uni-bivalent nature of the $[\text{RuCl}(\text{CO})_2(\text{L}_2)_3]\text{Cl}\cdot 3\text{H}_2\text{O}$ and $[\text{Ru}(\text{CO})_2(\text{L}_3)_4]\text{Cl}_2\cdot 3\text{H}_2\text{O}$ complexes, respectively. All the other complexes showed non-electrolytic behaviour.

TABLE I. Physical properties and analytical data of the ruthenium(II) carbonyl complexes with substituted benzimidazoles

Complex	Colour	M.p. °C	Λ^a $\text{S cm}^2 \text{mol}^{-1}$	Anal. (Calcd.), %		
				C	H	N
$[\text{RuCl}_2(\text{CO})_2(\text{L}_1)_2]$	Brown	>250	0.60	58.77 (58.60)	4.35 (3.74)	6.01 (6.51)
$[\text{RuCl}(\text{CO})_2(\text{L}_2)_3]\text{Cl}\cdot 3\text{H}_2\text{O}$	Pale-green	144	27	60.42 (60.49)	4.46 (4.42)	6.70 (6.82)
$[\text{Ru}(\text{CO})_2(\text{L}_3)_4]\text{Cl}_2\cdot 3\text{H}_2\text{O}$	Grey	174	55	63.42 (63.64)	4.77 (4.69)	7.50 (7.23)
$[\text{RuCl}_2(\text{CO})_2(\text{L}_4)_2]$	Straw	194	7.5	51.62 (51.86)	4.00 (3.10)	9.03 (8.63)
$[\text{RuCl}_2(\text{CO})_2(\text{L}_5)_2]$	Straw	216	12	51.26 (51.86)	4.02 (3.10)	9.10 (8.63)
$[\text{RuCl}_2(\text{CO})_2(\text{L}_6)_2]\cdot 3\text{H}_2\text{O}$	Grey	>250	0.20	51.05 (51.03)	3.81 (3.67)	7.07 (5.67)
$[\text{Ru}(\text{CO})_2\text{Cl}_2(\text{L}_7)_2]$	Grey	>250	0.30	54.40 (53.98)	3.34 (3.02)	6.70 (5.99)
$[\text{RuCl}_2(\text{CO})_2(\text{L}_8)_2]\cdot 2\text{H}_2\text{O}$	Dark green	128	5.0	53.18 (52.94)	4.59 (4.14)	7.45 (8.23)
$[\text{RuCl}_2(\text{CO})_2(\text{L}_9)_2]\cdot 2\text{H}_2\text{O}$	Yellow	>280	2.5	57.50 (57.05)	3.66 (3.64)	12.36 (12.66)
$[\text{RuCl}_2(\text{CO})_2(\text{L}_{10})_2]$	Grey	186	0.20	62.10 (61.97)	5.64 (5.40)	10.36 (11.56)

^aMolar conductance of $\approx 10^{-3}$ M solution in nitrobenzene

Spectral studies

The infrared spectra (in nujol mull) of the complexes were similar to those of the uncoordinated ligands except for slight shifts in the positions of some of the bands and some changes in their intensities due to coordination (Tables II and III). In the spectrum of the $[\text{RuCl}_2(\text{CO})_2(\text{L}_8)_2]\cdot 2\text{H}_2\text{O}$ complex, bands due to the

$\nu(\text{OH})$ of hydration water and $\nu(\text{NH})$ of the ligand appeared at 3440 and 3190 cm^{-1} , respectively.^{17,18} The band due to $\nu(\text{OH})$ of lattice water molecules^{19,20} was observed around 3350 cm^{-1} in the carbonyl complexes of L_2 , L_3 and L_6 . The $\nu(\text{OH})$ of the ligands containing a phenolic OH group and their complexes appeared around 3200 cm^{-1} . Bands due to $\nu(\text{C}=\text{N})$ and $\nu(\text{C}=\text{C})$ vibrations occurred around 1620 cm^{-1} , very close to each other, as weak bands in the spectra of free heterocycles and they were shifted to lower or higher wave numbers by 5–10 cm^{-1} on complexation. These shifts in the positions of $\nu(\text{C}=\text{N})$ and $\nu(\text{C}=\text{C})$ indicate coordination of the substituted benzimidazoles *via* the tertiary nitrogen of the imidazole moiety.²¹ The spectra of the complexes of L_8 , L_4 , L_5 and L_9 exhibited the NH out-of-plane bending vibration at around 730 cm^{-1} . A weak band in the spectrum of $[\text{RuCl}_2(\text{CO})_2(\text{L}_{10})_2]$ at 1480 cm^{-1} is assigned to the N–CH₃ deformation mode. Another band at around 1320 cm^{-1} is attributed to C–N stretching of the N–CH₃ group.²² Medium intensity bands in the spectra of the complexes at around 1490, 1200, 1100, 720 and 540 cm^{-1} are assignable to the *o*-, *m*-, *p*-disubstituted benzene ring. In the spectra of the $[\text{RuCl}_2(\text{CO})_2(\text{L}_6)_2] \cdot 2\text{H}_2\text{O}$ and $[\text{RuCl}_2(\text{CO})_2(\text{L}_7)_2]$ complexes, a strong band around 760 cm^{-1} is assigned to the C–Cl stretching vibration.²³ Two intense bands at ≈ 1900 and ≈ 2000 cm^{-1} were observed in the spectra of all the complexes. These are attributed to $\nu(\text{CO})$ and the data suggest that the two carbonyl groups are placed in the *cis* position.^{19,20} In the case of the $[\text{Ru}(\text{CO})_2(\text{L}_8)_2] \cdot 2\text{H}_2\text{O}$ and $[\text{Ru}(\text{CO})_2\text{Cl}_2(\text{L}_1)_2]$ complexes, one of the two $\nu(\text{CO})$ peaks splits further and to give a weak band which may be due to a mixture of two isomers.

TABLE II. IR spectral data (cm^{-1}) of the ruthenium(II) carbonyl complexes

Compound	$\nu(\text{NH})$	$\nu(\text{O}-\text{H})$ of lattice H_2O	$\nu(\text{O}-\text{H})$ coordinated $\text{H}_2\text{O}/\text{ligand}$	$\nu(\text{C}=\text{O})$	$\nu(\text{C}=\text{N})$ and $\nu(\text{C}=\text{C})$	$\nu(\text{N}-\text{CH}_2)$	<i>o</i> -, <i>m</i> -, <i>p</i> - Disubstituted benzene
L_1	–	–	–	–	1616 _s	1590 _s	1491 _m , 1057 _m , 740 _m , 540 _w
$[\text{Ru}(\text{CO})_2\text{Cl}_2(\text{L}_1)_2]$	–	–	3190 _{br}	2055 _s 1988 _s 1936 _s	1610 _s	1600 _s	1496 _m , 1052 _m , 748 _m
$[\text{Ru}(\text{CO})_2\text{Cl}(\text{L}_2)_3]\text{Cl} \cdot 3\text{H}_2\text{O}$	–	3320 _{br}	3178 _{br}	2040 1962	1624 _s	1590 _s	1310 _s , 1150 _s , 726 _{ms}
L_4	3170 <i>br</i>	–	3230 _w	–	1616 _s	–	1243 _w , 1090 _w , 722 _s

TABLE II. Continued

Compound	$\nu(\text{NH})$	$\nu(\text{O-H})$ of lattice H_2O	$\nu(\text{O-H})$ coordinated $\text{H}_2\text{O}/\text{ligand}$	$\nu(\text{C=O})$	$\nu(\text{C=N})$ and $\nu(\text{C=C})$	$\nu(\text{N-CH}_2)$	<i>o</i> -, <i>m</i> -, <i>p</i> - Disubstituted benzene
$[\text{Ru}(\text{CO})_2\text{Cl}_2(\text{L}_4)_2]$	3178 <i>br</i>	—	3238 w	2045 s 1967 s	1626 s	—	1243 s , 1093 w , 726 s
L_5	3160 <i>br</i>	—	3203 w	—	1616 s	—	1253 s , 1010 s , 736 m
$[\text{Ru}(\text{CO})_2\text{Cl}_2(\text{L}_5)_2]$	3166 <i>br</i>	—	3172 b	2034 s 1962 s	1605 s	—	1233 w , 1020 w , 730 m
L_8	3180 <i>br</i>	—	—	—	1600 s	1558 w	1108 w , 720 s , 548 s
$[\text{RuCl}_2(\text{CO})_2(\text{L}_8)_2] \cdot 2\text{H}_2\text{O}$	3190 <i>br</i>	3440 br	—	2034 s 2064 s 1988	1605 s	1554 w	1103 s , 731 s , 545 w
L_9	3150 <i>br</i>	—	—	—	1626 s	—	1226 s , 1090 s , 742 s , 540 w
$\text{Ru}(\text{CO})_2\text{Cl}_2(\text{L}_9)_2 \cdot 2\text{H}_2\text{O}$	3170 <i>br</i>	3400 br	—	2045 s 1962 s	1631 s	—	1220 s , 1090 s , 747 s , 529 w

TABLE III. IR spectral data (cm^{-1}) of the ruthenium(II) carbonyl complexes

Compound	$\nu^{\text{Coordinated}}$ lattice H_2O	$\nu(\text{OH/NH})$	$\nu(\text{C=O})$	$\nu(\text{C=C})$ and $\nu(\text{C=N})$	$\nu(\text{N-CH}_2)$	<i>o</i> -, <i>m</i> -, <i>p</i> -Substituted benzene
L_3	—	3260	—	1610 s	1594 s	1468 b , 1181 m , 1114 s , 752 m
$[\text{Ru}(\text{CO})_2(\text{L}_3)_4]\text{Cl}_2 \cdot 3\text{H}_2\text{O}$	3358 br	3198 br	2049 s 1972 s	1621 s	1600 s	1476 s , 1279 s , 1186 m , 726 s
L_{10}	—	—	—	1616 s	1590 s	1470 s , 1180 m
$[\text{Ru}(\text{CO})_2\text{Cl}_2(\text{L}_{10})_2]$	—	—	2050 s 1962 s	1610 s	1595 s	1455 s , 1171 s , 750 s , 653 s
L_6	—	—	—	1616 s	1590 s	1438 s , 1196 m , 788 s
$[\text{Ru}(\text{CO})_2\text{Cl}_2(\text{L}_6)_2] \cdot 3\text{H}_2\text{O}$	3369 s	—	2055 s 1983 s	1600 s	1584 s	1450 s , 1190 s , 780 s
L_7	—	—	—	1600 w	1590 s	1460 s , 1220 s , 1192 s , 780 s
$[\text{Ru}(\text{CO})_2\text{Cl}_2(\text{L}_7)_2]$	—	—	2052 s 1982 s	1616 s	1588 s	1464 s , 1234 s , 1198 s , 786 s

The electronic spectra of the complexes (recorded as solids in nujol) were recorded and the spectral data are listed in Table IV. The bands observed around 17700 and 25000 cm^{-1} are assigned to the transitions ${}^1A_{1g} \rightarrow {}^1T_{1g}$ and ${}^1A_{1g} \rightarrow {}^1T_{2g}$, respectively, based on the earlier assignments.^{24–27} A strong band observed around 34000 cm^{-1} is assigned to the charge transfer transition.

TABLE IV. Electronic spectral data (cm^{-1}) of the ruthenium (II) carbonyl complexes

Compound	Electronic transitions and assignments		
	$\pi \rightarrow \pi^*$	${}^1A_{1g} \rightarrow {}^1T_{2g}$	${}^1A_{1g} \rightarrow {}^1T_{1g}$
[Ru(CO) ₂ (L ₉) ₂ Cl ₂] \cdot 2H ₂ O	28570	25640	–
[Ru(CO) ₂ (L ₁) ₂ Cl ₂]	32786	27780	12500
[Ru(CO) ₂ Cl(L ₂) ₃]Cl \cdot 3H ₂ O	–	27027	20000
[Ru(CO) ₂ (L ₃) ₄]Cl ₂ \cdot 3H ₂ O	31250	25974	–
[Ru(CO) ₂ (L ₄) ₂ Cl ₂]	30300	26310	–
[Ru(CO) ₂ (L ₅) ₂ Cl ₂]	38460	29410	–
[Ru(CO) ₂ (L ₆) ₂ Cl ₂] \cdot 3H ₂ O	–	26500	17500
[Ru(CO) ₂ (L ₇) ₂ Cl ₂]	34722	31250	27780
[Ru(CO) ₂ (L ₈) ₂ Cl ₂] \cdot 2H ₂ O	–	26310	16950
[RuCl ₂ (CO) ₂ (L ₁₀) ₂]	26450	20490	12500

The ${}^1\text{H-NMR}$ spectra of the free ligands and their complexes were recorded in DMSO-*d*₆ and the spectra of the complexes displayed features similar to those of the ligands (Tables Va and Vb), suggesting their close similarity with the free ligands. The resonance due to the hydroxyl proton in the complexes of L₄ and L₅ was observed at δ 7.83 and 10.00 ppm, respectively, while the resonance due to the imine proton appeared in the range 12.65–13.45 ppm. In the complexes of L₁, the signal due to the OH protons of the benzyl group was found at 10.72 ppm, while it was found at around 9.7 ppm in the complexes of L₂ and L₃. The signal due to hydroxyl protons of the phenylene ring in the [RuCl₂(CO)₂(L₁)₂] complex was observed at 10.26 ppm and it appeared at around 9.72 ppm in the complexes of L₂ and L₃. The spectra of L₉ and its complexes showed a resonance around 13.5 ppm, due to the imine proton. In the complex [RuCl₂(CO)₂(L₁₀)₂], the signals due to the $-\text{CH}_3$ protons of the benzyl and phenylene groups were observed at around 2.90 and 2.80 ppm, respectively. The methylene proton resonances are found in the range 5.40–7.30 ppm in the carbonyl complexes of 1,2-disubstituted benzimidazoles. The proton signals of the benzyl ring in all the 1,2-disubstituted benzimidazole carbonyl complexes were found in the range 6.40–7.90 ppm, while those due to the phenylene protons were observed in the range 7.10–7.95 ppm. Furthermore, the resonances due to the $-\text{CH}_2-$ protons shifted by 0.15–0.40 ppm. The coordination induced larger shifts at positions 4 and 6' because of polarization of the electron density towards the metal ion after complexation.²⁸ The coordination-induced shifts (c.i.s.) for various protons of the coordinated N-heterocycles were either positive or negative, which indicates that M \rightarrow L (σ^-) or L \rightarrow M

(π -) electron transfer occurs. A similar observation was made earlier for the spectra of related complexes.^{21,29–32}

TABLE Va. ¹H-NMR spectral data (δ / ppm) of the ruthenium(II) carbonyl complexes (the values in the parentheses are coordination induced shifts (c.i.s.) = $\delta_{\text{complex}} - \delta_{\text{ligand}}$)

Compound	2''	6'	4	7	CH ₂	O–H _b	O–H _p	N–H
L ₁	–	7.39 <i>m</i>	7.71 <i>d</i>	7.39 <i>m</i>	5.42 <i>s</i>	9.90 <i>s</i>	9.90 <i>s</i>	–
[RuCl ₂ (CO) ₂ (L ₁) ₂]	–	7.44 <i>m</i> (0.05)	7.74 <i>m</i> (0.03)	1.74 <i>m</i> (0.35)	5.66 <i>m</i> (0.24)	10.72 <i>s</i> (0.82)	10.26 <i>s</i> (0.36)	–
L ₂	6.47 <i>s</i>	7.09 <i>m</i>	7.72 <i>m</i>	7.23 <i>m</i>	5.48 <i>s</i>	9.62 <i>s</i>	9.62 <i>s</i>	–
[Ru(CO) ₂ Cl(L ₂) ₃]Cl·3H ₂ O	7.16 <i>s</i> (0.69)	6.92 <i>d</i> (–0.17)	7.71 <i>d</i> (–0.01)	7.71 <i>d</i> (0.48)	5.48 <i>s</i> (0.0)	9.44 <i>m</i> (–0.18)	9.75 <i>s</i> (0.16)	–
L ₃	6.83	7.41	7.64	7.56	5.41 <i>s</i>	9.40 <i>s</i>	9.6 <i>s</i>	–
[Ru(CO) ₂ (L ₃) ₄]Cl ₂ ·3H ₂ O	6.84 (0.01)	7.40 (–0.01)	7.65 (0.01)	7.57 (0.01)	5.44 <i>s</i>	9.72 <i>b</i> (0.32)	9.72 <i>b</i> (–0.24)	–
L ₄	–	7.65 <i>d</i>	8.05 <i>d</i>	8.05 <i>d</i>	–	–	7.38 <i>s</i>	13.15 <i>s</i>
[Ru(CO) ₂ (L ₄) ₂ Cl ₂]	–	6.15 <i>d</i> (–1.50)	8.20 <i>d</i> (0.15)	7.67 <i>d</i> (–0.38)	–	–	7.83 <i>s</i> (0.45)	13.57 <i>s</i> (0.47)
L ₅	–	7.14 <i>m</i>	8.03 <i>d</i>	8.03 <i>d</i>	–	–	10.00 <i>s</i>	12.65
Ru(CO) ₂ (L ₅) ₂ Cl ₂]	–	7.17 <i>m</i> (0.03)	8.01 <i>d</i> (–0.02)	8.01 <i>d</i> (–0.02)	–	–	10.00 (0.0)	13.42 <i>s</i> (0.77)
L ₆	–	7.52 <i>d</i>	7.92 <i>m</i>	7.42 <i>d</i>	5.43 <i>s</i>	–	–	–
[Ru(CO) ₂ Cl ₂ (L ₆) ₂]·3H ₂ O	–	7.23 <i>d</i> (–0.29)	7.76 <i>d</i> (–0.16)	7.51 <i>d</i> (0.09)	5.42 <i>s</i> (–0.01)	–	–	–
L ₇	7.65 <i>m</i>	7.93 <i>m</i>	8.00 <i>d</i>	8.00 <i>d</i>	7.23 <i>d</i>	–	–	–
[Ru(CO) ₂ (L ₆) ₂ Cl ₂]	7.27 <i>m</i> (–0.38)	7.63 <i>m</i> (–0.30)	8.19 <i>d</i> (0.19)	8.19 <i>d</i> (0.19)	7.27 <i>m</i> (0.04)	–	–	–

TABLE Vb. ¹H-NMR spectral data (δ / ppm) of the ruthenium(II) carbonyl complexes (the values in the parentheses are coordination induced shifts (c.i.s.) = $\delta_{\text{complex}} - \delta_{\text{ligand}}$)

Compound	2''	3''	5''	6''	6'	4	CH ₂	N–H	2	Benzyl CH ₃	Phenyl CH ₃
L ₈	–	–	–	–	7.17 <i>q</i>	7.52 <i>m</i>	5.73 <i>s</i>	–	7.52 <i>m</i>	–	–
[Ru(CO) ₂ Cl ₂ (L ₈) ₂]·2H ₂ O	–	–	–	–	7.44 <i>m</i> (0.27)	7.80 <i>d</i> (0.28)	5.64 <i>d</i> (–0.09)	–	7.80 (–0.28)	–	–
L ₉	–	–	–	–	7.25 <i>m</i>	7.69 <i>d</i>	8.35 <i>s</i>	13.5 <i>s</i>	–	–	–
[Ru(CO) ₂ Cl ₂ (L ₉) ₂]·2H ₂ O	–	–	–	–	7.27 <i>m</i> (0.02)	7.66 <i>m</i> (–0.03)	8.38 <i>t</i> (0.03)	13.84 <i>m</i> (0.34)	–	–	–
L ₁₀	6.63 <i>t</i>	6.88 <i>d</i>	6.88 <i>d</i>	6.63 <i>t</i>	7.61 <i>m</i>	7.99 <i>d</i>	5.42 <i>s</i>	–	–	2.99 <i>s</i>	2.89 <i>s</i>
Ru(CO) ₂ Cl ₂ (L ₁₀)	6.91 <i>d</i> (0.28)	6.83 <i>d</i> (–0.05)	6.83 <i>d</i> (–0.05)	6.58 (–0.08)	7.23 <i>m</i> (–0.38)	7.15 <i>d</i> (–0.84)	4.70 <i>s</i> (–0.72)	–	–	2.83 <i>m</i> (–0.16)	2.77 <i>m</i> (–0.12)

The ¹³C-NMR spectral data of the free ligands and their complexes are tabulated in Table VI. The spectra of the complexes show resonances in the regions that are in agreement with those expected based on the carbon environments. The resonance at δ 47.20 ppm was assigned to the N–CH₃ carbon in the L₁₀ complex.

In the complexes of L₄ and L₅, the signal due to C–OH was found at 129.00 and 118.99 ppm, respectively. The resonance due to C–OH of the benzyl group of the L₁ complex was found at 110.50 ppm, while in the complexes of L₂ and L₃, it was observed at 153.30 and 156.60 ppm, respectively. The resonance of phenylene C–OH of L₁ appeared at 161.73 ppm and in the complexes of L₂ and L₃ at 157.64 and 158.87 ppm, respectively. The resonance of the CH₂ carbon occurred near 47.00 ppm in the L₂ and L₃ complexes. In the case of the [RuCl₂(CO)₂(L₉)₂] complex, the resonance signal due to the benzimidazole ring occurred in the range 112.15–150.0 ppm. In the [RuCl₂(CO)₂(L₈)₂]·2H₂O complex, the signals for C-4, 8, 9 and 1' were shifted to a greater extent and, therefore, have higher c.i.s. values. The resonance due to the CH₂ carbon was observed at 57.88 ppm. The resonance signal in the region 190–200 ppm was observed in all the complexes, which indicates the presence of coordinated carbonyl groups.

TABLE VI. ¹³C-NMR spectral data (δ / ppm) of the ruthenium(II) carbonyls with substituted benzimidazoles (the values in the parentheses are coordination induced shifts (c.i.s.) = $\delta_{\text{complex}} - \delta_{\text{ligand}}$)

Compound	CO	1''	1'	6'	4	8	9	2	CH ₂
L ₁	–	120.37 _s	120.37 _s	127.86 _s	136.66 _s	140.50 _s	146.98	157.33 _d	65.04 _s
[RuCl ₂ (CO) ₂ (L ₁) ₂]	190.6 _s	120.30 _s	120.30 _s	127.16 _s	137.45	140.48 _s	146.96 _s	157.56 _s	65.04 _s
		(–0.07)	(–0.07)	(–0.70)	(–0.21) _s	(–0.02)	(–0.02)	(–0.23)	(0.0)
L ₂	–	116.97 _s	116.97 _s	122.19 _s	131.23 _s	135.90 _s	138.33 _s	142.64 _s	47.48 _s
[Ru(CO) ₂ Cl(L ₂) ₃]Cl·3H ₂ O	199.0 _s	116.94 _s	116.91 _s	122.13 _d	131.20 _s	135.91 _s	138.34 _s	142.6 _s	47.90 _s
		(–0.03)	(–0.06)	(–0.06)	(–0.03)	(0.01)	(–0.04)	(–0.04)	(0.42)
L ₃	–	120.85	127.11 _s	115.53 _s	127.49 _s	135.87 _s	142.80 _s	153.50 _s	47.30 _s
[Ru(CO) ₂ (L ₃) ₄]Cl ₂ ·3H ₂ O	194.35 _d	120.87	129.27	115.56	127.59 _t	135.88 _s	142.76 _s	153.65 _s	47.12 _s
		(0.02)	(2.16)	(0.03)	(0.10)	(0.01)	(–0.04)	(0.05)	(–0.18)
L ₄	–	112.66 _s	–	117.18 _s	126.23 _s	131.67 _s	131.67 _s	158.09 _s	–
[Ru(CO) ₂ (L ₄) ₂ Cl ₂]	190.10 _s	109.54 _s	–	114.15 _s	131.89 _s	134.56 _s	134.56 _s	157.34 _s	–
		(–3.12)		(–3.03)	(5.66)	(2.86)	(2.86)	(–0.75)	
L ₅	–	114.63 _s	–	115.73 _s	128.21 _s	121.69	121.16 _s	159.18 _s	–
[RuCl ₂ (CO) ₂ (L ₅) ₂]	190.10 _s	114.47 _s	–	116.41 _s	129.98 _s	124.90 _s	124.90 _s	161.95 _s	–
		(–0.16)		(–0.68)	(1.77)	(3.21)	(3.74)	(2.77)	
L ₆	–	123.07 _s	129.67 _s	130.33 _s	132.06 _d	131.14 _s	139.03 _s	142.54 _s	46.14 _s
[Ru(CO) ₂ (L ₆) ₂ Cl ₂]·3H ₂ O	199.0 _s	118.64 _s	123.79 _s	128.00 _s	132.18 _s	130.66 _s	139.02 _s	142.36 _s	47.15 _s
		(–4.43)	(–5.88)	(–2.33)	(0.12)	(0.48)	(–0.01)	(–0.18)	(1.01)
L ₇	–	136.38 _s	142.94 _s	134.35 _m	147.94 _s	155.45 _s	171.79 _s	157.35 _d	54.17 _s
[Ru(CO) ₂ (L ₇) ₂ Cl ₂]	198.5 _s	133.49 _s	134.29 _s	125.58 _s	138.08 _s	149.76 _s	168.32 _s	149.76 _s	58.18 _s
		(–2.89)	(–8.65)	(–9.77)	(–9.86)	(–5.69)	(–3.47)	(–7.59)	(–4.01)
L ₈	–	115.12 _s	121.81 _s	128.81 _d	128.00 _s	153.49 _s	137.22 _s	61.23	
[[Ru(CO) ₂ (L ₈) ₂ Cl ₂]·2H ₂ O	201.0 _s	–	118.49 _s	122.18 _m	128.28 _s	153.2 _s	126.52 _d	57.88 _s	
			(3.38)	(0.37)	(–0.53)	(0.28)	(–0.29)	(–10.70)	(3.35)
L ₉	CO	–	131.19 _s	126.92 _s	111.41 _s	143.91 _s	131.19 _s	143.94 _s	–
[Ru(CO) ₂ Cl ₂ (L ₉) ₂]·2H ₂ O	200.0 _s	–	130.58 _s	127.22 _s	112.15 _s	138.4 _m	133.69 _s	150.15 _s	–
			(–0.61)	(0.30)	(0.74)	(–5.53)	(2.50)	(6.21)	
L ₁₀	–	115.84 _s	126.78 _s	125.84 _s	123.73 _s	131.83 _s	138.36 _s	154.39 _s	47.50 _s
[Ru(CO) ₂ (L ₁₀) ₂ Cl ₂]	199.5 _s	114.50 _s	128.33 _s	129.10 _s	123.69 _s	135.06 _s	137.9 _s	152.6 _s	47.20 _s
		(–1.34)	(1.55)	(4.74)	(–0.13)	(3.17)	(–0.6)	(–1.79)	(–0.30)

Stereochemistry

As discussed above, the analytical, infrared, electronic, ^1H - and ^{13}C -NMR data indicate coordination of the ligands to the metal ion. The dicarbonyl complexes show two intense CO stretching bands around 2000 cm^{-1} in the infrared spectra suggesting that the two carbonyl groups are in the *cis* position. In the cases of the $[\text{RuCl}_2(\text{CO})_2(\text{L}_8)_2] \cdot 2\text{H}_2\text{O}$ and $[\text{Ru}(\text{CO})_2\text{Cl}_2(\text{L}_1)_2]$ complexes, the spectra showed an additional, comparatively weak band, which is due to the presence of the *cis-trans* isomer. Furthermore, as the ruthenium(II) is in the low spin d^6 configuration and is diamagnetic, two bands are expected at 21000 and 25000 cm^{-1} for octahedral geometry. Similar to this, the discussed complexes also exhibited bands at around 17700 and 25000 cm^{-1} , which were assigned to the transitions: $^1\text{A}_{1g} \rightarrow ^1\text{T}_{1g}$ and $^1\text{A}_{1g} \rightarrow ^1\text{T}_{2g}$, respectively. In addition, the coordination environment around the metal ion in all the complexes were not symmetrical. Therefore, it is suggested they have distorted octahedral geometry, which makes *fac*-isomers impossible. The coordination of the benzimidazole ligands occurred through the tertiary nitrogen. The following are the five possible structures for the complexes and the complex may exist in one of these structures (Fig. 2).

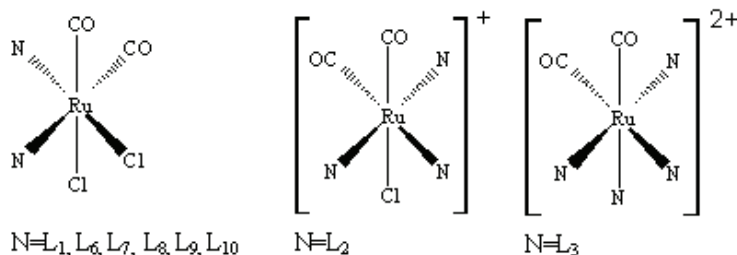


Fig. 2. The possible geometry of the complexes.

Acknowledgements. The authors are thankful to Professor D. N. Sathyanarayana, Indian Institute of Science, Bangalore, India and the authorities of the Central Drug Research Institute, Lucknow, India, for CHN analyses and the authorities of the Sophisticated Instrumentation Facility, Indian Institute of Science, Bangalore, for recording the NMR spectra. The authors are also thankful to UGC-DRS and FIST programme for financial assistance.

ИЗВОД

СИНТЕЗА РУТЕНИЈУМ(II) КАРБОНИЛ КОМПЛЕКСА СА 2-МОНОСУПСТИТУИСАНИМ И 1,2-ДИСУПСТИТУИСАНИМ БЕНЗИМИДАЗОЛИМА

GANGA NAIK KRISHNAMURTHY¹ и NARASHIMAIAH SHASHIKALA²

¹Department of Chemistry, Sahyadri Science College (Autonomous), Kuvempu University, Shimoga 577 203, Karnataka и ²Department of Chemistry, Central College Campus, Bangalore University,

Bangalore-560 001, Karnataka, India

Реакција полимерног карбонилног комплекса $[\text{RuCl}_2(\text{CO})_2]_x$ са 2-моносупституисаним и 1,2-дисупституисаним бензимидазолима и 1,4-бис(бензимидазол-2-ил)бенzenом (L_6) у 2-ме-

токсичности етанолу даје различито обојене комплексе формуле $[\text{Ru}(\text{CO})_2\text{Cl}_2(\text{L})_2] \cdot x\text{H}_2\text{O}$ ($\text{L} = 1$ -(*o*-хидроксибензил)-2-(*o*-хидроксифенил)бензимидазол (L_1), 1-(*o*-хидроксифенил)бензимидазол (L_4), 1-(*p*-хидроксифенил)бензимидазол (L_5), 1-(*p*-хлоробензил)-2-(*p*-хлорофенил)бензимидазол (L_7), 1-[*p*-(диметиламино)бензил]-2-[*p*-(диметиламино)фенил]бензимидазол (L_{10}), $x = 0$; $\text{L} = 2$ -бензилбензимидазол (L_8), 1,4-бис(бензимидазол-2-ил)бензен (L_9), $x = 2$; $\text{L} = 1$ -(*o*-хлоробензил)-1-(*o*-хлорофенил)бензимидазол (L_6); $x = 3$) $[\text{Ru}(\text{CO})_2\text{Cl}(\text{L}_2)_3]\text{Cl} \cdot 3\text{H}_2\text{O}$ и $[\text{Ru}(\text{CO})_2(\text{L}_3)_4]\text{Cl}_2 \cdot 3\text{H}_2\text{O}$ ($\text{L}_2 = 1$ -(*m*-хидроксибензил)-2-(*m*-хидроксифенил)бензимидазол; $\text{L}_3 = 1$ -(*p*-хидроксибензил)-2-(*p*-хидроксифенил)бензимидазол). Комплекси су окарактерисани елементалном анализом, мерењем проводљивости, IR, електронским, ^1H - и ^{13}C -NMR спектралним проучавањима.

(Примљено 16. јануара, ревидирано 31. марта 2009)

REFERENCES

1. N. E. Leadbeater, K. A. Scott, L. J. Scott, *J. Org. Chem.* **65** (2000) 3231
2. P. Kalck, J. Frances, P. Fister, T. G. Southern, A. Thorez, *J. Chem. Soc. Chem. Commun.* (1983) 510
3. E. G. Leelamani, N. M. Nanje Gowda, V. Gayathri, G. K. N. Reddy, *Recent Advances in Catalysis and Catalytic Reaction Engineering*, RRL, CSIR, Hyderabad, 1986
4. R. Uson, J. Gimano, L. A. Oro, M. Valderrama, R. Sariego, E. Martinez, *Transition Met. Chem.* **6** (1981) 103
5. N. H. Li, J. M. J. Frenchet, *J. Chem. Soc. Chem. Commun.* **16** (1985) 1100
6. R. S. Drago, *Coord. Chem. Rev.* **117** (1992) 185
7. M. Frigerio, M. Santagostino, S. Sputore, G. Palamisano, *J. Org. Chem.* **60** (1965) 727
8. G. S. Fink, G. F. Schmidt, *J. Mol. Catal.* **42** (1987) 361
9. M. Schroder, T. A. Stephenson, *Comprehensive Coordination Chemistry*, G. Wilkinson, Ed., Pergamon Press, New York, 1987, Vol. 4, p. 277
10. M. M. Taquikhan, G. Ramachandraiah, R. S. Shukla, *Inorg. Chem.* **27** (1988) 3274
11. M. M. Taquikhan, A. Hussain, K. Venkatasubramanian, G. Ramachandraiah, V. Oomen, *J. Mol. Catal.* **44** (1988) 117
12. J. Halpen, B. R. James, A. L. W. Kemp, *J. Am. Chem. Soc.* **88** (1996) 5142
13. M. M. Taquikhan, C. Sreelatha, S. A. Mirza, G. Ramachandraiah, S. H. R. Abdi, *Inorg. Chim. Acta* **154** (1988) 103
14. I. W. Hein, R. I. Arhum, J. J. Liquitt, *J. Am. Chem. Soc.* **79** (1957) 427
15. D. D. Perrin, W. L. F. Armarego, D. R. Perrin, *Purification of Laboratory Chemicals*, Pergamon Press, Oxford, 1966
16. N. V. Subba Rao, C. V. Ratnam, *Curr. Sci.* **24** (1955) 174
17. K. Takahashi, Y. Nishida, S. Kida, *Polyhedron* **3** (1984) 113
18. J. Tamm, H. J. Eggers, R. Batalannian, A. P. Wanger, K. Folkers, *Nature* **223** (1969) 785
19. K. Nakanishi, P. H. Solomon, *Infrared Absorption Spectroscopy*, Holden-Day Inc., Sydney, 1977
20. K. Nakamoto, *Infrared and Raman Spectra of Inorganic and Coordination Compounds*, 3rd ed., John Wiley, New York, 1978
21. G. Krishnamurthy, N. Shashikala, *J. Chem. Res.* **2006** (2006) 766
22. G. K. N. Reddy, B. R. Ramesh, *Indian J. Chem. A* **15** (1977) 621
23. L. J. Bellamy, *The Infrared Spectra of Complex Molecules*, Chapman and Hall, London, 1975

24. T. A. Stephenson, G. Wilkinson, *J. Inorg. Nucl. Chem.* **28** (1966) 945
25. J. Chatt, G. J. Leigh, D. M. P. Mingos, R. J. Paske, *J. Chem. Soc. A* (1968) 2636
26. L. R. Ramirez, T. A. Stephenson, *J. Chem. Soc. D* (1975) 2244
27. A. B. P. Lever, *Inorganic Electronic Spectroscopy*, Elsevier, New York, 1968
28. D. M. Grant, R. J. Pugmire, *J. Am. Chem. Soc.* **93** (1971) 1880
29. a) P. G. Douglas, B. L. Shaw, *J. Chem. Soc. D* (1969) 624; b) P. G. Douglas, B. L. Shaw, *J. Chem. Soc. A* (1970) 334
30. T. A. Stephenson, *J. Chem. Soc. A* (1970) 889
31. B. S. Hammes, M. T. Kieber-Emmons, R. Sommer, A. L. Rheingold, *Inorg. Chem.* **41** (2002) 1351
32. M. Haga, M. Ishizuya, T. Kanetsugu, T. Yutaka, D. Sakiyama, J. Fees, W. Kaim, *Ind. J. Chem.* **42A** (2003) 2290.



J. Serb. Chem. Soc. 74 (10) 1097–1104 (2009)
JSCS–3903

An unsymmetrical porphyrin and its metal complexes: synthesis, spectroscopy, thermal analysis and liquid crystal properties

CHANGFU ZHUANG, XUEXIN TANG, DONG WANG, AIQING XIA, WENHUI LIAN,
YUHUA SHI* and TONGSHUN SHI

College of Chemistry, Jilin University, Changchun 130023, P. R. China

(Received 25 January, revised 30 April 2009)

Abstract: The synthesis and characterization of a new unsymmetrical porphyrin liquid crystal, 5-(4-stearoyloxyphenyl)phenyl-10,15,20-triphenylporphyrin (SPTPPH₂) and its transition metal complexes (SPTPPM, M(II) = Zn, Fe, Co, Ni, Cu or Mn) are reported. Their structure and properties were studied by elemental analysis, and UV–Vis, IR, mass and ¹H-NMR spectroscopy. Their luminescent properties were studied by excitation and emission spectroscopy. The quantum yields of the S₁ → S₀ fluorescence were measured at room temperature. According to thermal studies, the complexes have a higher thermal stability (no decomposition until 200 °C). Differential scanning calorimetry (DSC) data and an optical textural photograph, obtained using a polarizing microscope (POM), indicate that the porphyrin ligand had liquid crystalline character and that it exhibited more than one mesophase and a low-lying phase transition temperature, with transition temperatures of 19.3 and 79.4 °C; the temperature range of the liquid crystal (LC) phase of the ligand was 70.1 °C.

Keywords: porphyrin; transition metal complex; fluorescence spectroscopy; liquid crystal.

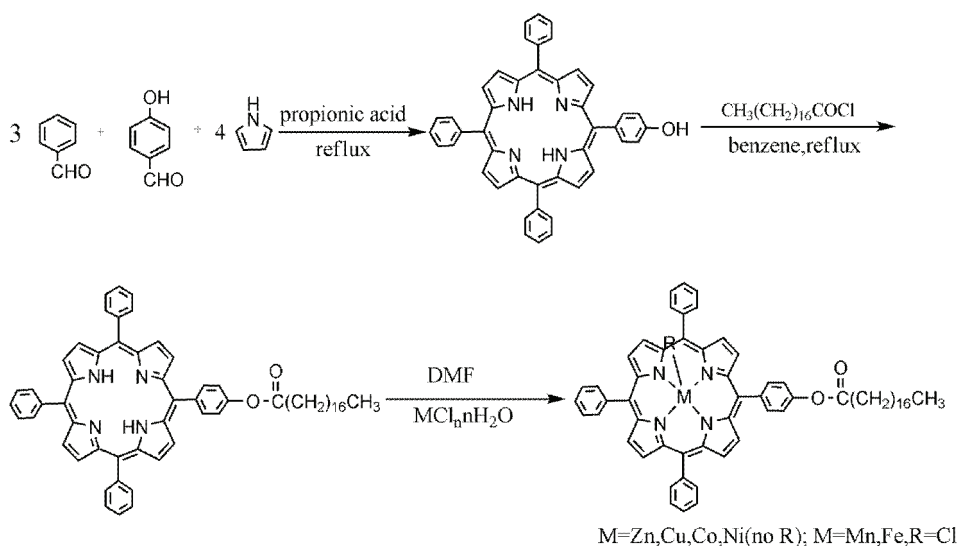
INTRODUCTION

Porphyrin and metalloporphyrins have always received considerable attention from scientists because of their photostability, high visible molar extinction coefficients, interesting excited state chemistry and electron transfer processes. These properties make them useful materials for charge transport, photoelectronic conversion, non-linear optics, organic light emitting diodes and optical information storage.^{1–5} Porphyrin liquid crystals⁶ are of interest for optoelectronic and other device applications due to their synthetic versatility, thermal stability, large electron systems and photochemical properties.⁷ Considerable scientific and technological effort has been devoted to discotic liquid crystals since the first

* Corresponding author. E-mail: cfzhuang_2008@yahoo.com.cn
doi: 10.2298/JSC0910097Z

discovery of discotic mesogens.⁸ The studies of previously reported liquid crystal compounds concentrated mainly on a certain aspect of their properties, such as fluorescence.⁹

Hence, chemists have made efforts to synthesize different porphyrins by peripheral modification of porphyrin.^{10–12} However, most of the porphyrin derivatives substituted with a conjugated system at the meso-position were symmetrical¹³ and limited to transition metal–porphyrin complexes.^{14,15} In this paper, the synthesis and characterization of a novel unsymmetrical porphyrin liquid crystal and its transition metal complexes are reported for the first time (Scheme 1).



Scheme 1. Synthesis route to the porphyrin ligand and its metal complexes.

RESULTS AND DISCUSSION

Characterization and spectroscopy

5-(4-Stearoyloxyphenyl)phenyl-10,15,20-triphenylporphyrin (SPTPPH₂). Yield: 81.7 %; purple solid. M.p. > 300 °C. Anal. Calcd. for C₆₂H₆₄N₄O₂: C, 82.94; H, 7.13; N, 6.22 %; found: C, 82.99; H, 7.13; N, 6.24 %. IR (KBr, cm⁻¹): 3319 (N–H (pyrrole)), 2919, 2850 (C–H), 1762 (C=O), 1199 (C–O), 966 (N–H (pyrrole)). 725 (–(CH₂)_n– (n > 4)). ¹H-NMR (500 MHz, CDCl₃, δ / ppm): –2.756 (2H, pyrrole N–H), 0.858–0.901 (3H, –CH₃), 1.544–1.932 (30H (–CH₂)₁₅), 2.721–2.772 (2H, OOCCH₂–), 7.452–8.230 (19H, meso-phenyl protons), 8.844–8.856 (8H, pyrrole ring). MS (*m/z*): 897.3 (M⁺). UV–Vis (CHCl₃) (λ_{max} / nm): 420 (Soret band), 515, 550, 590, 645 (four Q bands).

SPTPPZn. Yield: 88.3 %, purple red solid. M.p. > 300 °C. Anal. Calcd. for C₆₂H₆₂N₄O₂Zn: C, 77.45; H, 6.45; N, 5.82 %; found: C, 77.52; H, 6.50; N, 5.83

%. IR (KBr, cm^{-1}): 2917, 2850 (C–H), 1760 (C=O), 1193 (C–O), 719 ($-(\text{CH}_2)_n-$ ($n > 4$)). $^1\text{H-NMR}$ (CDCl_3 , 500 MHz): 0.845–0.881 (3H, $-\text{CH}_3$), 1.533–1.937 (30H, $-(\text{CH}_2)_{15}$), 2.721–2.772 (2H, OOCCH_2-), 7.471–8.233 (19H, meso-phenyl protons), 8.950–8.948 (8H, pyrrole ring). MS (m/z): 960.5 $[\text{M}]^+$. UV–Vis (CHCl_3) (λ_{max} / nm): 425 (Soret band), 555, 595 (two Q bands).

SPTPPCu. Yield: 87.6 %, green solid. M.p. > 300 °C. Anal. Calcd. for $\text{C}_{62}\text{H}_{62}\text{N}_4\text{O}_2\text{Cu}$: C, 77.61; H, 6.47; N, 5.82 %; found: C, 77.67; H, 6.51; N, 5.84 %. IR (KBr, cm^{-1}): 2919, 2850 (C–H), 1760 (C=O), 1199 (C–O), 717 ($-(\text{CH}_2)_n-$ ($n > 4$)). MS (m/z): 957.9 $[\text{M}+1]^+$. UV–Vis (CHCl_3) (λ_{max} / nm): 415 (Soret band), 540 (Q bands).

SPTPPNi. Yield: 83.2 %, purple red solid. M.p. > 300 °C; Anal. Calcd. for $\text{C}_{62}\text{H}_{62}\text{N}_4\text{O}_2\text{Ni}$: C, 77.98; H, 6.49; N, 5.85 %; found: C, 78.06; H, 6.55; N, 5.87. IR (KBr, cm^{-1}): 2917, 2848 (C–H), 1762 (C=O), 1199 (C–O), 721 ($-(\text{CH}_2)_n-$ ($n > 4$)). MS (m/z): 953.1 $[\text{M}]^+$. UV–Vis (CHCl_3) (λ_{max} / nm): 415 (Soret band), 530 (Q bands).

SPTPPCo. Yield: 81.3 %, purple red solid. M.p. > 300 °C. Anal. Calcd. for $\text{C}_{62}\text{H}_{62}\text{N}_4\text{O}_2\text{Co}$: C, 77.98; H, 6.55; N, 5.84 %; found: C, 78.04; H, 6.55; N, 5.87 %. IR (KBr, cm^{-1}): 2917, 2848 (C–H), 1760 (C=O), 1197 (C–O), 717 ($-(\text{CH}_2)_n-$ ($n > 4$)). MS (m/z): 954.1 $[\text{M}+1]^+$. UV–Vis (CHCl_3) (λ_{max} / nm): 410 (Soret band), 530, 575 (two Q bands).

SPTPPFeCl. Yield: 80.1 %, purple black solid. M.p. > 300 °C. Anal. Calcd. for $\text{C}_{62}\text{H}_{62}\text{N}_4\text{O}_2\text{ClFe}$: C, 75.46; H, 6.29; N, 5.64 %; Found: C, 75.48, H, 6.33; N, 5.67 %. IR (KBr, cm^{-1}): 2919, 2850 (C–H), 1764 (C=O), 1202 (C–O), 721 ($-(\text{CH}_2)_n-$ ($n > 4$)). MS (m/z): 953.1 $[\text{M}]^+$. UV–Vis (CHCl_3) (λ_{max} / nm): 420 (Soret band), 510 (Q bands).

SPTPPMnCl. Yield: 80.8 %, purple black solid. M.p. > 300 °C. Anal. Calcd. for $\text{C}_{62}\text{H}_{62}\text{N}_4\text{O}_2\text{ClMn}$: C, 75.48, H, 6.29; N, 5.65 %; found: C, 75.55; H 6.34; N, 5.68 %. IR (KBr, cm^{-1}): 2923, 2854 (C–H), 1758 (C=O), 1201 (C–O), 715 ($-(\text{CH}_2)_n-$ ($n > 4$)). MS (m/z): 953.1 $[\text{M}]^+$. UV–Vis (CHCl_3) (λ_{max} / nm): 480 (Soret band), 580 (Q bands).

The characteristic Q and B (Soret) bands of the ligand and metal porphyrins in the visible and near UV ranges were assigned as transitions from the ground state (S_0) to the lowest excited singlet (S_1) and second lowest excited singlet state (S_2), respectively. *SPTPPH₂* has one Soret band (420 nm) and four Q bands (515, 550, 590 and 645 nm). Compared with the ligand, the number of Q band decreased and the absorption frequencies shifted after the metal ion entered the hole of the porphyrin because of the increase in molecular symmetry from D_{2h} to D_{4h} .¹⁶

The spectral bands at 3319 and 966 cm^{-1} in the IR spectrum of the porphyrin ligand are due to the N–H stretching vibration and the winding vibration of the porphyrin core, respectively. The two vibration bands of in the spectra of the

complexes disappeared because the two hydrogen atoms of the porphyrin core are replaced by the transition metal ion to form an M–N bond. The bands found in the 1758–1764 cm^{-1} range in the spectra of the ligand and complexes are assigned to the C=O stretching vibration. The bands at 715–725 cm^{-1} correspond to the methylene in-plane rocking vibration of the straight alkyl chain consisting of over four carbon atoms.

The fluorescence emission spectra of SPTPPH₂ and SPTPPM at room temperature were measured. Their peak values and the quantum yields of the fluorescent emission of SPTPPH₂ and SPTPPZn are given in Table I.

TABLE I. Fluorescence spectral data of the ligand and Zn complex

Compound	$\lambda_{\text{emmax}} / \text{nm}$		Quantum yields (ϕ_f)
Ligand	650	709	0.050
SPTPPZn	594	639	0.035

The samples were dissolved in dry chloroform and deaerated under argon. Two emission bands, Q (0–1) bands at 650 and 594 nm and Q (0–2) bands at 709 and 639 nm were registered for SPTPPH₂ and SPTPPZn, respectively. The quantum yields (ϕ_f) of the Q bands of the complexes were calculated to be 0.050 and 0.035. The quantum yield was determined from the following equation:

$$\phi_{\text{sample}} = \frac{F_{\text{sample}}}{F_{\text{ZnTPP}}} \frac{A_{\text{ZnTPP}}}{A_{\text{sample}}} \phi_{\text{ZnTPP}}$$

where F_{sample} and F_{ZnTPP} are the measured integral areas of the fluorescence peaks of the sample and the reference ZnTPP, respectively; A_{sample} and A_{ZnTPP} are the absorbencies of the sample and the reference (ZnTPP), respectively, at the same excitation wavelength, and ϕ_{ZnTPP} (equals 0.033)¹⁷ is the quantum yield of the reference. Porphyrin exhibited two fluorescence peaks: one from S₂ (B band) and the other from S₁ (Q band). The fluorescence of the B (Soret) band is attributed to the transition from the second excited singlet state S₂ to the ground state S₀, S₂ → S₀. The Soret fluorescence was about two orders of magnitude weaker than the S₁ → S₀ transition of the Q band emission. Its quantum yield is so low that the fluorescence sometimes becomes unobservable. This fluorescence emission was not observed at room temperature, which indicates certainly that the spin forbidden process S₁ → T_n is predominant for the radiationless deactivation of S₁ in porphyrin complexes.

Thermal analysis

Non-isothermal thermogravimetric analyses were performed in an air atmosphere at a heating rate of 10 °C/min. The TG and DTA curves of the ligand SPTPPH₂ are shown in Fig. 1. There are four stages in the TG curve of the ligand. The ligand began to decompose at 200 °C. At 360 °C, about 40 % of the

mass had been lost due to loss of the meso-phenyl and palmitoyl groups. At 445 °C, about 66 % of the mass had been lost, corresponding to loss of the triphenyl group. The residual mass was zero at 600 °C. Simultaneously, there were three exothermic peaks at 310, 505 and 595 °C on the DTA curve of the ligand. The exothermic peaks correspond to the decomposition of the ligand. Decomposition began at 200 °C and was completely finished at 600 °C. It is a continuous decomposition process; the small exothermic peaks correspond to the loss of chains of the porphyrin ring and the large exothermic peak at 505 °C corresponds to the collapse of the porphyrin skeleton. It is very easy to see that this porphyrin complex is so stable in air that it could be dried at temperatures up to 200 °C.

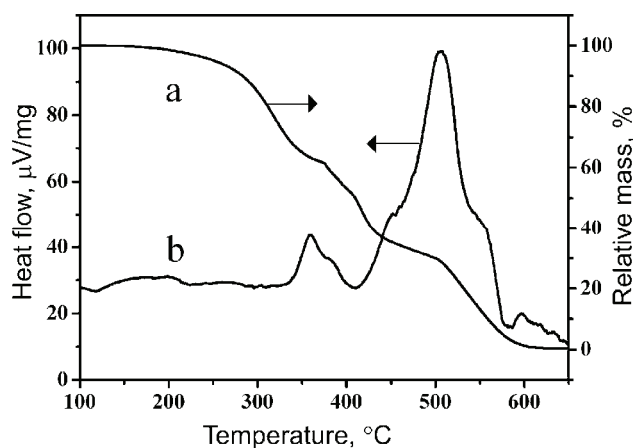
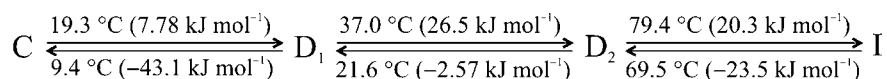


Fig. 1. TG Curve (a) and DTA curve (b) of SPTPPH₂.

Liquid crystalline behaviour

The liquid crystal properties were investigated by DSC and POM. The results showed that only the porphyrin ligand exhibited liquid crystalline behaviour, while all the investigated metal porphyrin complexes were not liquid crystals. The phase change temperatures and enthalpies for SPTPPH₂ are as follows at heating and cooling rate of 10 °C min⁻¹:



where → represents heating and ← cooling; C is crystal phase, D₁ and D₂ are discotic mesophases and I is isotropic liquid phase.

Importantly, the ligand porphyrin exhibited an enantiotropy mesophase. A melting similar transition temperature of 19.3 °C for the ligand was observed during the first heating scan. Moreover, the porphyrin resulting from the ligand could be melted; a melting transition temperature of 37.0 °C for the ligand col-

lected from the second heating scan was obtained. On cooling from the isotropic liquid, the ligand changed to the mesophase D at 69.5 °C, which persisted until about 9.4 °C. The phases were identified by their characteristic optical texture as shown in Fig. 2. Single liquid domains were obtained by annealing them from their clearing temperature. Due to alignment of the molecules with the polarizer and the analyzer, a classic Maltese cross extinction pattern was observed in the polarizer direction (vertical in the figure) and the analyzer direction (horizontal in the figure).

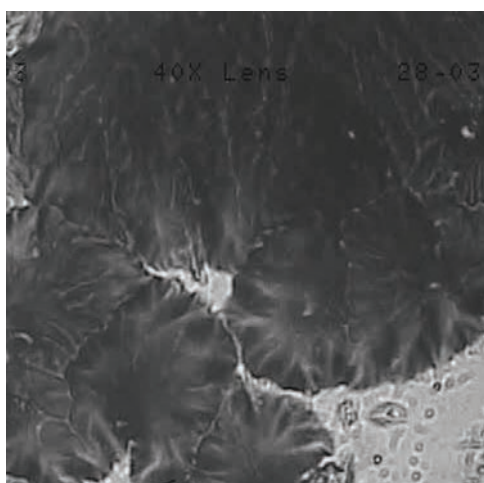


Fig. 2. Optical texture of SPTPPH₂ at 40 °C.

EXPERIMENTAL

Chemicals

All reagents and solvent were commercial reagent grade and were used without further purification except DMF that was predried over activated 4 Å molecular sieve and vacuum distilled from calcium hydride (CaH₂) prior to use. Pyrrole was distilled under reduced pressure.

Stearoyl chloride was prepared and purified according to a published procedure. Meso-5-(*p*-hydroxy)phenyl-10,15,20-triphenylporphyrin (HTPPH₂) was prepared and purified by known procedures.¹⁸

Synthesis of ligand (SPTPPH₂)

HTPPH₂ (1.5 g) was dissolved in 400 mL of heated distilled benzene in a 250 mL round bottom flask and 2.00 mL triethylamine was added. Then a solution of stearoyl chloride in 10 mL benzene was added dropwise over 0.5 h to the above solution under vigorous stirring at 70 °C. The solution was refluxed for 8 h under the protection of a dry nitrogen stream. The benzene was removed from the mixture by distillation. Then the mixed residue was extracted three times with two volumes of distilled water. A concentrated chloroform solution was added to a neutral aluminum oxide column and eluted with CHCl₃. The first band (purple red) was collected and evaporated to dryness to give a purple solid, which was further recrystallized from CHCl₃.

Synthesis of SPTPPZn

The complex SPTPPZn was prepared according to a published procedure. The ligand and $ZnCl_2$ were added to a mixture of DMF (20 mL) and CH_2Cl_2 (20 mL) and the solution refluxed for about 20 min. The extent of the reaction was monitored by measuring the UV-Vis spectrum of the reaction solution every 5 min. After cooling to room temperature, 200 mL distilled water was added to the reaction mixture and extracted three times. The chloroform solution was concentrated and the crude product was chromatographed on a silica gel column using $CHCl_3$ as the eluent. The second band was collected, condensed and dried under vacuum to give a purple red solid.

The other complexes were synthesized in a similar manner to the above-described procedure.

Instrumentation

The UV-Vis spectra were recorded on a Shimadzu UV-240 spectrometer using chloroform as the solvent. The IR spectra were recorded on a Nicolet 5PC-FT-IR spectrometer in the region $400-4000\text{ cm}^{-1}$ using KBr pellets. The 1H -NMR spectra were recorded on a Varian Unity-500 (MHz) NMR spectrometer. The chemical shifts are reported on the δ -scale relative to tetramethylsilane (TMS). The elemental analyses were realized using a Perkin-Elmer 240 C auto elementary analyzer. The mass spectra (FBA) were obtained on an AXIMA-CFR spectrometer. The fluorescence spectra were recorded on a Shimadzu RF5301PC spectrofluorometer. The thermogravimetric analyses (TGA) and differential thermal analyses (DTA) were performed on a TA SDT 2960 thermoanalyzer in air atmosphere at a heating rate of $10\text{ }^\circ\text{C}/\text{min}$.

CONCLUSIONS

A new unsymmetrical porphyrin and its transition metal complexes (SPTPPM, $M(II) = Zn, Fe, Co, Ni, Cu$) were prepared. The application of fluorescence, thermal studies, differential scanning calorimetry (DSC) and polarized optical microscopy (POM) in the analyses were illustrated. The fluorescence intensities of the ligand and SPTPPZn were much larger than the other transition metal complexes. The thermal studies showed that the porphyrin complexes were stable up to nearly $200\text{ }^\circ\text{C}$ and that the decomposition of the complexes was a continuous process. Importantly, the porphyrin is a new class of liquid-crystal material, as verified by the combination of the DSC and POM techniques. This research may open a new vista in materials and devices using porphyrin.

Acknowledgement. This work was supported by the National Natural Science Foundation of People's Republic of China.

ИЗВОД

АСИМЕТРИЧНИ ПОРФИРИН И ЊЕГОВИ МЕТАЛНИ КОМПЛЕКСИ: СИНТЕЗА, СПЕКТРОСКОПИЈА, ТЕРМИЧКА АНАЛИЗА И СВОЈСТВА ТЕЧНОГ КРИСТАЛА

CHANGFU ZHUANG, XUOXIN TANG, DONG WANG, AIQING XIA, WENHUI LIAN, YUHUA SHI и TONGSHUN SHI

College of Chemistry, Jilin University, Changchun 130023, P. R. China

Приказана је синтеза и карактеризација новог асиметричног течног кристала порфирина 5-(4-стеарилоксифенил)фенил-10,15,20-трифенилфосфин (SPTPPH₂) и његових

металних комплекса (SPTPPM, M(II) = Zn, Fe, Co, Ni, Cu, Mn). Њихова структура и својства су изучавани елементалном анализом, UV-Vis, IR, MS и ¹H-NMR спекторскопијом. Луминисцентна својства су проучавана екситационим и емисионим спектрима, квантним приносима S₁→S₀ флуоресценције и мерене на собној температури. На основу термалне анализе комплекси имају већу стабилност (распадају се до 200 °C). Подаци диференцијалне скенирајуће калориметрије (DSC) и оптичке текстуралне фотографије помоћу поларизујућег микроскопа (POM) указују да порфирински лиганд има карактер течног кристала и поседује више од једне мезофазе и ниско-лежеће фазе температурног прелаза, чије се температуре фазног прелаза мењају од 19,3 до 79,4 °C; температурни опсег за фазу течног кристала (LC) лиганда одржава се на 70,1 °C.

(Примљено 25. јануара, ревидирано 30. априла 2009)

REFERENCES

1. W. J. Ruan, Y. Li, X. J. Zhao, C. Z. Wang, Z. A. Zhu, F. M. Miao, *Chin. J. Chem.* **21** (2003) 1451
2. P. I. Premović, I. R. Tonsa, D. M. Đorđević, M. S. Pavlović, *J. Serb. Chem. Soc.* **65** (2000) 113
3. R. E. Hughes, S. P. Hart, D. A. Smith, B. Movaghar, R. J. Bushby, N. Boden, *J. Phys. Chem. B* **106** (2002) 6638
4. S. Kumar, S. K. Varshney, *Org. Lett.* **4** (2002) 157
5. K. Q. Jian, H. S. Shim, D. Tuhus-Dubrow, S. Bernstein, C. Woodward, D. Steingart, *Carbon* **41** (2003) 2073
6. A. Segade, M. Castella, F. Lopez-Calahorra, D. Velasc, *Chem. Mater.* **17** (2005) 5366
7. C. Y. Liu, H. L. Pan, M. A. Fox, A. J. Bard, *Science* **261** (1993) 897
8. S. Chandrasekhar, B. K. Sadashiva, K. A. Suresh. *Pramana* **9** (1977) 471
9. I. A. Levitsky, K. Kishikawa, S. H. Eichhorn, T. M. Swager, *J. Am. Chem. Soc.* **122** (2000) 2474
10. C. P. Wong, R. F. Venteicher, W. D. Horrocks Jr., *J. Am. Chem. Soc.* **96** (1974) 7149
11. J. E. Rogers, K. A. Ngugen, D. C. Hufnagle, D. G. McLean, W. Su, K. M. Gossett, A. R. Burke, S. A. Vinogradov, R. Pachter, P. A. Fleitz, *J. Phys. Chem. A.* **107** (2003) 11331
12. Y. Inokuma, A. Osuka, *Org. Lett.* **6** (2004) 3663
13. Z. X. Zhao, G. F. Liu, *Synth. React. Inorg. ME* **32** (2002) 461
14. J. Otsuki, K. Harada, K. Araki, *Chem. Lett.* (1999) 269
15. K. Ichihara, Y. Naruta, *Chem. Lett.* (1998) 185
16. W. D. Horrocks Jr., C. P. Wong, *J. Am. Chem. Soc.* **98** (1976) 7157
17. W. Liu, Y. H. Shi, T. S. Shi. *Chem. J. Chinese. U* **24** (2003) 200
18. L. N. Ji, X. Qin, Y. W. Huang, *Acta Sci. Natur. Univ. Sunyatseni* **32** (1993) 1.



J. Serb. Chem. Soc. 74 (10) 1105–1111 (2009)
JSCS–3904

Theoretical insights into the properties of the borazine...X⁻ complexes (X⁻ = H, F, Cl, CN, NC or NCO)

REZA GHIASI*

Department of Chemistry, East Tehran Branch (Qiam Dasht) – Islamic Azad University,
Tehran, Iran

(Received 20 February, revised 12 March 2009)

Abstract: The character of the NH...X⁻ (X⁻ = H, F, Cl, CN, NC or NCO) interactions of borazine with anions was studied using *ab initio* method. The interaction energies were calculated at the B3LYP/6-311++G(d,p) level. The energetic and geometric characteristics of the complexes were compared. The “atoms in molecules” methodology was used to analyze the electron density and to obtain atomic contributions to the total energy and charge of the systems. Natural bond orbital (NBO) analysis demonstrated the charge transfer in the study of the nature of the intermolecular interactions. The aromaticity of these compounds was predicted in light of the nucleus-independent chemical shift (NICS).

Keywords: borazine; borazine complexes; interaction energy; NBO; AIM methodology.

INTRODUCTION

Inorganic cyclic ring systems that are isoelectronic with benzene, of which borazine is a textbook example of a six- π -electron six-membered ring, have been known for many years.¹ Many derivatives of borazine have been synthesized and well characterized.² Theoretical studies showed that the six π -electrons are significantly localized on the nitrogen atoms, due to the large electronegativity difference between boron and nitrogen.³ Whether borazine is aromatic remains a controversy,⁴ but it is a fact that borazine is considerably less aromatic than benzene.

This paper studies the complex formed by interaction between borazine and X⁻ anions (X⁻ = H, F, Cl, CN, NC or NCO). The optimized structures, the interaction energies and natural population analysis (NPA) are discussed.

The “atom in molecules” (AIM) methodology of Bader was also applied to study the properties of the bond critical point of the X⁻ and borazine contacts to

* E-mail: rezaghiasi1353@yahoo.com

doi: 10.2298/JSC0910105G

analyze the dependencies between topological, energetic, and geometrical parameters of the complexes.

CALCULATION METHODS

The structures of borazine and X^- ($X^- = H, F, Cl, CN, NC$ or NCO) were optimized by the B3LYP method and 6-311++G(d,p) was chosen as the basis set.

The optimization was realized together with a frequency calculation for each complex to verify that the geometry was the real minimum without any imaginary frequency.

The interaction energy, IE , can be evaluated from the difference between the energy of the complex and the sum of the energies of borazine and X^- :

$$IE = E(\text{complex}) - (E(\text{borazine}) + E(X^-))$$

The calculated interaction energies were corrected for basis set superposition errors (BSSE), which were computed for all calculations using the counterpoise correction method of Boys and Bernardi.⁵

All electronic structure calculations were performed using the Gaussian 98 program.⁶

Population analysis was also performed by the natural bond orbital method⁷ at the B3LYP/6-311++G(d, p) level of the theory using the NBO program⁸ under the Gaussian 98 program package.

AIM Methodology was applied to analyze the electron density and its corresponding Laplacian at the critical point of the $B_3N_3H_6 \cdots X^-$ contact from the structures of $B_3N_3H_6 \cdots X^-$ optimized at the B3LYP/6-311++G(d, p) level. Topological analyses was performed with the AIM 2000 program⁹ using B3LYP/6-311++G(d, p) wave functions as the input.

RESULTS AND DISCUSSION

Energetic

The computed interaction energies (IE) and the corrected interaction energies ($IE^{\text{corrected}}$) for the $B_3N_3H_6 \cdots X^-$ complexes ($X = H, F, Cl, NC, CN$ or NCO) (Fig. 1) are presented in Table I. For a given complex, IE was the largest for $X = F$, which is in agreement with analyses from the distance $r(H \cdots X)$.

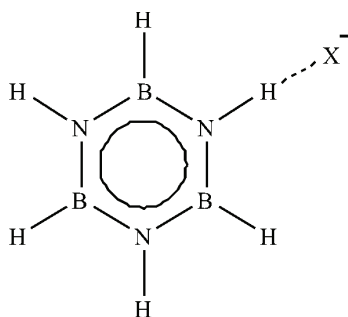


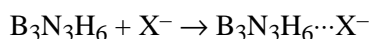
Fig. 1. Geometry of the borazine $\cdots X^-$ complexes ($X^- = H, F, Cl, CN, NC$ or NCO).

Thermochemical analysis

Thermochemical analysis was performed for all the complexes. The values of ΔH , ΔS and ΔG are reported in Table II, whereby the individual terms refer to a temperature of 298 K. The reaction can be considered as:

TABLE I. Calculated energy (Hartree), interaction energy (*IE*), *BSSE*, corrected interaction energy, *r*(H...X) for borazine...X⁻ complexes by the B3LYP method with the 6-311++G(d,p) basis set

X ⁻	<i>E</i> Hartree	<i>IE</i> kcal mol ⁻¹	<i>BSSE</i> ×10 ³ Hartree	<i>IE</i> ^{corrected} kcal mol ⁻¹	<i>r</i> (H...X) Å
H	-243.3064214	-14.8644	1.264305116	-14.0710	1.45814
F	-342.6796508	-26.5987	3.227830862	-24.5732	1.34335
Cl	-703.0702164	-11.2445	0.682776676	-10.8161	2.19947
CN	-335.6559382	-11.8542	0.271105435	-11.6841	2.00025
NC	-335.6566621	-12.3085	0.337451621	-12.0967	1.86189
NCO	-410.9556042	-12.8988	0.452088312	-12.6151	1.82806



As can be seen, the ΔS values are similar for all complexes. Since in this reaction two particles form one, ΔS should have a negative value, although the relative difference of ΔG is almost the same as that for the ΔH . The equilibrium constants of the all complexes are also given in Table II, from which it can be seen that the equilibrium constant is the largest for X⁻ = F.

TABLE II. Calculated thermodynamic parameters for the for the borazine...X⁻ (X⁻ = H, F, Cl, CN, NC or NCO) complexes by the B3LYP method with the 6-311++G(d,p) basis set

X ⁻	ΔG / kcal mol ⁻¹	ΔH / kcal mol ⁻¹	ΔS / kcal mol ⁻¹ K ⁻¹	<i>K</i>
H	-9.45657	-15.908	-0.02165	8.6×10 ⁶
F	-21.4715	-28.5925	-0.0239	5.6×10 ¹⁵
Cl	-5.27171	-11.4615	-0.02077	7.3×10 ³
CN	-4.31789	-11.4044	-0.02378	1.5×10 ⁶
NC	-4.49171	-11.7777	-0.02445	2.0×10 ³
NCO	-5.97828	-12.3343	-0.02133	2.4×10 ⁴

Atoms in molecules analysis

Analysis of the electron density by means of the Bader atoms in molecules (AIM) methodology provides useful tools to confirm the presence of NH...X⁻ interactions between borazine and X⁻.

The values of ρ , eigenvalues of the Hessian matrix of density (λ_1 , λ_2 and λ_3), and $\nabla^2\rho$ of the complexes at the B3LYP/6-311++G(d,p) level are listed in Table III. It contains the electron densities at the bond critical points of the NH...X⁻ interactions. Different features of the electron densities analysis obtained in the AIM framework are summarized as follows:

1. All the BCPs of NH...X⁻ interactions are characterized by small $\rho(r)$ values and a positive Laplacian of the electron density. The sign of the Laplacian is determined by the positive curvature of $\rho(r)$ along the interaction line, as the Pauli exclusion principle leads to a relative depletion of the charge density in the interatomic surface. These interactions are dominated by a contraction of the char-

TABLE III. Electron densities $\rho(e/a_0^3)$, eigenvalues of the Hessian matrix of density (λ_1 , λ_2 and λ_3) and Laplacians $\nabla^2\rho(e/a_0^5)$ at the intermolecular bond critical points of borazine... X^- ($X^- = H, F, Cl, CN, NC$ or NCO), calculated at the B3LYP/6-311++G(d,p) level within the AIM theory

X^-	ρ	λ_1	λ_2	λ_3	$\nabla^2\rho$
H	0.046	-0.069	-0.068	0.160	0.023
F	0.104	-0.261	-0.260	0.701	0.180
Cl	0.026	-0.030	-0.030	0.123	0.062
CN	0.031	-0.041	-0.040	0.141	0.060
NC	0.035	-0.051	-0.050	0.196	0.094
NCO	0.036	-0.053	-0.053	0.208	0.102

ge density away from the interatomic surface toward each of interacting species. It was confirmed that the electron density at the bond critical point can be used as a measure of the binding strength. The Laplacians $\nabla^2\rho$ are all positive, indicating a typical closed-shell kind of interactions in the complexes. A plot of the calculated interaction energies of the borazine... X^- interaction of the complexes vs. their electron density at the BCP(NH... X^-) is presented in Fig. 2, which indicates a regression coefficient of 0.9984.

2. Among all the complexes, the obtained value for electron density was the highest for the interaction $NH...F^-$.

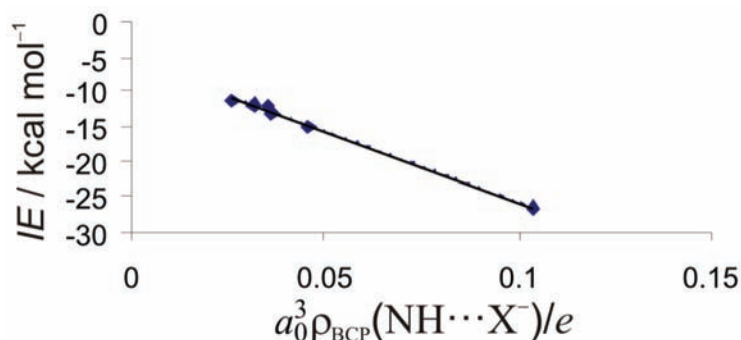


Fig. 2. A plot of the calculated interaction energies ($IE = -201.56\rho_{BCP} - 5.6114$; $R^2 = 0.9984$) of borazine... X^- ($X^- = H, F, Cl, CN, NC$ or NCO) interaction complexes vs. their electron density at the BCP(NH... X^-).

Natural population analysis

Natural bond orbital analysis stresses the role of intermolecular orbital interactions in a complex, particularly charge transfer ones. This analysis is carried out by considering all possible interactions between filled donor and empty acceptor NBOs and estimating their energetic importance by a second-order perturbation theory. For each donor NBO (i) and acceptor NBO (j), the stabilization

energy $E^{(2)}$ associated with electron delocalization between donor and acceptor is estimated as:

$$E^{(2)} = -q_i \frac{(F_{i,j})^2}{\epsilon_j \epsilon_i}$$

where q_i is the orbital occupancy, ϵ_i and ϵ_j are diagonal elements and $F_{i,j}$ is the off-diagonal NBO Fock matrix element.

The results of the second-order perturbation theory analysis of the Fock matrix at the B3LYP/6-311++G(d,p) level of theory are collected in Table IV. For the borazine...X⁻ complexes, most of the charge transfer energies reported in Table IV are related to the dominant interaction, which is between donor species and acceptor species.

TABLE IV. The results of second-order perturbation theory analysis of the Fock matrix within the NBO basis

X ⁻	Donor	Acceptor	$E^{(2)}$ / kcal mol ⁻¹	$\epsilon_j - \epsilon_i$	$F_{i,j}$
H	LP (1) H	$\sigma^*(\text{N-H})$	58.05	0.51	0.154
F	LP (4) F	$\sigma^*(\text{N-H})$	82.38	0.81	0.230
Cl	LP (4) Cl	$\sigma^*(\text{N-H})$	15.43	0.71	0.093
CN	LP (1) C	$\sigma^*(\text{N-H})$	27.90	0.78	0.132
NC	LP (1) N	$\sigma^*(\text{N-H})$	21.43	0.91	0.125
NCO	LP (1) N	$\sigma^*(\text{N-H})$	22.12	0.94	0.129

Interaction of NH...X⁻ in borazine has an attractive aspect. The strongest interaction is between the LP(4) F donor and the $\sigma^*(\text{NH})$ acceptor.

It is interesting to note that the obtained results based on the NBO are completely accordant with the results obtained within the AIM framework.

A comparison between the results of the $IE^{\text{corrected}}$ in Table I and the $E^{(2)}$ in Table IV showed that, from all the considered anions, the interaction energy is the greatest when the borazine interacts with F⁻.

The natural population analysis (NPA) shows that the charge on X⁻ decreases in the order H, F, Cl, CN (Table V). These results are compatible with charge transfer from X⁻ to borazine.

TABLE V. Natural population analysis (NPA) for the borazine...X⁻ (X⁻ = H, F, Cl, CN, NC or NCO) complexes by the method B3LYP with 6-311++G(d,p) basis set

X ⁻	X	X(monomer)	H	H(borazine)
H	-0.74268	-1.00	0.40502	0.39928
F	-0.83744	-1.00	0.48555	0.39928
Cl	-0.93896	-1.00	0.46306	0.39928
CN	-0.20834	-1.00	0.45176	0.39928
NC	-0.94379	-1.00	0.47455	0.39928
NCO	-0.94288	-1.00	0.47771	0.39928

Nucleus independent chemical shifts (NICS)

In order to further study the aromaticity of borazine complexes, the nucleus independent chemical shifts (NICS) of the optimized structures were calculated at the ring center and at 0.5 and 1.0 Å perpendicularly away from the successions of points of the plane, as listed in Table VI.

TABLE VI. NICS(0.0), NICS(0.5) and NICS(1.0) values for borazine...X⁻ (X⁻ = H, F, Cl, CN, NC or NCO) complexes by the B3LYP method with the 6-311++G(d,p) basis set

Species	NICS(0.0)	NICS(0.5)	NICS(1.0)
Borazine	-1.5844	-2.2813	-2.6670
H	-1.7779	-2.6086	-3.0760
F	-1.8756	-2.5839	-2.9570
Cl	-1.8172	-2.5660	-2.9647
CN	-2.0349	-2.8114	-3.1570
NC	-1.8252	-2.5911	-3.0052
NCO	-2.1471	-2.9309	-3.2172

In this study, first the values of NICS(0.0) at the geometrical centers of the planar six-membered ring, which provide a direct measure of the ring current effects, were calculated. The calculated results are listed in Table VI. The NICS values of borazine and the other species are all negative. It can be seen that all complexes are more aromatic than borazine. In order to further analyze the aromaticity, the values of NICS(0.5), NICS(1.0) were calculated by placing a ghost atom 0.5 and 1.0 Å, respectively, above the center of the six-membered ring. The values of NICS(0.5) and NICS(1.0) for all species were negative, supporting the existence of delocalization and aromaticity in these complexes. The most negative values of NICS(0.0), NICS(0.5) and NICS(1.0) were obtained for X⁻ = NCO.

CONCLUSIONS

Calculations on borazine...X⁻ (X⁻ = H, F, Cl, CN, NC or NCO) complexes were performed at the B3LYP level with the 6-311++G(d,p) basis set. A good correlation between $\rho_{\text{BCP}}(\text{NH}\cdots\text{X}^-)$ and the interaction energy was found for the complexes.

The aromaticity of these compounds was predicted in light of the nucleus-independent chemical shift (NICS). All of the molecules were found to be highly π -aromatic in nature.

ИЗВОД

ТЕОРИЈСКО САГЛЕДАВАЊЕ СВОЈСТАВА БОРАЗИН...X⁻
КОМПЛЕКСА (X⁻ = H, F, Cl, CN, NC ИЛИ NCO)

REZA GHIASI

Department of Chemistry, East Tehran Branch (Qiam Dasht) – Islamic Azad University, Tehran, Iran

Карактер интеракција NH...X⁻ (X⁻ = H, F, Cl, CN, NC or NCO) између боразина и ањона испитиван је *ab initio* методом. Енергије интеракције израчунате су на V3LYP/6-311++G(d,p) нивоу. Упоредне су енергетске и геометријске карактеристике комплекса. Коришћена је методологија „атома у молекулима“ за анализу густине и атомског доприноса укупној енергији и наелектрисању система. Анализа орбитале природне везе (NBO) показала је пренос наелектрисања при испитивању природе међумолекулских интеракција. Ароматичност једињења претпостављена је на основу хемијског помераја који не зависи од типа језгра (NICS).

(Примљено 20. фебруара, ревидирано 12. марта 2009)

REFERENCES

1. J. E. Huheey, A. E. Keiter, R. L. Keiter, *Inorganic chemistry: principle of structure and reactivity*, Harper Collins College Publishers, New York, 1993
2. R. Steudel, *The Chemistry of Inorganic Ring Systems*, Elsevier, New York, 1992
3. a) R. Miao, G. Yang, C. Zhao, J. Hong, L. Zhu, *J. Mol. Struct. (THEOCHEM)* **715** (2005) 91; b) J. K. Parker, S. R. Davis, *J. Phys. Chem. A* **101** (1997) 9410
4. a) P. von Ragué Schleyer, H. Jiao, N. J. R. van Eikema Hommes, V. G. Malkin, O. L. Malkina, *J. Am. Chem. Soc.* **119** (1997) 12669; b) B. Kiran, A. K. Phukan, E. D. Jemmis, *Inorg. Chem.* **40** (2001) 3615
5. S. F. Boys, F. Bernardi, *Mol. Phys.* **19** (1970) 553
6. M. J. Frisch, G. W. Trucks, H. B. Schlegel, G. E. Scuseria, M. A. Robb, J. R. Cheeseman, V. G. Zakrzewski, J. A. Montgomery, Jr., R. E. Stratmann, J. C. Burant, S. Dapprich, J. M. Millam, A. D. Daniels, K. N. Kudin, M. C. Strain, O. Farkas, J. Tomasi, V. Barone, M. Cossi, R. Cammi, B. Mennucci, C. Pomelli, C. Adamo, S. Clifford, J. Ochterski, G. A. Petersson, P. Y. Ayala, Q. Cui, K. Morokuma, D. K. Malick, A. D. Rabuck, K. Raghavachari, J. B. Foresman, J. Cioslowski, J. V. Ortiz, A. G. Baboul, B. B. Stefanov, G. Liu, A. Liashenko, P. Piskorz, I. Komaromi, R. Gomperts, R. L. Martin, D. J. Fox, T. Keith, M. A. Al-Laham, C. Y. Peng, A. Nanayakkara, C. Gonzalez, M. Challacombe, P. M. W. Gill, B. Johnson, W. Chen, M. W. Wong, J. L. Andres, C. Gonzalez, M. Head-Gordon, E. S. Replogle, J. A. Pople, *Gaussian 98, Revision A.7*, Gaussian Inc., Pittsburgh, PA, 1998
7. A. E. Reed, L. A. Curtiss, F. Weinhold, *Chem. Rev.* **88** (1988) 899
8. E. D. Glendening, A. E. Reed, J. E. Carpenter, F. Weinhold, *NBO Version 3.1*, Theoretical Chemistry Institute and Department of Chemistry, University of Wisconsin, Madison, WI, USA
9. F. Biegler-Konig, *AIM 2000 version 1.0*, University of Applied Science, Bielefeld, 2000.



J. Serb. Chem. Soc. 74 (10) 1113–1123 (2009)
JSCS–3905

The use of NaX zeolite as a template to obtain a mono-atomic Pt dispersion by impregnation with Pt(II) acetylacetonate/acetone solution

SLAVKO MENTUS^{1*#}, ZORICA MOJOVIĆ² and VELIMIR RADMILOVIĆ³

¹University of Belgrade, Faculty of Physical Chemistry, Studentski trg 12, 11000 Belgrade,

²ICTM – Department for Catalysis and Chemical Engineering, Njegoševa 12, 11000

Belgrade, Serbia and ³National Center for Electron Microscopy, Lawrence Berkeley National Laboratory, University of California, Berkeley, USA

(Received 26 October 2008, revised 11 June 2009)

Abstract: The incorporation of platinum into the cavities of NaX zeolite was realized by impregnation and thermal decomposition of the organometallic compound Pt(II)-acetylacetonate dissolved in acetone. A high dispersion of platinum to predominantly mono-atomic particles was achieved thanks to the tight fit of the Pt(II)-acetylacetonate molecules in the aperture of the zeolite supercage. Using the high angle annular dark field imaging technique of HRTEM, individual Pt particles situated within the zeolite crystals were, for the first time, clearly visible. This offers new possibilities of studying the distribution of incorporated metal particles along the crystal depth.

Keywords: HRTEM imaging; impregnation technique; NaX zeolite; Pt(II)-acetylacetonate; platinum-modified zeolite.

INTRODUCTION

Zeolites are aluminosilicates with an ordered open porosity and very developed inner surface area, which approaches several hundred square meters per gram.¹ Aluminum(III) sites present the positive-deficient sites, which are compensated usually by alkali or alkali-earth cations. The charge compensating cations may be replaced by other cationic species by ion-exchange. Zeolites are known as very strong sorbents for molecules interacting with the inner zeolite surface, *i.e.*, those being small enough to penetrate through the cavity orifices.

The cations of transition metals have been introduced into the zeolite cavities either by ion exchange or by impregnation techniques.^{2–12} According to numerous literature reports, metals such as Pt, Pd, Ni and Mo, as well as alloys have

* Corresponding author. E-mail: slavko@ffh.bg.ac.rs

Serbian Chemical Society member.

doi: 10.2298/JSC0910113M

been incorporated within the cavities of zeolites either by chemical reduction of their cations introduced by ion-exchange or by thermal decomposition of appropriate precursors (in the presence of hydrogen, if necessary).² Reducing agents other than hydrogen may be used. For instance, Wang *et al.*³ introduced Co²⁺ ions into the cavities of NaX zeolite and reduced them to metallic Co clusters by means of sodium borohydride.

Considerable catalytic effects of metal-zeolite systems have been demonstrated in numerous, particularly organic, chemical reactions.^{13–19} Barthomont,²⁰ in particular, indicated the role of the aluminosilicate support in suppressing the agglomeration of metal cluster to during prolonged catalyst exploitation.

In various ways, zeolites were the subject of investigations by electrochemical methods.^{21–23} Quite recently, zeolites were used as templates to produce metal particle of uniform, sub-nanometer dimensions for electrocatalysis purposes. For instance, Coker *et al.*^{11,24} incorporated Pt nanoclusters in NaX zeolite (faujasite type) by the ion-exchange technique, and, upon zeolite dissolution, transferred them to a carbon support to obtain Pt/C electrocatalysts. Furthermore, following literature reports relating to Ag⁺-exchanged zeolites,^{10,25} Senthilkumar *et al.*²⁶ incorporated Pt cluster into the pores of type Y zeolite by cathodic reduction of a previously introduced Pt-salt. They attempted to use so-prepared Pt-loaded zeolite in the form of a membrane for electrochemical reduction of oxygen and oxidation of methanol.²⁶

The hitherto published impregnation techniques to incorporate Pt clusters into zeolites involved a solution of Pt(IV) chloride^{2,12} or Pt(IV) tetra-aminenitrate¹¹ as the impregnation agent. Pt(II) acetylacetonate was used by Yao *et al.*²⁷ to synthesize Pt catalysts (0.5–2 % loading) on a mesoporous MCM-41 support. Metal acetylacetonates were rarely used in conjunction with zeolites and the studies published to date do not report their decomposition to metals. For example, Ferreira *et al.*²⁸ investigated NaX zeolite with incorporated Cu acetylacetonate, and de Souza *et al.*²⁹ investigated NaX and NaY zeolites with incorporated Ni acetylacetonate, in both cases without their thermal degradation.

The size and shape of metal clusters both in zeolites^{4–8} and silicate-based mesoporous materials⁹ were examined preferably by high-resolution transmission electron microscopy (HRTEM). The dimensions of metal clusters are expected to be limited by the pore dimensions, for instance, in the case of zeolite, to approx. 1 nm. Many HRTEM microphotographs of zeolites with incorporated metal particles were published,^{3–9,11,26} however, they never provided sufficiently clear insight into the distribution of the metal particles along the crystal depth. Usually, insufficient resolution and sample transparency limited the quality of the microphotographs. In some cases, problems arose from the formation of metal clusters of random size on the outer surface of the zeolite crystals,^{3,10} as well as

the growth of huge clusters inside the crystals,^{7,11} accompanied obviously by destruction of the local zeolite structure.

In this study, NaX zeolite was impregnated with a Pt(II) acetylacetonate/acetone solution and the Pt(II) acetylacetonate decomposed in order to produce Pt particles within the zeolite cavities. The high angle annular dark field imaging technique of HRTEM, capable of visualizing individual atoms,³⁰ was used to investigate the distribution of platinum particles within the zeolite crystals.

EXPERIMENTAL

Preparation of platinum-loaded NaX zeolite

Faujasite type NaX zeolite, with the formula $\text{Na}_{86}(\text{AlO}_2)_{86}(\text{SiO}_2)_{106} \cdot x\text{H}_2\text{O}$ ($0 < x < 264$, depending on the partial pressure of water), approx. 2 g cm^{-3} in density, was the product of Linde Co., while Pt(II) acetylacetonate ($\text{Pt}(\text{C}_5\text{H}_7\text{O}_2)_2$) was purchased from Aldrich.

A recently published procedure for the thermal decomposition of noble metal acetylacetonates to deposit noble metal clusters on the surface of a solid support,³¹ which was subsequently adapted to introduce noble metal clusters into zeolite cavities,^{32,33} was employed in this study. Briefly, after heating to $350 \text{ }^\circ\text{C}$ in order to remove adsorbed water and subsequent cooling to room temperature in a dry atmosphere, the zeolite sample was slightly wetted with a dilute acetone solution of platinum(II) acetylacetonate. The sample was then dried at $90 \text{ }^\circ\text{C}$ to evaporate the acetone, and heated at $350 \text{ }^\circ\text{C}$ under a hydrogen atmosphere to both decompose the Pt(II) acetylacetonate and remove its gaseous decomposition products. The impregnation/decomposition procedure was repeated about 20 times until a Pt/zeolite weight ratio of 0.1 was achieved. After this procedure the zeolite was dark brown in color.

X-Ray diffractometry

X-Ray powder diffractograms of the original and Pt-modified NaX zeolite samples were recorded on a Siemens-D500 diffractometer with Ni filtered Cu $\text{K}\alpha$ radiation ($\lambda = 1.54178 \text{ \AA}$).

Electron microscopy

Specimens were prepared for transmission electron microscopy by suspending the catalyst powders in ethanol using an ultrasonic bath and adding a drop of the suspensions onto clean holey carbon grids, which were then dried in air. The samples were examined by high angle annular dark field imaging using a Tecnai F20 FEG electron microscope operating at 200 kV. The particle shapes were determined by real space crystallography using high resolution images taken from particles near or on the edge of the carbon black substrate. Conventional bright-field and dark-field imaging were also utilized in order to investigate the overall distribution of the Pt particles. Local structural information from single particles was obtained by numerical Fourier filtering of the digitized image intensity spectrum.

RESULTS AND DISCUSSION

Usually, the impregnation techniques employed to date for the incorporation of platinum into zeolite cavities involved soaking the zeolite in solutions of inorganic thermodegradable platinum compounds (chloride, tetra-aminonitrate).^{2,11,12} The impregnation of NaX zeolite with acetylacetonates, although studied experimentally,^{32,33} was never considered on the level of molecular structure. This aspect of impregnation will be discussed herein.

As is well known from the literature, the structure of NaX-type zeolite (Fig. 1) consists of small sodalite cages interconnected by means of hexagonal prisms, which together surround almost spherical supercages. The supercages are interconnected mutually by 12-membered rings.^{1,34} The inner diameter of the sodalite cages and supercages, with the charge compensating cations placed inside, amount to 0.26 and 0.9 nm, respectively, while their entrance apertures amount to 0.22 and 0.74 nm, respectively.^{34,35} Small molecules, such as helium or water, may enter both the sodalite cages and supercages, while even the smallest organic molecules, such as methane, may enter the supercages only. The mean number of molecules which may simultaneously enter a supercage depends on both the volume ratio and molecule geometry. This number is, for example, 5.2 for benzene (planar molecule with a diameter of approx. 0.5 nm) and 3.6 for mezytilene.³⁶

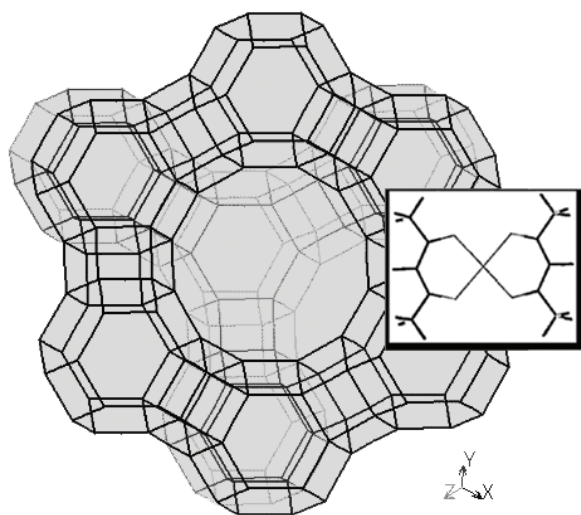


Fig 1. Wire model of the NaX (FAU) zeolite structure, the view directed to the (111) plane, which shows the orifice of a zeolite supercage; a wire model of the planar Pt(II) acetylacetonate molecule in nearly natural proportions is added as an inset.

The structure of the Pt(II)-acetylacetonate molecule is planar.³⁷ The Pt atom, located at the centre of the molecule, is bonded to the pairs of oxygen atoms of the 2,4-pentanedionato ions *via* one ionic and one coordinative bond, equalized mutually by resonance of the structures. Using Chem3D Ultra (CambridgeSoft) package to analyze intramolecular distances in space, the distance between the centers of the hydrogen atoms situated in the outermost methyl groups along the pentanedione chain, due to their rotation, vary between 0.45 and 0.65 nm. Kevin *et al.*³⁷ for Cu(II) acetylacetonate, being similar both in dimensions and in geometry to Pt(II) acetylacetonate, found from monolayer-adsorption measurements on Cab-O-Sil 200 m² g⁻¹ surface that one molecule occupies 0.588 nm² of the surface, which is in good agreement with the dimensions 0.65×0.9 nm² found

by Chem3D Ultra software for one molecule of Pt(II)-acetylacetonate. Therefore, regarding even the van der Waals radii of the hydrogen atoms, the Pt(II) acetylacetonate molecule should experience no substantial obstacles when penetrating into the supercages, particularly assuming free rotation of the outermost methyl groups around the C–C bond. This is in accordance with the work of Ferreira *et al.*²⁸. Namely, these authors reported that the complex compound Cu(II)-acetylacetonate diffuses freely through the channels of NaX zeolite, while complexation of Cu(II) acetylacetonate with aliphatic triamines, which led to more voluminous molecules, restricted completely their movement.²⁸ According to the paper by de Souza *et al.*,²⁹ the isostructural and dimensionally similar Ni(II) acetylacetonate may also be incorporated into NaX zeolite cavities.

This consideration indicates that Pt(II)-acetylacetonate may serve effectively as a transporting agent for the incorporation of platinum into NaX zeolite cavities. However, due to its complex configuration and greater dimensions in comparison to benzene,³⁶ a very low probability for a Pt(II) acetylacetonate molecule to enter a previously already occupied supercage. Therefore, the impregnation/thermal decomposition procedure in this case may be considered as the introduction of Pt atoms one after another. The impregnation/thermal decomposition procedure must, therefore, be repeated many times in order to obtain Pt clusters greater than a single atom.

The SEM microphotographs of the zeolite sample used in this study before and after platinum incorporation are shown in Fig. 2. A comparison of these pictures indicates no visible change in the crystal form and mean diameter. However, the platinum-modified sample enabled photographs of better contrast to be taken, indicating better reflectivity to electrons.

Knowledge of the zeolite structure enables the calculation of the population of the supercages by Pt atoms under the assumption of uniform filling. The formula of a unit cell of anhydrous NaX is $\text{Na}_{86}(\text{AlO}_2)_{86}(\text{SiO}_2)_{106}$ (relative mass 13836). The unit cell is cubic with the length of the axis 2.4975 nm, *i.e.*, roughly 2.5 nm. Thus, one gram of zeolite contains 3.38×10^{19} unit cells. Each unit cell contains 8 supercages, which means 2.7×10^{20} supercages per gram of zeolite.³⁵ The platinum loaded NaX zeolite sample synthesized in this work contained 0.1 g (*i.e.*, 3×10^{20} atoms) of Pt per gram of NaX. Assuming uniform distribution, Pt-modified NaX zeolite with 10 wt. % of Pt should contain, on average, 1.1 Pt atoms per supercage. Since, according to recent HRTEM observation of Pt nanocrystals, the most reliable diameter of a Pt atom is about 0.26 nm,^{38–40} assuming that the sample is transparent, in the present case, particles close to 0.26 nm in size in the plane of the photograph should be seen and, for the case of a quite uniform distribution, on average, 8 individual atoms per unit cell.

The picture shown in Fig. 3 was taken by a high angle annular dark field imaging technique using a Tecnai F20 FEG transmission microscope. This tech-

nique is the best one for observation of atomic arrays of supported nanoparticles of catalyst.^{39,40} If the microscope is adjusted to observe platinum, the structural details composed of lighter elements (Si, Al) remain invisible. The microphotograph shown in Fig. 3 is the best picture of a metal-loaded zeolite taken to date, even in comparison to recently published ones.^{3,12,24,26}

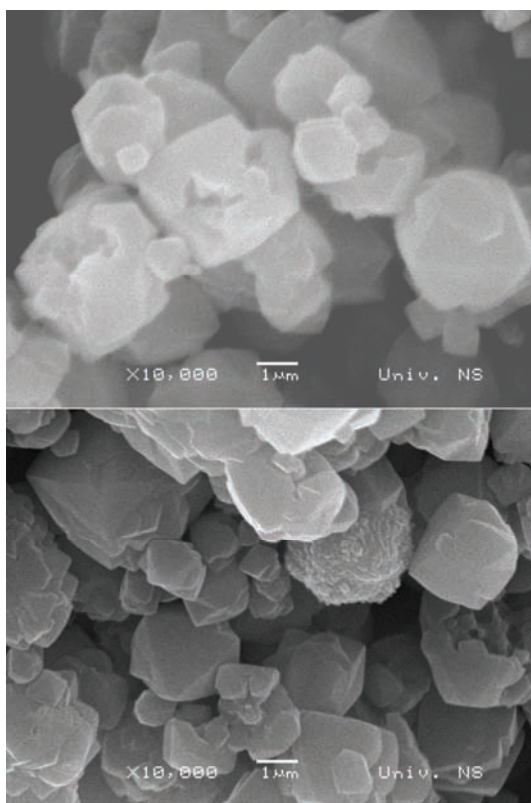


Fig. 2. SEM Microphotographs of the original NaX zeolite (top) and Pt-loaded NaX zeolite (10 wt. % Pt), taken at a magnification of 10000; the mean crystal diameter is approx. 3 μm .

In order to analyze the distribution of particles along unit cells, the transparency of the sample should be discussed.

Aluminum metal of thickness 1.5 and 8 μm is transparent for electrons accelerated to 100 and 1000 keV, respectively. Based on the closeness in the atomic weights, a similar transparency may be expected for silicon. Therefore, for NaX zeolite, being an aluminosilicate material, it may be assumed that, for the 200 keV electron beam used in this study, the depth of transparency is of the order of 1 μm .

Since Fig. 3 presents the tip of a Pt-loaded NaX zeolite monocrystal, from purely geometric considerations, it may be concluded that the largest depth along the axis vertical to the plane of the picture may not exceed 25 nm. Such a depth is

obviously quite transparent for the employed electron beam and, consequently, Fig.3 presents all the Pt particles placed within the piece of zeolite crystal caught by this microphotograph.

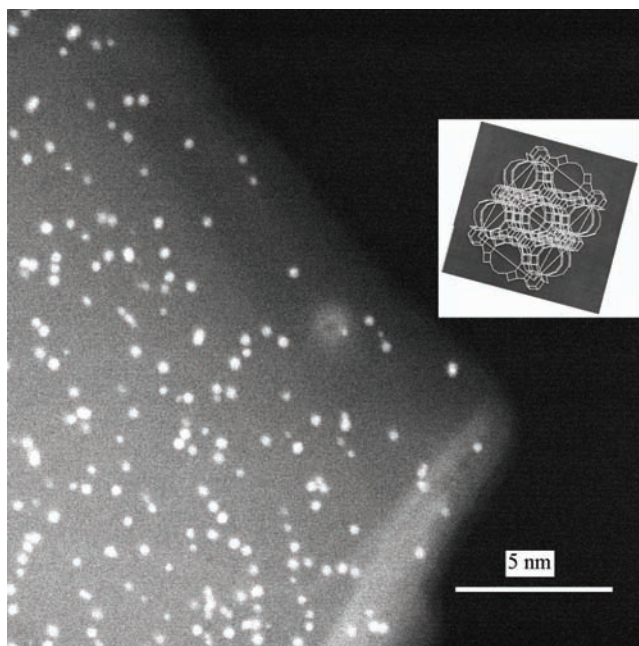


Fig. 3. High angle annular dark field image (200 kV) of a tip of a Pt-loaded NaX zeolite (10 wt. % Pt) monocrystal. Inserted figure presents the model of a (cubic) unit cell of NaX zeolite, with only the Si-Si bonds presented, for sake of clarity. The size and orientation of the model of the unit cell really fits the tip of the photographed crystal.

In the inset of Fig. 3, presents by wire-modeled Si-Si bonds, the details of the structure of a (cubic) NaX unit cell ($a = 2.5$ nm), in natural proportions to the photographed crystal and properly oriented in space to fit the tip of the photographed crystal. For the photographed crystal, the presented network of Si-Si bonds depicts the real dimensions and positions of the supercages. Based on Fig. 3, statistical analysis of the particle distribution per unit cell may be performed, bearing in mind that the number of unit cells distributed along the electron beam path increases progressively as the distance from the crystal tip increases. Considering the most reliable data for the diameter of a Pt atom,³⁸⁻⁴⁰ Fig. 3 evidences that the number of Pt-atoms per supercage is preferably one, rarely two or three, which might amount to not more than 3 wt. % of the platinum in the zeolite. The missing amount, supplementing the 10 % of platinum in the zeolite, should exist in another form than that perceived in Fig. 3. However, the particles located within

the supercages obviously completely experienced the templating effect of the supercage dimensions.

The dimensions of metal particles incorporated into zeolite crystals were not always limited by the zeolite host.^{7,10} For example, silver particles ranging in size from 1 to 18 nm were found in the Faujasite host,¹⁰ which means that silver tends to destroy the local crystal structure and to grow outside the volume of the zeolite cavities. Similarly, Tonscheidt *et al.*⁷ observed very large Ir and Rh particles in X zeolite samples modified by ion exchange. They also outlined the problem of instability of the zeolite lattice under the impact of the electron beam during TEM observations.

Additional characterization of the Pt-loaded NaX zeolite sample was realized by means of X-ray diffractometry. The X-ray diffractograms of both the original and platinum-modified NaX zeolite used in this study are shown in Fig. 4. The diffractogram of the original 13 X sample overlaps with the one filed in the JCPDS library.⁴¹ The diffractogram of the Pt- modified sample contains all the diffraction lines visible in that of the original NaX sample. The deviation of the baseline of the X-ray diffractogram over a broad range of 2θ values is a characteristic feature in this case. A deviation of the baseline of X-ray diffractograms was observed by de Souza *et al.*²⁹ in the case of NaX zeolite with incorporated Ni(II)-acetylacetonate. In terms of crystallography, this feature corresponds to

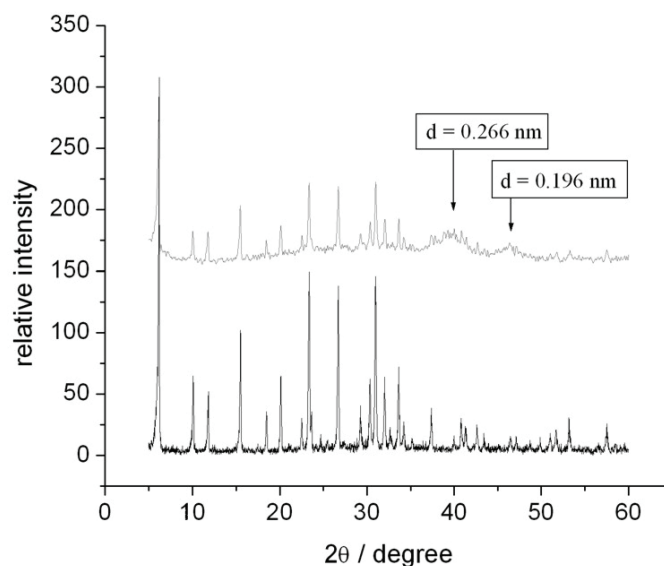


Fig. 4. The X-ray diffractograms of NaX zeolite (lower) and Pt loaded NaX zeolite (upper). The d -values labeling the humps on the base-line correspond to reflections from the (111) and (200) crystallographic planes of platinum.

amorphization of the sample. It is not due to crushing of the zeolite crystals, since the SEM microphotographs (Fig. 2) taken before and after Pt incorporation did not evidence such an event. Amorphization in this case may be attributed only to slight local deformations of the zeolite lattice caused by the presence of Pt particles. Contrary to data pertaining to NaX zeolite impregnated with Ni-acetylacetonate,²⁹ the amorphization in this case did not influence the adsorption capacity: as proven by thermogravimetry, the adsorption capacity for water was reduced only by the volume occupied by the incorporated platinum.

Based on the microphotograph shown in Fig. 3, which shows that the Pt particles incorporated in the zeolite crystals contain only few atoms, any feature pertaining to the crystal structure of platinum are not to be expected. However, in the diffractogram of the modified zeolite (Fig 4, upper diagram), two broad humps are visible in the $35^\circ < 2\theta < 50^\circ$ region, at 2θ values approaching the angles 39.75° and 46.20° . These angles correspond to the two strongest, (111) ($d = 0.266$ nm) and (200) ($d = 0.196$ nm), reflections of polycrystalline platinum.⁴² The half-width of these humps, with the help of the famous Scherrer formula, show that somewhat larger Pt-particles, with a diameter around 1 nm, also exist in the observed system. Such particles may grow outside of crystal pores by chemical vapor-deposition caused by precursor evaporation during the thermal decomposition procedure. This is in accordance with the fact that a mirror-like layer of platinum condensed on the wall of the glass tube in which the impregnation/decomposition procedure was performed. The simultaneous existence of larger clusters, most probably outside the zeolite crystals, does not distort the finding depicted in Fig. 3 that the procedure employed in this study produces predominantly mono-atomic platinum particles within the zeolite host.

CONCLUSIONS

Platinum was incorporated into the cavities of NaX zeolite crystals by multiple impregnations with Pt(II) acetylacetonate and its subsequent thermal decomposition. Molecular structure considerations indicate that the Pt(II) acetylacetonate molecules may enter the zeolite supercages without molecular rearrangement. However, thanks to the tight fit of the precursor molecule in the supercage orifice, most probably only sequentially may other Pt atoms be introduced inside the zeolite supercages during repetitions of the impregnation/decomposition procedure. This procedure may be characterized as a soft one, which does not cause crushing of the zeolite crystals during the multiple repetitions. The Pt particles were visualized by the high angle annular dark field imaging HRTEM technique, which evidenced that the population of one to a few atoms per supercage prevails.

Acknowledgement. The paper was supported by and realized within the projects No. 142047 (S. M.), and No. MHT.2.09.0022.B (Z. M.) of the Ministry of Science of the Republic Serbia.

ИЗВОД

ЗЕОЛИТ NaX КАО ТЕМПЛАТ ЗА ДОБИЈАЊЕ МОНОАТОМСКИ
ДИСПЕРГОВАНЕ ПЛАТИНЕ ИМПРЕГНАЦИЈОМ СА РАСТВОРОМ
Pt(II)-АЦЕТИЛАЦЕТОНАТА У АЦЕТОНУ

СЛАВКО МЕНТУС¹, ЗОРИЦА МОЈОВИЋ² и ВЕЛИМИР РАДМИЛОВИЋ³

¹Универзитет у Београду, Факултет за физичку хемију, Студентски брз 12, 11000 Београд, ²ИХТМ – Центар за катализу и хемијско инжењерство, Њевошева 12, 11000 Београд и ³National Center for Electron Microscopy, Lawrence Berkeley National Laboratory, University of California, Berkeley, USA

Платина је уграђена у кавезе зеолиита NaX импрегнацијом и термалним разлагањем органометалног једињења Pt(II)-ацетилацетоната, раствореног у ацетону. Висока дисперзност платине претежно у виду једноатомних честица, постигнута је захваљујући блискости димензија молекуле Pt(II)-ацетилацетоната и пречника улазног отвора супекавеза зеолиита. Техником широкоугаоне дифракције и тамног поља ултрависокорезолутивне електронске микроскопије, први пут су учињене видљивим индивидуалне честице платине смештене унутар кристала зеолиита, што отвара нове могућности у проучавању расподеле уграђених металних честица по дубини кристала.

(Примљено 26. октобра 2008, ревидирано 11. јуна 2009)

REFERENCES

1. D. W. Breck, *Zeolite Molecular Sieves: Structure, Chemistry and Use*, Wiley, New York, 1974
2. G. H. K uhl, *Modification of Zeolites in Catalysis and Zeolites: Fundamentals and Applications*, J. Weitkamp, L. Puppe, Eds., Springer, Berlin, 1999, p. 81
3. Y. Wang, H. Wu, Q. Zhang, Q. Tang, *Micropor. Mesopor. Mater.* **86** (2005) 38
4. P. Gallezot, I. Mutin, G. Dalmai-Imelik, B. Imelik, *J. Microsc. Spectrosc. Electron.* **1** (1976) 1
5. P. Gallezot, *Surf. Sci.* **106** (1981) 459
6. A. Tonscheidt, P. L. Ryder, N. I. Jaeger, G. Schulz-Ekloff, *Surf. Sci.* **281** (1993) 51
7. A. Tonscheidt, P. L. Ryder, N. I. Jaeger, G. Schulz-Ekloff, *Zeolites* **16** (1996) 271
8. V. Alfredsson, O. Terasaki, Z. Blum, Jan-Olov Bovin, G. Karlsson, *Zeolites* **15** (1995) 111
9. M. Hartman, C. Bischof, Z. Luan, L. Kevan, *Micropor. Mesopor. Mater.* **44–45** (2001) 385
10. J. W. Li, K. Pfanner, G. Calzaferri, *J. Phys. Chem.* **99** (1995) 2119
11. E. N. Coker, W. A. Steen, J. E. Miller, *Micropor. Mesopor. Mater.* **104** (2007) 236
12. B. Imre, I. Hannus, Z. K onya, J. Kiriczi, *J. Mol. Struct.* **651–653** (2003) 191
13. A. M. Ferrari, K. M. Neyman, T. Belling, M. Mayer, N. R sch, *J. Phys. Chem. B* **103** (1999) 216
14. A. L. Yakovlev, K. M. Neyman, G. M. Zhidomirov, N. R sch, *J. Phys. Chem.* **100** (1996) 3482
15. R. E. Jentoft, M. Tsapatsis, M. E. Davis, B. C. Gates, *J. Catal.* **179** (1998) 565
16. W. A. Weber, B. C. Gates, *J. Catal.* **180** (1998) 207
17. W. A. Weber, B. L. Phillips, B. C. Gates, *Chem. European J.* **5** (1999) 2899
18. W. A. Weber, A. Zhao, B. C. Gates, *J. Catal.* **182** (1999) 13
19. A. G. F. de Souza, A. M. P. Bentes Jr., A. C. C. Rodrigues, L. E. P. Borges, J. L. F. Monteiro, *Catal. Today* **107–108** (2005) 493

20. D. Barthoment, *Catal. Rev.* **38** (1996) 521
21. M. Xu, W. Horsthemke, M. Schell, *Electrochim. Acta* **38** (1993) 919
22. Z. Li, C. M. Wang, L. Persaud, T. E. Mallouk, *J. Phys. Chem.* **92** (1988) 2592
23. C. Iwakura, S. Miyazaki, H. Yoneyama, *J. Electroanal. Chem.* **246** (1988) 63
24. E. N. Coker, W. A. Steen, J. T. Miller, A. J. Kropf, J. E. Miller, *Micropor. Mesopor. Mater.* **101** (2007) 440
25. Y. Zhang, F. Chen, J. Zhuang, Y. Tang, D. Wang, Y. Wang, A. Dong, N. Ren, *Chem. Commun.* (2002) 2814
26. S. Senthilkumar A. Adisa, R. Saraswathi, R. A. W. Dryfe, *Electrochem. Commun.* **10** (2008) 141
27. N. Yao, C. Pinckney, S. Lim, C. Pak, G. L. Haller, *Micropor. Mesopor. Mater.* **44–45** (2001) 377
28. R. Ferreira, M. Silva, C. Freire, B. de Castro, J. L. Figueiredo, *Micropor. Mesopor. Mater.* **38** (2000) 391
29. M. O. de Souza, F. M. T. Mendes, R. F. de Souza, J. H. Z. dos Santos, *Micropor. Mesopor. Mater.* **69** (2004) 217
30. D. O. Klenov, S. Stemmer, *Ultramicroscopy* **106** (2006) 889
31. M. Okumura, T. Tanaka, A. Ueda, M. Haruta, *Solid State Ionics* **95** (1997) 143
32. S. Mentus, Z. Mojović, N. Cvjetičanin, Z. Tešić, *J. New Mater. Electrochem. Syst.* **7** (2004) 213
33. Z. Mojović, S. Mentus, N. Cvjetičanin, Z. Tešić, *Mat. Sci. Forum* **453–454** (2004) 257
34. M. Barrer, A. J. Walzer, *Trans. Faraday Soc.* **60** (1964) 171
35. O. Ursini, E. Lilla, R. Montanari, *J. Hazardous Mater. B* **137** (2006) 1079
36. I. Daems, P. Leflaive, A. Méthivier, G. V. Baron, J. F. M. Denayer, *Micropor. Mesopor. Mater.* **96** (2006) 149
37. J. C. Kevlin, M. G. White, M. B. Mitchell, *Langmuir* **7** (1991) 1198
38. M. Tsuji, P. Jiang, S. Hikino, S. Lim, R. Yano, S.-M. Jang, S.-H. Yoon, N. Ishigami, X. Tang, K. S. N. Kamarudin, *Coll. Surf. A* **317** (2008) 23
39. N. V. Krstajić, Lj. M. Vračar, V. R. Radmilović, S. G. Neophytides, M. Labou, J. M. Jakšić, R. Tunold, P. Falaras, M. M. Jakšić, *Surf. Sci.* **601** (2007) 1949
40. Web Elements, http://www.webelements.com/periodicity/atomic_radius_empirical/
41. Joint Committee on Powder Diffraction Standards (JCPDS), Powder Diffraction File, International Center for Diffraction Data, Swarthmore, PA, 1987, card No. 04-0802.



J. Serb. Chem. Soc. 74 (10) 1125–1132 (2009)
JSCS–3906

The effect of gamma radiation on the properties of activated carbon cloth

DANIJELA R. SEKULIĆ, BILJANA M. BABIĆ, LJILJANA M. KLJAJEVIĆ,
JELENA M. STAŠIĆ and BRANKA V. KALUDJEROVIĆ*

“Vinča” Institute of Nuclear Sciences, Laboratory for Materials Science,
P.O. Box 522, 11001 Belgrade, Serbia

(Received 23 February, revised 9 April 2009)

Abstract: Activated carbon cloth dressing is an appropriate wound healing material due to its biocompatibility and adsorption characteristics. The influence of gamma radiation as a sterilization process on the adsorption and mechanical properties of activated carbon cloth was investigated. The specific surface area, micropore volume, pore size distribution, surface chemistry as well as the breaking load of activated carbon cloth before and after gamma radiation were examined. Characterization by nitrogen adsorption showed that the activated carbon cloth was a microporous material with a high specific surface area and micropores smaller than 1 nm. Gamma radiation decreased the specific surface area and micropore volume but increased the pore width. The sterilization process changed the surface chemistry quantitatively, but not qualitatively. In addition, the breaking load decreased but without any influence considering the further application of this material.

Keywords: activated carbon cloth; dressing material; gamma radiation; adsorption; surface modification.

INTRODUCTION

The potential of activated carbon cloth (ACC) in wound management relates to its ability to adsorb small gas molecules released from a wound, which are produced by anaerobic or proteolytic bacteria.^{1–3} These molecules, which are responsible for the production of malodor, are attracted to the surface of the carbon and are held there by electrical forces.⁴ This occurs due to the microporous structure of ACC consisting of thin slit-like pores that increase the effective surface area of the carbon fibers.^{4,5} The ease of containment, formability, handling and especially the apparent biocompatibility are positive attributes and significant advantages for the application of ACC for dressings. The advantages of

* Corresponding author. E-mail: branka@vinca.rs
doi: 10.2298/JSC0910125S

activated carbon cloth over granulated active carbon or medical gauze are generally a higher pore volume (especially micropore volume) and surface area, which lead to a higher adsorption capacity and faster adsorption–desorption processes.⁶ ACC appears to be useful for the adsorption of low and medium molecular weight organic compounds and bacteria.³

Such dressings can also be supports for therapeutic or antiseptic materials.⁷ The disadvantage is that the agent incorporated into the dressing, inherently limits the bacteria-adsorbing characteristics of the carbon cloth and could adversely affect wound healing.

The adsorption capacity of ACC is controllable and depends on the raw material and the methods and conditions used in the production processes (carbonization and activation processes).^{6,8–12} The pore size, specific surface area and surface chemistry of ACC significantly influence the adsorption capacity. For the adsorption of inorganic and polar organic molecules, both the porous structure and surface chemistry of the adsorbents are important. Carbon–oxygen surface structures, such as carboxyls, lactones, and phenols, are the most important ones affecting the surface characteristics and the properties of activated carbons. The activation is usually achieved by exposing a carbon material to an oxidizing gas, such as steam, air, CO₂, *etc.*, or by mixing the precursor with oxidizing solutions. In addition, the exposure of carbon cloth to CO and CO₂ laser irradiation enhanced the content of surface oxygen complexes.¹¹ The surface chemistry of ACC can be modified using a microwave device as a heat source.¹²

The sterilization process of the examined ACC was performed by γ -radiation. Hence, it is important to determine whether the sterilization process influences the characteristics of the ACC. In this study, the influence of γ -radiation on the adsorption and mechanical characteristics of the ACC were examined.

EXPERIMENTAL

The viscose rayon cloth used as the carbon cloth precursor was soaked in an aqueous solution of a mixture of NH₄Cl and ZnCl₂ before the carbonization process. The carbonization process was performed in a nitrogen flow, which was followed by activation process in a CO₂ flow between 1123 K and 1273 K for 1 h. The ACC samples were washed in distilled water to remove traces of chlorides and other soluble impurities.

The samples were cut to a dressing form and wrapped in an aluminum package and sealed. These packages were then sterilized by γ -radiation. Packages were irradiated with a dose of 25 kGy over three days using a ⁶⁰Co-source.

The adsorption characteristics of the ACC were determined before and after γ -radiation by the standard N₂ adsorption technique at 77 K.¹³ The adsorption and desorption isotherms of N₂ were determined gravimetrically using a McBain balance. From the adsorption isotherm, the specific surface area, S_{BET} , the total pore volume V_{tot} , the micropore volume, V_{mic} , the mesopores and macropores including the external surface area, S_{ext} , and the pore size distribution for the samples were calculated. The specific surface area, S_{BET} , was calculated using the Brunauer–Emmet–Teller (BET) method.¹³ The total pore volume, V_{t} , was expressed

by the Gurwitsch rule using the quantity adsorbed (n) close to saturation, at a relative pressure $p/p_0 = 0.95$.¹³ The Dubinin–Radushkevich (DR) equation was used to calculate the volume of the micropores ($V_{\text{micD-R}}$) of the ACC and the characteristic adsorption energy (E_0).¹⁴

The high resolution α_s -plot proposed by Kaneko *et al.*¹⁵ was used to calculate the external surface area (S_{ext}), the total surface area (S_{tot}) and the micropore volume (V_{mic}). The micropore surface area, S_{mic} , was calculated by subtracting S_{ext} from S_{tot} .

The characteristic size of the slit-shaped pores is their average pore width (L_{sr}). The pore size distribution was estimated by applying the Horvath and Kawazoe (HK)¹⁶ method and the numerical method of Pierce modified by Orr and Dalla Valle.¹³ The HK method is valid for micropores (less than 2 nm) and the modified Pierce method for mesopores (over 2 nm).

The content of oxygen containing surface groups was investigated by the acid–base titration method proposed by Boehm.¹⁷ The samples were contacted with 0.10 M NaHCO_3 , 0.050 M Na_2CO_3 and 0.10 M NaOH solutions. After equilibration for at least 24 h, the excess of each base was estimated by titration with 0.10 M HCl using methyl orange as the indicator.

The breaking loads of the ACC before and after γ -radiation were measured with a Universal Testing Machine, model Instron 1185.

The morphological modification of the surface was examined by scanning electron microscopy (SEM) using a model JEOL-JSM-35 microscope.

RESULTS AND DISCUSSION

The adsorption characteristics of activated carbon cloth before (ACC) and after γ -radiation (ACC_γ) are shown in Fig. 1 by the nitrogen adsorption and desorption isotherms at 77 K. These adsorption isotherms belong to type I isotherms according to IUPAC classification and indicate a microporous material.¹⁸ Many type I isotherms exhibit no hysteresis at all, but the isotherms for ACC display a low pressure hysteresis and the isotherms for ACC_γ display hysteresis over the whole range of measurement (Fig. 1).

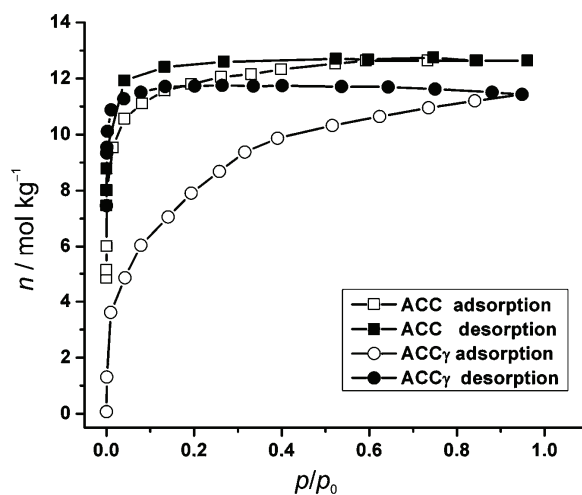


Fig. 1. Nitrogen adsorption/desorption isotherm at 77 K on activated carbon cloth before (ACC) and after γ -irradiation (ACC_γ).

A hysteresis for a relative pressure higher than 0.4 indicates the presence of mesopores. On the other hand, low pressure hysteresis, when the relative pressure is lower than 0.4, means that some adsorbate is retained in the pores. The retained adsorbate persists after prolonged outgassing and can be removed only by pumping at elevated temperatures.

The knees of the nitrogen adsorption isotherms for ACC and ACC γ at 77 K are different (Fig. 1). In the case of adsorption by the ACC (sharp knee), the uptake reached a limiting value, manifested by the plateau in the adsorption isotherm. This means that the net heat of adsorption is high and the micropores are narrow. Slit pores with smaller widths are characterized by having greater adsorption energy due to the superposition of the adsorption potentials of the opposite pore walls. In addition, the plateau of the isotherm was nearly or completely horizontal, and the value of the microporous capacity was close to the uptake at saturation pressure.

When the knee of the isotherm is rounded, as was the case for the ACC γ isotherm (see Fig. 1), the net heat of adsorption is smaller and the micropores are wider. The value of the capacity of the micropores is hard to locate. Therefore, it is quite different from the value of the total capacity derived from the isotherm plateau, and even mesopores could be present. The presence of mesopores was confirmed by the existence of hysteresis (Fig. 1). These observations are quantitatively confirmed by analysis of the further experimental results.

TABLE I. Adsorption characteristics of ACC and ACC γ determined from BET, D-R and α_s -plots

Sample	S_{BET} m ² /g	V_t cm ³ /g	$V_{\text{micD-R}}$ cm ³ /g	E_0 kJ/mol	$V_{\text{mic}\alpha}$ cm ³ /g	S_{tot} m ² /g	S_{ext} m ² /g	S_{mic} m ² /g
ACC	985	0.438	0.393	23.75	0.378	1025	16	1009
ACC γ	668	0.396	0.263	12.59	0.325	884	76	808

The values of specific surface area (S_{BET} and S_{tot}), as well as S_{mic} , were higher for the ACC samples before γ -radiation (Table I). Moreover, the total pore volume V_t was higher before radiation. In addition, S_{ext} was 8.6 % of S_{tot} after the sterilization process, which is higher compared to the proportion of the external area to the total surface area of the starting material (1.6 %). This confirms formation of mesopores during γ -radiation. The values of the microporous volume were higher for the material before radiation, which is confirmed by calculations from both D-R and α_s -plots (Table I).

The values of V_{mic} obtained from these two methods are in disagreement, which was more pronounced for the ACC γ . The branch that corresponds to micropore filling in the D-R plot for ACC γ was not linear, which may cause the lower estimated value for $V_{\text{mic}\alpha}$ (Fig. 2). In addition, this could be a consequence of the broad size distribution of the micropores present in the ACC γ . This was con-

firmed by analysis of the pore size distribution (Fig. 3). The presence of mesopores (pores larger than 2 nm) in the ACC γ samples was also corroborated by this analysis.

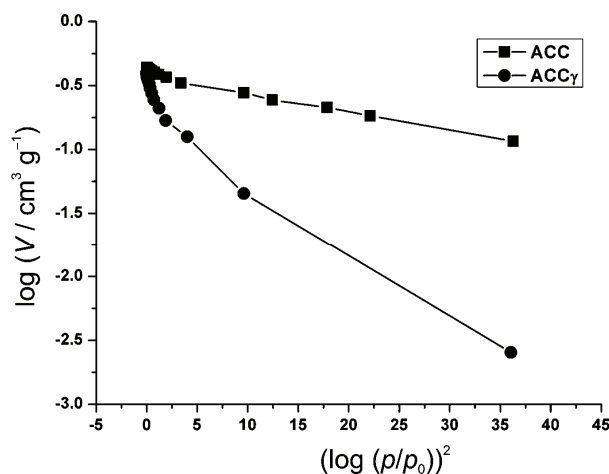


Fig. 2. D-R plots for nitrogen adsorption at 77 K on ACC and ACC γ .

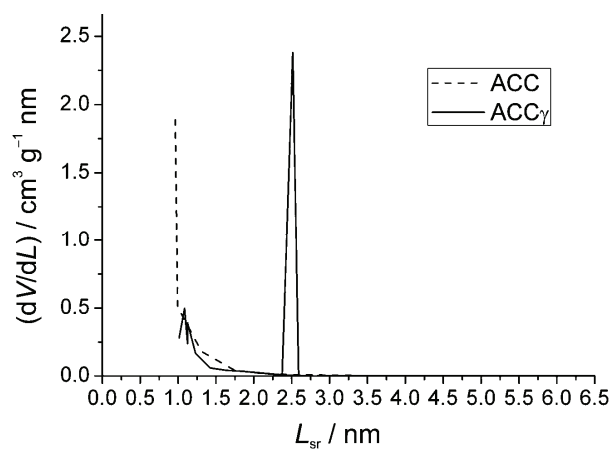


Fig. 3. Pore size distributions for ACC and ACC γ .

The size of the majority of the micropores in the ACC before γ -radiation was below 1 nm (Fig. 3). In such micropores, the mechanism of adsorption is pore filling rather than surface coverage explained by the D-R theory. Hence, the D-R plot, which describes the micropore filling of the ACC, is linear, as shown in Fig. 2. The D-R plot for the ACC γ deviated from linearity at low pressures. This arose from the overlap of the micropore filling process and multilayer adsorption, as a consequence of the broad distribution of pore sizes (Fig. 3). The micropore

volume decreased after the sterilization process. The characteristic energy of adsorption, E_0 , also decreased, which indicates an increase in the pore size (Table I and Fig. 3).

The α_s -analysis also indicated that the sterilization process induced changes in the porous structure. The micropore volume and the total surface area decreased, while the external surface area increased. The decrease of V_{mic} could be explained by changes in the pore size induced by γ -radiation, but the mechanism itself that induced the changes cannot.

TABLE II. Content of acidic oxygen-containing groups on the ACC and ACC γ surface

Sample	Total acidity mol/kg	Content, %		
		Phenolic groups	Lactonic groups	Carboxylic groups
ACC	8.8	41	17	42
ACC γ	12.8	43	16	41

The decrease of the total surface area could be provoked by the increase of the content functional groups on the surface after the sterilization process (Table II). These groups occupied sites at the edges of the pores and in that way decreased surface area.⁶ It can be seen that the content of each group remained the same but the total acidity increased. The small amount of air remaining in the sealed ACC packages, together with the high energy of γ -radiation, was sufficient to induce the formation of oxygen-containing groups in the ACC γ .

The breaking load (the maximum load that the specimen can tolerate without breaking) of the ACC was slightly decreased after γ -irradiation, from 21 to 18 N. This behavior was expected – the wider the pores are, the smaller is the break resistance of the cloth. In addition, sporadic fiber damage is induced by γ -irradiation, especially on the side directly exposed to the radiation, which can be seen in the SEM microphotographs of the ACC γ shown in Fig. 4.

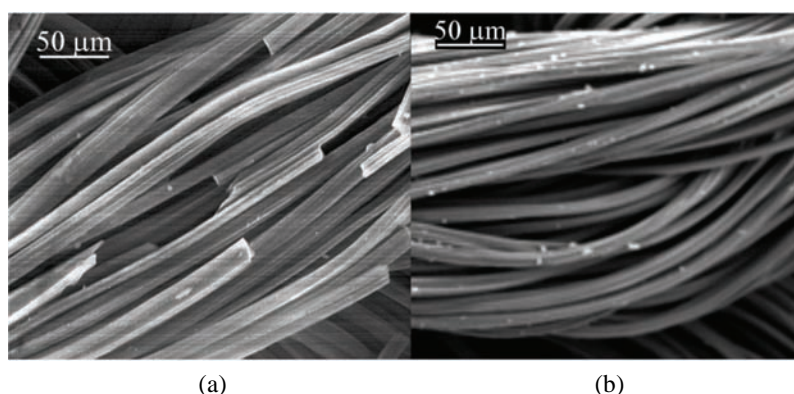


Fig. 4. SEM Microphotographs of ACC γ from: a) side directly exposed to the γ -radiation; b) the opposite side.

CONCLUSIONS

Due to its biocompatibility and developed adsorption characteristics, ACC could be used as a dressing material for healing wounds even without drugs. For this purpose, the influence of ACC irradiation by γ rays on the adsorption and mechanical properties of the activated carbon cloth was examined.

Gamma radiation induced pore widening and the formation of mesopores in the material, which provoked a broad distribution of the pore sizes. These changes promote the retention of adsorbates in the pores and make the material more convenient for further application as a dressing or as a filter material.

Although the content of functional groups after gamma radiation of the ACC remained the same, the total acidity was increased. This induced a decrease of the specific surface area, which was nevertheless still high. Functional groups on the ACC surface, as well as a high surface area, are very important for the adsorption of inorganic and polar organic molecules.

The decrease in the mechanical properties of the ACC after gamma radiation was not so drastic as to make them inappropriate for their future usage.

The obtained results suggest that gamma-irradiation is a suitable technique for the sterilization of activated carbon cloth.

Acknowledgement. This paper was supported by the Ministry of Science and Technical Development of the Republic of Serbia, under Contract No. 142016.

ИЗВОД

УТИЦАЈ ГАМА ЗРАЧЕЊА НА СВОЈСТВА АКТИВНЕ УГЉЕНИЧНЕ ТКАНИНЕ

ДАНИЈЕЛА П. СЕКУЛИЋ, БИЉАНА М. БАБИЋ, ЉИЉАНА М. КЉАЈЕВИЋ,
ЈЕЛЕНА М. СТАШИЋ И БРАНКА В. КАЛУЂЕРОВИЋ

Институт за нуклеарне науке "Винча", Лабораторија за материјале, п. бр. 522, 11001 Београд

Захваљујући биокompatibilности и адсорпционим својствима, завоји од активног угљеничног материјала су врло погодни за лечење рана. Испитиван је утицај процеса стерилизације гама зрачењем на адсорпциона и механичка својства активне угљеничне тканине. Специфична површина, запремина микропора, расподела величине пора, хемија површине, као и прекидна сила, су одређиване пре и после гама зрачења. Карактеризација материјала помоћу адсорпције азота је показала да је активна угљенична тканина микропорозна, велике специфичне површине са микропорама мањим од 1 nm. Гама зрачење смањује специфичну површину и запремину микропора, а повећава ширину пора. Процес стерилизације мења хемију површине квантитативно, али не и квалитативно. Такође се смањује и прекидна сила, али без неког утицаја за даљу примену материјала.

(Примљено 23. фебруара, ревидирано 9. априла 2009)

REFERENCES

1. C. Williams, *Br. J. Nurs.* **9** (2000) 1016
2. C. Williams, *Br. J. Nurs.* **10** (2001) 122
3. P. G. Bowler, B. J. Davies, S. A. Jones, *J. Wound Care* **8** (1999) 216

4. S. Thomas, B. Fisher, P. J. Fram, M. J. Waring, *J. Wound Care* **7** (1998) 246
5. D. A. Morgan, *Formulary of Wound Management Products*, Euromed Communications Ltd., Surrey, 2007, p. 35
6. R. C. Bansal, J. B. Donnet, F. Stoeckly, *Active Carbon*, Marcel Dekker Inc., New York, 1988, p. 27
7. J. Verdu Soriano, J. Rueda Lopez, F. Martinez Cuervo, J. Soldevilla Agreda, *J. Wound Care* **13** (2004) 421
8. L. R. Radović, F. Rodrigues-Reinoso, in *Chemistry and Physics of Carbon*, Vol. 25, P. A. Throter, Ed., Marcel Dekker Inc., New York, 1992, p. 243
9. T. J. Bandoz, M. J. Biggs, K. E. Gubbins, Y. Hattori, T. Iiyama, K. Kaneko, J. Pikunic, K. T. Thomson, in *Chemistry and Physics of Carbon*, Vol. 28, L. R. Radović, Ed., Marcel Dekker Inc., New York, 2003, p. 41
10. P. Burg, D. Cagniant in *Chemistry and Physics of Carbon*, Vol. 30, L. R. Radović, Ed., Marcel Dekker Inc., New York, 2008, p. 130
11. B. V. Kaludjerović, M. Z. Srećković, M. S. Trtica, A. A. Ionin, B. M. Babić, L. M. Milovanovic, *Carbon* **42** (2004) 443
12. J. A. Menéndez, E. M. Menéndez, M. J. Iglesias, A. García, J. J. Pis, *Carbon* **37** (1999) 1115
13. S. J. Gregg, K. S. W. Sing, *Adsorption, Surface Area and Porosity*, Academic Press, London, 1982, p. 195
14. M. M. Dubinin, in *Chemistry and Physics of Carbon*, Vol. 16, P. L. Walker Jr., Ed., Marcel Dekker Inc, New York, 1966, p. 51
15. K. Kaneko, C. Ishii, M. Ruike, H. Kuwabara, *Carbon* **30** (1992) 1075
16. G. Horvath, K. Kawazoe, *J. Chem. Eng. Jpn.* **16** (1983) 470
17. H. P. Boehm, *High Temp.–High Pres.* **22** (1990) 275
18. K. S. W. Sing, D. H. Everett, R. A. W. Haul, L. Moscou, R. A. Pierotti, J. Rouquerol, *Pure Appl. Chem.* **57** (1985) 603.



J. Serb. Chem. Soc. 74 (10) 1133–1142 (2009)
JSCS–3907

Solid phase extraction and a spectrophotometric method for the determination of trace amounts of gold with 4-rhodanineazo benzoic acid

ZHANG JIE HUANG*, XIAO GUO WANG and JUN ZHANG

Department of Chemistry, Yunnan University, Kunming, 650091, P. R. China

(Received 19 January, revised 18 May 2009)

Abstract: The synthesis and application of 4-rhodanineazo benzoic acid (4-BARA) as a new chromogenic reagent for the determination of gold is described. A highly sensitive, selective, and fast method for the determination of gold based on its rapid reaction with 4-rhodanineazo benzoic acid and the solid phase extraction of the colored complex on a reversed phase Clean-up[®] C₅ cartridge was developed. In the presence of 0.02–0.2 mol/L phosphoric acid solution and a polyoxyethylene nonylphenol ether (emulsifier-OP) medium, 4-rhodanineazo benzoic acid reacted with gold to form a colored complex with a gold-to-4-BARA molar ratio of 1:2. The complex was enriched by solid phase extraction with a reversed phase Clean-up[®] C₅ cartridge. The complex was eluted from the cartridge with ethanol and an enrichment factor of 50 was achieved. In ethanol medium, the molar absorptivity of the complex was $2.39 \times 10^5 \text{ L mol}^{-1} \text{ cm}^{-1}$ at 505 nm. The Beer Law was obeyed in the concentration range 0.01–1.2 $\mu\text{g/mL}$. The relative standard deviation for eleven replicate samples at the 0.001 $\mu\text{g/mL}$ level was 2.3 %. In the original sample, the detection limit was $8.0 \times 10^{-5} \mu\text{g/mL}$. This method was applied to the determination of trace amounts of gold in ore samples with good result.

Keywords: 4-rhodanineazo benzoic acid; gold; spectrophotometry; solid phase extraction.

INTRODUCTION

Gold is one of most important noble metals due to its wide application in industry and economic value, yet it is not naturally abundant. Several sophisticated techniques, such as total reflection X-ray fluorescence spectrometry (TXRF), inductively coupled plasma mass spectrometry (ICP–MS), neutron activation analysis, inductively coupled plasma optical emission spectrometry (ICP–OES), electrochemical, spectrofluorimetry, atomic absorption spectrometry, *etc.* have been

* Corresponding author. E-mail: zhjhuang@ynu.edu.cn
doi: 10.2298/JSC0910133H

widely applied to the determination of gold.^{1–12} Some factors, including the cost of the instrumentation, technical know-how, and costly maintenance of equipment restrict wider applicability of these techniques, particularly in fieldwork and in laboratories in developing countries with limited budgets. Thus, the development of a simple, sensitive, and selective method for determination of trace amounts of gold is required.

Spectrophotometric methods are essentially applicable in trace analysis due to their simplicity and low operating costs. Usually they involve the use of chromogenic agents. The already reported chromogenic systems for the determination of gold have specific advantages and disadvantages with respect to sensitivity, selectivity and rapidity.^{13–18} Standard spectrophotometric methods are, however, often not sensitive enough to determine gold ions in geological samples at the $\mu\text{g/L}$ levels. Determination of such low concentrations of gold usually requires a pre-concentration step. For this purpose, solid phase extraction may be utilized due to its apparent advantages.

In this paper, the solid phase extraction of the Au(III)–4-BARA complex on a reversed phase Clean-up[®] C₅ cartridge is described. Based on this, a highly sensitive, selective and rapid method for the determination of gold in ore samples was developed.

EXPERIMENTAL

Apparatus

A UV-1800 spectrophotometer (Shimadzu, Japan) equipped with 1 cm microcell (0.5 mL) was used for all absorbance measurements. The pH was measured using a PHS-3C precision pH meter (REX Instrument Factory, Shanghai, China). The extractions were realized on an UCT solid phase extraction device capable of performing 20 extractions simultaneously and using a reversed phase Clean-up[®] C₅ cartridge (Unitie Chemical Technologies Corporation, United States).

Synthesis of 4-BARA

4-BARA was synthesized according to a previously proposed procedure:¹⁹ 1.37 g (0.0100 mol) of 4-aminobenzoic acid was dissolved in 25 mL of 95 % ethanol in a 100 mL beaker under stirring. To this solution, 10.0 mL of 6.0 mol/L HCl was added and the solution was cooled to 0 °C, 7.0 mL of a 10 % sodium nitrite solution was then slowly added and the reaction was stirred for 15 min to give the respective diazonium salt. In another 200 mL beaker, 1.33 g (0.01 mol) of rhodanine was dissolved in 14 mL of 7.5 mol/L aqueous ammonia and the solution was cooled to 0 °C. The diazonium salt was then added dropwise to the rhodanine solution and the mixture was stirred overnight. The precipitate was isolated by filtration. The crude product was re-crystallized three times with 95 % ethanol to give pure 4-BARA in 75 % yield; its melting point was 258 °C.

Reagents

All employed reagents were of the highest available purity (at least of analytical grade). All solutions were prepared with ultra-pure water obtained from a UPHW-1-90 reagent water system (Ulupure Corporation, China). A 6.0×10^{-3} mol/L 4-BARA solution was prepared by

dissolving 4-BARA in 95 % ethanol. A stock standard solution of gold (1000 $\mu\text{g/mL}$) was obtained from the Chinese Standard Material Center, and a working solution of 0.20 $\mu\text{g/mL}$ was prepared by diluting the stock standard solution. A 1.0 mol/L phosphoric acid was used. Polyoxyethylene nonylphenol ether (emulsifier-OP) solution (2.0 % w/v) was prepared by dissolving 2.0 g of emulsifier-OP in 100 mL of water.

General procedure

To either a standard or a sample solution containing no more than 1.2 μg of Au(III) in a 50 mL volumetric flask, 4.0 mL of a 1.0 mol/L phosphoric acid solution, 4.0 mL of a 6.0×10^{-3} mol/L 4-BARA solution and 3.0 mL of a 2.0 % emulsifier-OP solution were added. The mixture was diluted to the mark and mixed well. After 6 min, the solution was passed through a Clean-up[®] C₅ cartridge at a flow rate of 10 mL/min. After completion of the enrichment step, the retained complex was eluted from the cartridge with 1.0 mL of ethanol at a flow rate of 1.0 mL/min in the reverse direction. The volume of the eluent was adjusted to 1.0 mL in a 1.0 mL volumetric flask by adding a microamount of ethanol with a 200 μL syringe. The absorbance of this solution was measured at 505 nm in a 1.0 cm microcell (0.50 mL) against a reagent blank prepared in a similar way but without gold.

Determination of gold in ores

An ore sample (1.0000 g) was transferred into a porcelain crucible and roasted for 2 h in a muffle furnace at 650 °C. After roasting, the sample was transferred to a 250 mL beaker and 50 mL freshly prepared *aqua regia* was added to the sample. NaCl (0.50 g) was added to stabilize the gold chloride complex during evaporation on a hot plate. The beaker was covered with a watch glass and heated on a hot plate. Heating was continued for at least 4 h and more *aqua regia* was added at regular intervals to maintain the free acid level at about 1 cm above the sample level. The watch glass was then removed and the content was evaporated slowly until the residue became nearly dry. Then 40 mL of 6.0 mol/L HCl was added to the beaker and the solution was warmed until it became clear. Subsequently, the sample solution was cooled and filtered through an 11 μm Whatman No. 1 filter paper. The residue was washed with the minimum amount of 0.10 mol/L HCl. The filtrate was quantitatively collected into a 100 mL volumetric flask and the gold content was analyzed according to the general procedure.

RESULTS AND DISCUSSION

Absorption spectra

The absorption spectra of 4-BARA and the Au(III)–4-BARA complex were recorded. The maximum absorbance of 4-BARA and the Au(III)–4-BARA complex were registered at 415 and 505 nm, respectively. The wavelength of 505 nm was chosen for further quantitative analysis (Fig. 1).

Effect of acidity

The pH of the solution is one of the important factors affecting the formation of complexes; the highest signal intensity of Au was obtained in acidic medium. Therefore, the effect of hydrochloric acid, sulfuric acid, perchloric acid, phosphoric acid, acetic acid, *etc.* on the color reaction of Au(III) with 4-BARA was studied. The results (Fig. 2) showed that phosphoric acid had the best effect and a

concentration of phosphoric acid within the 0.02–0.2 mol/L range was found to give the maximum and constant absorbance. Thus, 4.0 mL of 1.0 mol/L phosphoric acid is recommended.

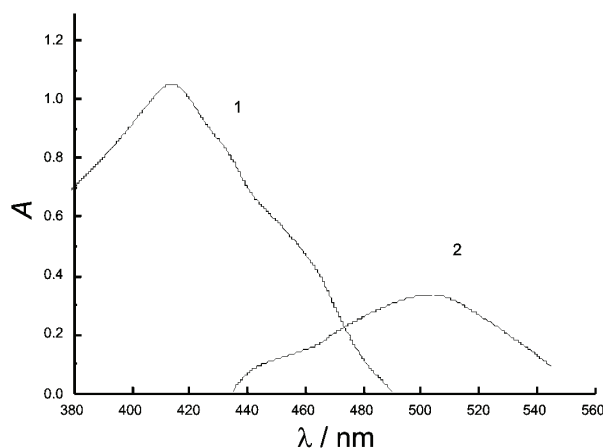


Fig. 1. Absorption spectra of 4-BARA and Au(III)-4-BARA: 1) 4-BARA-emulsifier-OP blank against water; 2) 4-BARA-emulsifier-OP-Au(III) chelate against reagent blank. The concentration of Au(III) was 0.30 $\mu\text{g/mL}$.

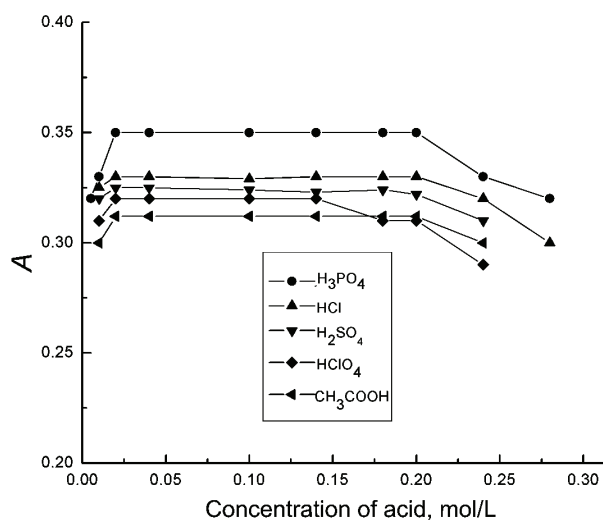


Fig. 2. The effect of acidity on the color reaction of Au(III) with 4-BARA. The absorbance was measured at 505 nm against the corresponding reagent blank. The concentration of Au(III) was 0.30 $\mu\text{g/mL}$. The other conditions were as given in the general procedure.

Effect of surfactants

The Au(III)–4-BARA complex was poorly soluble in aqueous solution. To enhance its solubility, a suitable amount of surfactant had to be added. The experiments showed that all types of surfactants: nonionic (Emulsifier-OP, Tween-20, Tween-60, and Tween-80), cationic (CTAB, CPC) and anionic (SDS and SLES) enhanced the solubility of the complex. Moreover, the nonionic surfactants improved the sensitivity of the determination of the Au(III)-4- BARA complex (Table I).

TABLE I. The effect of the surfactants on the Au(III)–4-BARA chromogenic system

Quantity	Absence	Emulsifier-OP	Tween-			CTAB	CPC	SDS	SLES
			80	60	20				
$\lambda_{\max} / \text{nm}$	490	500	500	500	500	490	490	490	490
$\varepsilon / 10^4 \text{L mol}^{-1} \text{cm}^{-1}$	5.97	23.9	14.3	12.8	10.9	7.68	7.12	6.54	6.38

The molecule of sodium dodecyl sulfate (SDS) has a tail of 12 carbon atoms attached to a sulfate group, giving the molecule amphiphilic properties. Sodium laureth sulfates (SLES) are characterized by the alkyl chain length, the average ethylene oxide (EO) level and the EO distribution. The critical micelle concentration (CMC) value of cetyltrimethylammonium bromide (CTAB) is 0.987 mM in pure water at 298 K. Cetylpyridinium chloride (CPC) is a cationic quaternary ammonium compound containing a pyridinium group and a 16 carbon hydrophobic tail. Polysorbate 20 (Tween-20), polysorbate 60 (Tween-60) and polysorbate 80 (Tween-80) are polysorbate surfactants. The number following the polysorbate part is related to the type of fatty acid associated with the polyoxyethylene sorbitan part of the molecule. Monolaurate is indicated by 20, monostearate by 60 and monooleate by 80.

From the data in Table I, it can be seen that polyoxyethylene nonylphenol ether (emulsifier-OP) is the most appropriate surfactant. Emulsifier-OP is a nonionic surfactant, the molecule of which contains both a hydrophobic tail (nonylphenol part) and a hydrophilic polar head group (ethoxy chain part), which imparts solubility in both aqueous and oil phases and reduces the surface tension of liquids. Emulsifier-OP does not dissociate in aqueous solutions, unlike anionic surfactants with negatively charged molecules and cationic surfactants of positively charged molecules in aqueous solution. Emulsifier-OP is non-ionic in solutions; hence its molecules have no electric charge. Thus, it can be successively employed in hard water at low temperatures and is stable in acidic and alkaline solutions. Emulsifier-OP shows excellent solvency and chemical stability, and is more widely used as a solubilizer than ionic surfactants. A 0.080–0.20 % solution of emulsifier-OP solution provided constant and maximum absorbance in the pre-

sent studies. Accordingly, 3.0 mL of a 2.0 % solution of emulsifier-OP was added in the further measurements.

Effect of 4-BARA concentration

For up to 1.2 μg of Au(III), the use of about 2–6 mL of a 6.0×10^{-3} mol/L 4-BARA solution (Fig. 3) was found to be sufficient for complete reaction. Accordingly, 4.0 mL 4-BARA solution was added in all further measurements.

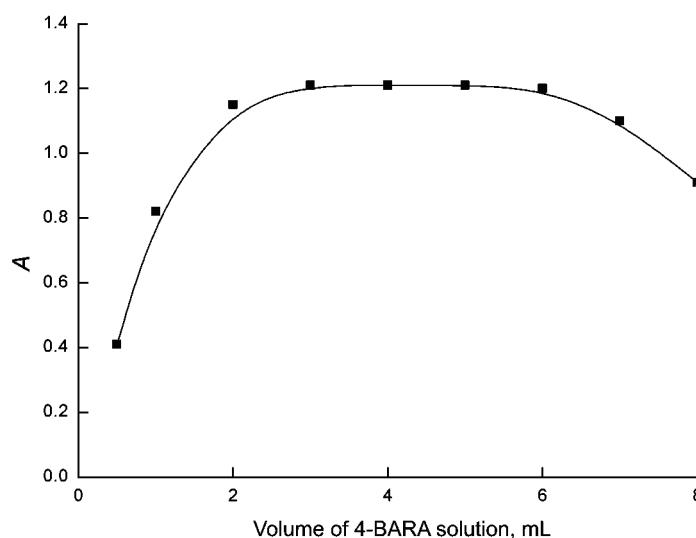


Fig. 3. The effect of the 4-BARA concentration on the color reaction of Au(III) with 4-BARA. The absorbance was measured at 505 nm against the corresponding reagent blank. The concentration of Au(III) was 1.0 $\mu\text{g}/\text{mL}$. The other conditions were as given in the general procedure.

Solid phase extraction

It was shown that 4-BARA forms a stable complex with Au(III) in phosphoric acid medium. To meet the requirement of metal complex enrichment by solid phase extraction in phosphoric acid medium, a Clean-up[®] C₅ cartridge was used. Both enrichment and elution were performed on a UCT SPE device. The flow rate was set to 10 mL/min during the enrichment and to 1 mL/min during elution. It was found experimentally that 4-BARA and its Au(III) complex are quantitatively retained on the cartridge in phosphoric acid medium.

0.10 g of Clean-up[®] C₅, C₈, C₁₀, C₁₂ and C₁₈ sorbents were placed in conical flasks (one cartridge of the Clean-up[®] contained 1.0 g of the sorbent). Stock solutions of Au(III), emulsifier-OP, phosphoric acid and 4-BARA were added to the flask. The solutions were thoroughly mixed using a mechanical shaker. The concentration of Au(III) was measured by ICP-MS as soon as the equilibrium

was attained. The adsorption capacities of the Clean-up[®] cartridges for Au(III) were measured and are given in Table II.

TABLE II. The adsorption capacity of different Clean-up[®] cartridges for Au(III)

Clean-up [®] cartridges	C ₅	C ₈	C ₁₀	C ₁₂	C ₁₈
Adsorption capacity, mmol/g	0.254	0.203	0.178	0.127	0.107

The Clean-up[®] C₅ cartridge was found to have the maximum adsorption capacity for Au(III). It appears that Clean-up[®] C₅ is the most appropriate sorbent for the considered purpose.

Since the maximum amount of Au(III) in the performed experiments was only 6.1×10^{-9} mol, the cartridge (1.0 g) had more than enough capacity to enrich the Au(III)–4-BARA complex.

In order to choose an appropriate eluent for the retained Au(III)–4-BARA complex, after extraction of 6.1×10^{-9} mol of gold from the solution, the gold ions were eluted with different eluting agents, *i.e.*, ethanol, methanol, acetonitrile, isopentylol and acetone. Their elution efficiency decreased in the following sequence: ethanol > isopentylol > methanol > acetonitrile > acetone. Finally, ethanol was selected as the appropriate eluent. Quantitative recovery (>98 %) was obtained using 1.0 mL of ethanol at a flow rate of 1.0 mL/min. In the subsequent experiments, 1.0 mL of ethanol was used as the eluent to desorb the Au(III)–4-BARA complex from the cartridge.

Stability of the chromogenic system

After mixing the components, the absorbance attained its maximum within 6 min at room temperature and remained stable for 5 h in aqueous solution. After extraction into ethanol, the complex was stable for at least 9 h.

Calibration curve and sensitivity

The calibration curve showed that the Beer Law was obeyed in the concentration range ~0.01 to ~1.2 µg Au(III) per mL in the measured solution. The obtained linear regression equation was: $A = 1.23c$ (µg/mL) – 0.0142 ($r = 0.9991$). The molar absorptivity was calculated to be 2.39×10^5 L mol⁻¹ cm⁻¹ at 505 nm. The detection limit, based on 3 times the relative standard deviation of the blank, was 8.0×10^{-5} µg/mL in the original sample.

The relative standard deviation at the concentration level 0.001 µg/mL of Au(III) (11 repeats) was 2.3 %. The quantification limit (*LOQ*) of developed methods was 2.0×10^{-4} µg/mL.

Composition of the complex

The composition of the complex was determined by the continuous variation and the molar ratio method. Both showed that the molar ratio of Au(III) to 4-BARA was 1:2.

Interference

The selectivity of the proposed method is shown in Table III for the determination of 12 µg/mL of Au(III) in the presence of various ions with a relative error of ±5 %. It is evident that most common ions do not interfere with the determination. This method has a high selectivity.

TABLE III. Tolerance limits for the determination of 0.60 µg of Au(III) with 4-BARA (relative error ±5 %)

Ion added	Tolerance, mg
NO ₂ ⁻ , F ⁻ , Cl ⁻ , K ⁺ , SO ₄ ²⁻ , Ca ²⁺	60
Fe ³⁺ , Pb ²⁺ , NO ₃ ⁻ , Cu ²⁺ , Zn ²⁺	30
Na ⁺ , SO ₃ ²⁻ , ClO ₃ ⁻ , Ni ²⁺ , I ⁻	10
Al ³⁺ , S ₂ O ₃ ²⁻ , ClO ₄ ⁻	5
Mg ²⁺ , Ba ²⁺ , Cd ²⁺ , IO ₃ ⁻ , BrO ₃ ⁻	3
Mn ²⁺ , Li ⁺ , Ce(IV), W(VI), Mo(VI), Co ²⁺	2
Ti(IV), Bi(III), Cr(VI), Zr(IV), Fe ²⁺	1
Cr ³⁺ , La ³⁺ , Ag ⁺ , Sn(IV), U(IV), V(V), Th(IV)	0.5
Sr ²⁺ , Sb ³⁺ , Br ⁻ , Os(VIII)	0.2
Se(IV), Rh(III), Te(IV), Hg ²⁺	0.1
Ir(IV), Ru(III)	0.05
Pd ²⁺	0.04

Application to real samples

The developed method was successfully applied to the determination of gold in ore samples (Table IV).

TABLE IV. Determination of gold in ore samples (*n* = 5)

Samples	ICP-MS method	Found	RSD	Recovery
	µg/g	µg/g	%	%
GBW(E)070021	1.38	1.42	3.1	95
GBW(E)070022	1.53	1.56	2.7	97
GBW(E)070023	2.12	2.07	2.9	94

CONCLUSIONS

The proposed method has the following characteristics: 1) 4-BARA is a sensitive and selective spectrophotometric reagent for the determination gold. The molar absorptivity of the Au(III)-4-BARA complex is $2.39 \times 10^5 \text{ L mol}^{-1} \text{ cm}^{-1}$. Most foreign ions do not interfere during the determination. The method is especially selective with respect to noble metal elements, which commonly interfere seriously in the determination of gold performed by literature methods. This is advantageous if traces of gold in ore samples are to be determined directly and 2) the Au(III)-4-BARA complex in 50 mL solution can be concentrated to 1.0 mL, representing an enrichment factor of 50, when solid phase extraction on a Clean-

-up[®] C₅ cartridge is applied. The detection limit is 8.0×10^{-5} $\mu\text{g/mL}$ in original sample and gold can be determined at the $\mu\text{g/L}$ level with good results. 4-Rhodanineazo benzoic acid (4-BARA) is cheap and can be easily synthesized. Its synthesis requires a short reaction time and simple conditions and proceeds with a high yield. Therefore, the proposed method can be applied in routine analysis.

Acknowledgements. This work was supported by the National Natural Science Foundation of China (50764008) and the Development Program of China (2006AA06Z127).

ИЗВОД

ЕКСТРАКЦИЈА ЧВРСОМ ФАЗОМ И СПЕКТРОФОТОМЕТРИЈСКА МЕТОДА ЗА ОДРЕЂИВАЊЕ ТРАГОВА ЗЛАТА СА 4-РОДАНИНАЗОБЕНЗОЕВОМ КИСЕЛИНОМ

ZHANG JIE HUANG, XIAO GUO WANG и JUN ZHANG

Department of Chemistry, Yunnan University, Kunming, 650091, P. R. China

У раду је описана синтеза и примена 4-роданиназо-бензоеве (4-БАРА) киселине као новог хромогеног реагенса. Високо осетљива, селективна и брза метода за одређивање злата базирана је на реакцији са 4-БАРА и екстракцији обојеног комплекса на Clean-up[®] C₅ колони реверсних фаза. У присуству 0,02–0,2 mol/L раствора фосфорне киселине и полиокси-етиленнонилфенил етра (emulsifier-OP) 4-БАРА формира са златом комплекс у стехиометријском односу 2:1. После сорпције на колони комплекс се елуира етанолом, са фактором концентрације 50. У етанолу, коефицијент моларне апсорпције комплекса износи $2,39 \times 10^5$ L mol⁻¹ cm⁻¹ на 505 nm. Зависнос апсорбације од концентрације следи Веер-ов закон у опсегу ~0,01–1,2 $\mu\text{g/mL}$. Релативна стандардна девијација на концентрационом нивоу од 0,001 $\mu\text{g/mL}$ износи 2,3 %, а границе детекције у оргиналном узорку $8,0 \times 10^{-5}$ $\mu\text{g/mL}$. Метода је успешно примењена за одређивање злата у узорцима руда.

(Примљено 19. јануара, ревидирано 18. маја 2009)

REFERENCES

1. C. M. Wang, H. L. Zhang, Y. Sun, H. L. Li, *Anal. Chim. Acta* **361** (1998) 133
2. M. Dequaire, C. Degrand, B. Limoges, *Anal. Chem.* **72** (2000) 5521
3. J. Medved, M. Bujdos, P. Matús, J. Kubová, *Anal. Bioanal. Chem.* **379** (2004) 60
4. Z. Navrátilová, P. Kula, *Fresenius J. Anal. Chem.* **367** (2000) 369
5. T. Venugopal, L. Giridharan, C. Anbuselvan, J. Gandhiraj, *J. Indian Chem. Soc.* **82** (2005) 368
6. Q. S. Pu, P. Liu, Q. Y. Sun, Z. X. Su, *Microchim. Acta* **143** (2003) 45
7. Q. S. Pu, Z. X. Su, Z. D. Hu, X. J. Chang, M. Yang, *J. Anal. At. Spectrom.* **13** (1998) 249
8. B. Tang, H. Zhang, Y. Wang, *Anal. Chim. Acta* **525** (2004) 305
9. R. D. Ye, S. B. Khoo, *Analyst* **124** (1999) 353
10. K. Oguri, G. Shimoda, Y. Tatsumi, *Chem. Geol.* **157** (1999) 189
11. J. Messerschmidt, A. Vonbohlen, F. Alt, R. Klockenkämper, *Analyst* **125** (2000) 397
12. K. Pyrzyńska, *Spectrochim. Acta B* **60** (2005) 1316
13. Z. T. Zeng, Q. H. Xu, *Talanta* **39** (1992) 409
14. Z. T. Zeng, T. McCreedy, A. Townshend, *Anal. Chim. Acta* **401** (1999) 237
15. M. Gangadharappa, R. P. Raveendra, R. V. Krishna, R. T. Sreenivasulu, *J. Indian Chem. Soc.* **81** (2004) 525

16. Z. J. Li, J. M. Pan, J. Tang, *Anal. Bioanal. Chem.* **375** (2003) 408
17. A. Pal, *Talanta* **46** (1998) 583
18. F. M. El-Zawawy, M. F. El-Shahat, A. A. Mohamed, M. T. M. Zaki, *Analyst* **120** (1995) 549
19. Z. J. Huang, F. Huang, Q. Y. Xie, *Chinese J. Anal. Lab.* **26** (2007) 38.



J. Serb. Chem. Soc. 74 (10) 1143–1153 (2009)
JSCS–3908

Validation of an HPLC–UV method for the determination of digoxin residues on the surface of manufacturing equipment

ZORAN B. TODOROVIĆ^{1*#}, MIODRAG L. LAZIĆ^{1#}, VLADA B. VELJKOVIĆ^{1#}
and DRAGAN M. MILENOVIĆ^{2#}

¹Faculty of Technology, Bulevar oslobođenja 124, 16000 Leskovac, University of Niš and

²“Zdravlje-Actavis“ Company, Analytical Department, Vlajkova 199, 16000 Leskovac, Serbia

(Received 25 February, revised 15 May 2009)

Abstract: In the pharmaceutical industry, an important step consists in the removal of possible drug residues from the involved equipments and areas. The cleaning procedures must be validated and methods to determine trace amounts of drugs have, therefore, to be considered with special attention. An HPLC–UV method for the determination of digoxin residues on stainless steel surfaces was developed and validated in order to control a cleaning procedure. Cotton swabs, moistened with methanol were used to remove any residues of drugs from stainless steel surfaces, and give recoveries of 85.9, 85.2 and 78.7 % for three concentration levels. The precision of the results, reported as the relative standard deviation (*RSD*), were below 6.3 %. The method was validated over a concentration range of 0.05–12.5 µg mL⁻¹. Low quantities of drug residues were determined by HPLC–UV using a Symmetry C18 column (150×4.6) mm, 5 µm) at 20 °C with an acetonitrile–water (28:72, v/v) mobile phase at a flow rate of 1.1 mL min⁻¹, an injection volume of 100 µL and were detected at 220 nm. A simple, selective and sensitive HPLC–UV assay for the determination of digoxin residues on stainless steel was developed, validated and applied.

Keywords: cleaning validation; digoxin; swab analysis; residues.

INTRODUCTION

An important step in the manufacture of pharmaceutical products is the cleaning of equipment and surfaces. The cleaning procedures for the equipment must be validated according to good manufacture practice (GMP) rules and guidelines. The main objective of cleaning validation is to avoid contamination between different productions or cross-contamination. This cleaning is verified by determining the amount of residues on surfaces involved in the manufacture process.

* Corresponding author. E-mail: todoroviczoran@yahoo.com

Serbian Chemical Society member.

doi: 10.2298/JSC0910143T



Cleaning validation consists of two separate activities: the first is the development and validation of the cleaning procedure used to remove drug residues from manufacturing surfaces and the second involves the development and validation of methods for quantifying residuals from the surfaces of manufacturing equipment. Furthermore, many sampling points of the manufacturing facility and the manufacturing equipment have to be tested to verify the occurrence of contamination. For these reasons, an analytical method for residue monitoring should also be rapid and simple.¹

The acceptable limit for residue in equipment is not established in the current regulations. According to the FDA, the limit should be based on logical criteria, involving the risks associated with residues of a determined product. The calculation of an acceptable residual limit, the maximum allowable carryover of active products in production equipment should be based on therapeutic doses, the toxicological index and a general limit (10 ppm). Several mathematical formulas were proposed to establish the acceptable residual limit.¹⁻⁷

Digoxin (Fig. 1) is a cardioactive glycoside isolated from the leaves of *Digitalis lanata* and is the most frequently used drug in the treatment of congestive heart failure.⁸ Numerous methods have been published for the quantitative determination of digoxin in raw materials,⁹⁻¹³ tablets,¹⁴⁻¹⁸ other solid dosage forms,¹⁹ human plasma, urine, serum²⁰⁻²³ and *Digitalis* leaves.^{24,25}

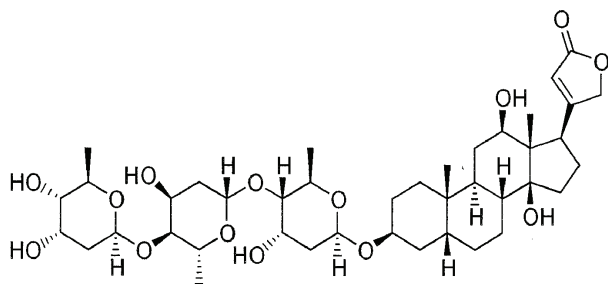


Fig. 1. Chemical structure of digoxin.

A literature survey revealed that no validation of cleaning methods for digoxin is to be found. Due to their high sensitivity and selectivity, analytical methods such as liquid chromatography were previously reported to be used for the determination of residues to control cleaning procedures.^{5-7,26-32}

Taking the above-mentioned consideration into account, the aim of this study was to develop and validate a simple analytical method that allows the determination of trace levels of digoxin residues in production area equipment and to confirm the efficiency of the cleaning procedure. The analytical method reported was validated considering selectivity, linearity, accuracy, precision and limits of detection (*LOD*) and quantification (*LOQ*). The stability of digoxin samples was also studied.³³

EXPERIMENTAL

Chemicals and reagents

The certified digoxin, working standard was purchased from Roche Diagnostics GmbH (Mannheim, Germany). Acetonitrile and methanol (HPLC gradient grade) were purchased from J. T. Baker (Deventer, Holland). Purified water was obtained from Arium Laboratory Equipment (RO, UV) Sartorius AG (Gottingen, Germany). The extraction–recovery sampling was realized with Alpha[®] Swab polyester on a polypropylene handle – TX714A (ITW Tex-wipe[®], Mahwah, NJ, USA). The mobile phase was filtered through a 0.45 µm Sartorius membrane filter (Gottingen, Germany).

Equipment

The HPLC system consisted of a degasser G1379B, a bin pump G1312A, an automatic injector G1329A, a thermostated column oven G1316A and a multiwavelength detector G1365B, all 1200 Series from Agilent Technologies, which were controlled by an HP Chemstation software (Waldbrook, Germany). The employed ultrasonic bath was from Elma, Transonic 470/H (Singen, Germany) and the analytical balance was from Sartorius AG, CP224S – OCE (Gottingen, Germany); accuracy of the balance: ± 0.0001 g.

Chromatographic conditions

All chromatographic experiments were performed in the isocratic mode. The mobile phase was acetonitrile-water (28:72, v/v) at a flow rate of 1.1 mL min⁻¹. The separation was performed at 20 °C on a Symmetry C18 column ((150×4.6) mm, 5 µm) from Waters (Milford, MA, USA). UV detection was realized at 220 nm. The injection volume was fixed at 100 µL.

Standard solutions preparation

The stock solution of standard was prepared by accurately weighing digoxin standard (approximately 12.5 mg) and transferring it into a 100 mL volumetric flask. Approximately, 20 mL of methanol was added and the content of the flask was sonified for 15 min. The solution in the flask was diluted to volume with 20 mL acetonitrile and water; the final concentration being 125 µg mL⁻¹ digoxin. Dilutions were later prepared with water to obtain solutions for calibration (0.05–12.5 µg mL⁻¹) and standard solution for the positive swab control at three concentration levels (0.625, 3.125, and 15.625 µg per swab level). These solutions were filtered through a 0.45 µm regenerated cellulose filter before analysis and injected in triplicate.

Sample preparation

The selected surfaces (5 cm×5 cm) of stainless steel, previously cleaned and dried, were sprayed with 500 µL of a standard solution, for the positive swab control at all concentration levels, and the solvent was allowed to evaporate (approximate time was 2 h). The surfaces were wiped with the first cotton swab soaked with methanol, passing it in various directions, to remove the residues from the stainless steel. The other dry cotton swab was used to wipe the wet surfaces. The swabs were placed into a 25 mL screw cap test tube, and 5.0 mL of the purified water was pipetted into adequate sample tubes. The background control sample was prepared from the extraction media. The negative swab control was prepared in the same way as the samples, using swabs, which had not been in contact with the test surface. In addition, test and excipient solutions were prepared according to the content of tablets to assure that they did not interfere with digoxin. Subsequently, the tubes were placed in an ultrasonic bath for 15 min and the solutions were analyzed by HPLC–UV.

RESULTS AND DISCUSSION

Acceptance limit calculation

The maximum allowable carryover (MACO) is the acceptable transferred amount from the previous to the following product. The MACO is determined based on the therapeutic dose, toxicity and generally 10 ppm criterion. Once the maximum allowable residue limit in the subsequent product was determined, the next step was the determination of the residue limit in terms of the contamination level of active ingredient *per* surface area of equipment. The total surface area of the equipment in direct contact with the product was accounted for in the calculations. The limit per surface area was calculated from the equipment surface area and the most stringent maximum allowable carryover (the most stringent criterion being based on the therapeutic dose in this case). The 0.1 % dose limit criterion is justified by the principle that an active pharmaceutical ingredient (API) at a concentration of 1/1000 of its lowest therapeutic dose will not produce any adverse effects on human health. The calculated limit per surface area (LSA) in the case of digoxin was $1.20 \mu\text{g swab}^{-1}$ *pro* 25 cm^2 . A stainless steel surface area of $5 \text{ cm} \times 5 \text{ cm}$ was chosen for practical reasons.

Optimization of the chromatographic conditions

To obtain the best chromatographic conditions, the wavelength for detection, the column and the mobile phase composition were adequately selected. The main objective was to develop an HPLC–UV method that, running in the isocratic mode, allowed the determination of digoxin residues collected by swabs, without interference of impurities originating from the swabs, plates and extraction media.

For the analysis, 220 nm was selected for detection because the drug has a sufficient absorption at this wavelength and low quantities of digoxin may be detected correctly. Furthermore, the calibration curve obtained at 220 nm showed good linearity.

Regarding the chromatographic procedure, different C18 columns were evaluated: LiChrosorb RP-18, Nucleosil C-18, μ Bondapak C-18, but Symmetry C-18 ((150 \times 4.6) mm, 5 μm) was preferred to improve the peak symmetry and to obtain an appropriate retention time.

A mixture of acetonitrile–water in different proportions is frequently used as the mobile phase. In order to improve the selectivity and sensitivity, the amount of acetonitrile was varied between 20 and 40 vol. %. The best separation was achieved with the proposed mobile phase acetonitrile–water (28:72, v/v) at a flow rate of 1.1 mL min^{-1} . Furthermore, with decreasing flow rate, the column back-pressure is lower and hence the column life is prolonged.

The injection volume was varied between 10 and 100 μL and was finally set at 100 μL in order to increase the sensitivity of the method without sacrificing the chromatographic peak shape. Taking into account the results obtained with

different C18 columns and the tested mobile phases, the already defined chromatographic conditions were finally chosen. The sensitivity achieved by this method was much better than the initial method given by Song *et al.*,⁹ which was modified in order to accommodate the requirements of trace analysis specific for a cleaning validation study.

Optimization of the sample treatment

Cotton swabs were spiked with different quantities of digoxin and placed into glass tubes. After the addition of different solvents (water, methanol and the mobile phase), the tubes were sonified for different times (5, 15 and 30 min) and the solutions analyzed by HPLC. The optimum conditions were achieved with water as the extracting solvent and a sonification time of 15 min. In all cases, the best results were obtained using two cotton swabs (the first wetted with methanol and the second dry); hence, this technique was applied in the subsequent work.

Validation of the method

Once the chromatographic conditions had been selected, the method was validated, whereby attention was paid to the selectivity, linearity, limit of detection, limit of quantification, precision, accuracy and sample stability.

Suitability test. System suitability testing is essential for the assurance of the quality performance of a chromatographic system. During performing the system suitability tests, in all cases, *RSD* of the peak areas was $< 2\%$, the average number of theoretical plates per column was > 5500 and the USP tailing factor was about 1.08.

Selectivity. The selectivity of the method was checked by injecting the digoxin standard, the background control sample, the negative swab control, the unspiked stainless steel 5 cm \times 5 cm plate swabbed as described and the excipient mixture (according to the content of the tablets). The results are shown in Fig. 2, from which it can be observed that there were no mutual interferences.

Linearity. Linearity data were obtained by plotting the area of the digoxin peak, expressed in area units, against the concentration of digoxin, expressed as $\mu\text{g mL}^{-1}$. A linear regression least square analysis was performed in order to determine the slope, intercept and coefficient of determination. The standard curve was linear from 0.05–12.5 $\mu\text{g mL}^{-1}$. The values of the slope, intercept and coefficient of determination of the calibration curve for digoxin are given in Table I. The high value of the coefficient of determination indicated good linearity.

Limit of detection and quantification. *LOD* and *LOQ* were determined based on the standard deviation of the response (*y*-intercept) and the slope of the calibration curve at low concentration levels according to ICH guidelines. The *LOD* and *LOQ* for digoxin were found to be 0.010 and 0.030 $\mu\text{g mL}^{-1}$, respectively.

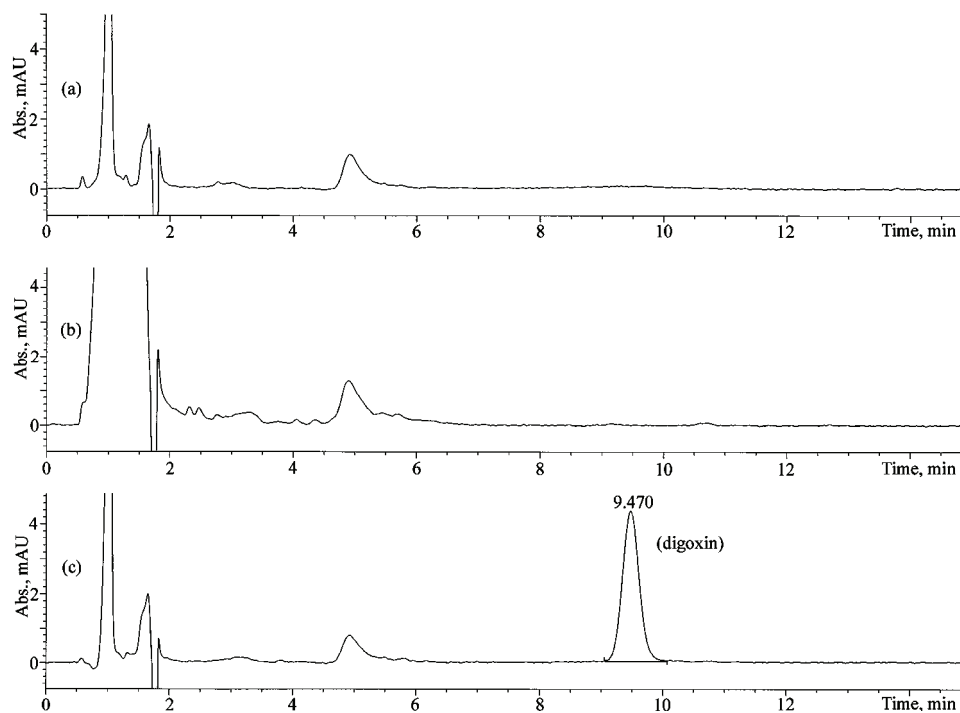


Fig. 2. Chromatograms obtained from: a) non-spiked stainless steel surface, b) excipient mixture and c) standard solution of digoxin ($1.25 \mu\text{g mL}^{-1}$).

TABLE I. Linear regression data in the analysis of digoxin

Statistical parameters	Values
Concentration range, $\mu\text{g mL}^{-1}$	0.050–12.50
Regression equation	$y = 64.342x + 4.7658$
Coefficient of determination	$r^2 = 0.9999$
$S(a)$ -error in intercept	2.684
$S(b)$ -error in slope	0.428
$S(y/x)$ -error for y -est	0.195

Precision and accuracy. The precision and accuracy of the procedure, reported as relative standard deviation (*RSD*) and the recovery (%), respectively, were assessed by comparing the amount of analyte determined *versus* the known amount spiked at three different concentration levels with 6 replicates ($n = 6$) for each investigated concentration level. The method precision and accuracy were determined for spiked and dried swabs and plates. The recovery, 95 % confidence interval, and the *RSD* values obtained on spiked and dried swabs and plates (Table II) for each level illustrated the good precision and accuracy of the method. These precision and recovery results are acceptable for the purpose of residue monitoring.

TABLE II. Precision and accuracy of the results obtained from swabs and plates spiked with digoxin

Samples	Amount added $\mu\text{g mL}^{-1}$	Amount found $\mu\text{g mL}^{-1}$	95 % Confidence interval, %	Recovery %	RSD / % $n = 6$
Swabs	0.125	0.116	92.3–93.2	92.7	3.1
	0.625	0.580	89.8–95.2	92.5	3.6
	3.125	2.836	89.9–91.6	90.7	0.6
Plates	0.125	0.107	83.5–86.3	85.9	3.0
	0.625	0.530	80.9–89.5	85.2	6.3
	3.125	2.461	77.1–80.4	78.7	1.3

The intermediate precision of the method was investigated by performing five consecutive injections of standard solutions on two different days by different analysts. On both days, the *RSD* was calculated for peak area responses obtained for the digoxin peak. The data obtained suggested that the method exhibited an acceptable intermediate precision with less than 1.0 % *RSD* for the digoxin standard solution when analyzed on two different days by two different analysts.

Sample stability. The stability of the digoxin in the swab matrix was tested. The spiked samples at all concentration levels were stored after analyses in the injector vials in the auto-sampler tray at ambient temperature for 7 days. All the samples were injected into the appropriate HPLC system after 24 h, 48 h and 7 days against fresh standard solutions. The stability of the standard digoxin solution ($1.25 \mu\text{g mL}^{-1}$) was also inspected after storage for 7 days at ambient temperature and refrigerated. No changes in the chromatography of the stored samples were found and no additional peaks were registered when compared with the chromatograms of the freshly prepared samples (Table III).

TABLE III. Stability results obtained from digoxin swab extract samples

Sample ($n = 3$) $\mu\text{g per swab}$	Mean recovery $\pm IC^a$, %			
	0 h	24 h	48 h	7 days
0.625	92.2 \pm 1.7	93.5 \pm 1.8	92.6 \pm 1.0	93.2 \pm 0.6
3.125	90.2 \pm 1.3	90.6 \pm 1.5	90.7 \pm 0.8	90.1 \pm 0.8
15.62	88.9 \pm 1.2	89.3 \pm 0.8	89.3 \pm 1.1	88.9 \pm 1.3

^aInterval of confidence

Assay of swab samples collected from different locations within the equipment train

Swab samples from different locations within the manufacturing equipment train were submitted to the laboratory for analysis of residual digoxin. These samples were prepared and analyzed by the proposed method. Some of the results obtained for these samples are presented in Table IV. An example of a chromatogram which originated from Glatt WSG (Bowl bottom mesh point), which is below the limit per surface area (LSA) and above the LOQ is shown in Fig. 3.

TABLE IV. Results obtained for the determination of digoxin in actual swab samples collected from 25 cm² swabbed area from different locations within the equipment train

Equipment swabbed	Location swabbed	Digoxin detected, µg per swab
Material dispensing scoops	Internal surface	<LOQ
	Back round plate	<LOQ
	External surface	<LOQ
High shear mixer – Diosna	Bottom of gran. bowl	<LOQ
	Chopper shaft	<LOQ
	Impeller blade	<LOQ
Turbo sieve – Bohle	Stainless steel inlet ring	0.24(<LSA ^a)
	Product inlet, side wall	<LOQ
	Sieve unit	<LOQ
Fluid bed dryer – Glatt WSG	Inside wall	<LOQ
	Viewing window	<LOQ
	Bowl bottom mesh	0.87(<LSA)
Pillar hoist – FBD bowl inverter	Internal surface-top	<LOQ
	Internal surface-bottom	<LOQ
	Collar	<LOQ
Washer – extractor Miele	Drum back plate	<LOQ
	Drum perforated surface	<LOQ
	Door-middle	<LOQ
Metal detector – Lock Met 30+	In-feed chute	0.223(<LSA)
	Reject device, corner	<LOQ
	Reject flap	<LOQ
Deduster – Kramer	Inlet plate	0.277(<LSA)
	Dedusting helix	<LOQ
	Outlet	<LOQ
Tablet press – Kilian	The table	0.357(<LSA)
	Tablet chute cover	<LOQ
	Main gate	0.355(<LSA)

^aLimit per surface area

CONCLUSIONS

In conclusion, a simple to use HPLC–UV method to quantify residues of the active pharmaceutical ingredient digoxin on swabs, in support of cleaning validation of pharmaceutical manufacturing equipment, was developed. Validation studies showed that the HPLC–UV method is selective, linear, precise and accurate. To extract the digoxin residues from the surfaces, a wipe test procedure using two cotton swabs is recommended. The recoveries obtained from the stainless steel surfaces were close to 80 % or higher and there was no interference from the cotton swab. Stability studies show that the digoxin swab samples are, at least, stable over the investigated 7 days. The overall procedure can be used as part of a cleaning validation program in the pharmaceutical manufacture of digoxin.

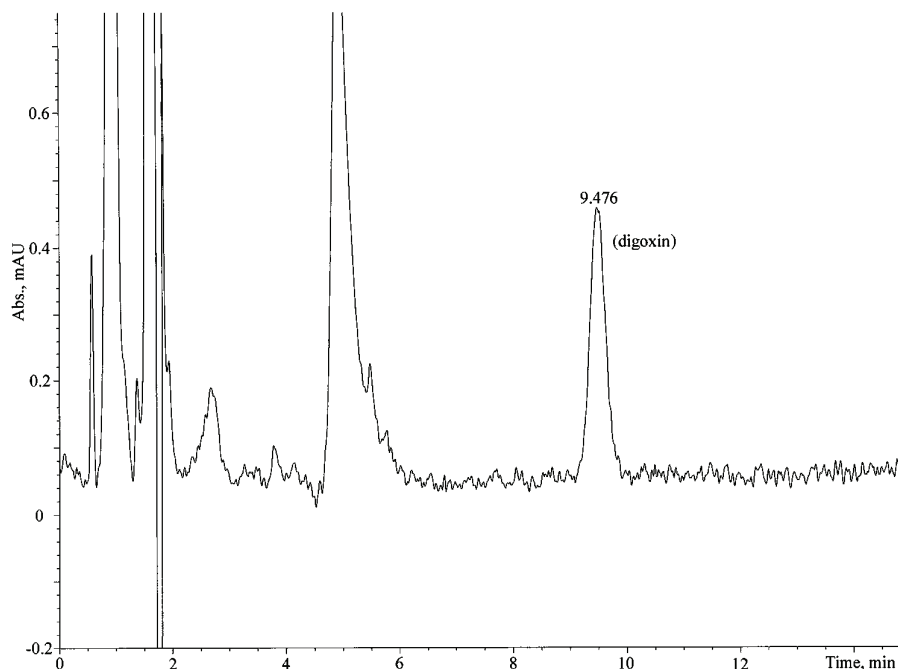


Fig. 3. Example of a chromatogram from a swab sample (Glatt WSG-Bowl bottom mesh point).

ИЗВОД

ВАЛИДАЦИЈА HPLC–UV МЕТОДЕ ЗА ОДРЕЂИВАЊЕ ОСТАКА
ДИГОКСИНА НА ПОВРШИНИ ПРОИЗВОДНЕ ОПРЕМЕ

ЗОРАН Б.ТОДОРОВИЋ¹, МИОДРАГ Л. ЛАЗИЋ¹, ВЛАДА Б. ВЕЉКОВИЋ¹ и ДРАГАН М. МИЛЕНОВИЋ²

¹Технолошки факултет, Булевар ослобођења 124, 16000 Лесковац, Универзитет у Нишу

²“Здравље-Actavis“, Одељење аналитичког развоја, Влајкова 199, 16000 Лесковац

У фармацеутској индустрији, веома битан елемент представља уклањање могућих остатака активних супстанци са опреме и других површина укључених у производни процес. Процедура чишћења мора бити потврђена, те се стога мора посветити посебна пажња методи за одређивање остатака активних супстанци у траговима. Развијена је и потврђена HPLC–UV метода за одређивање остатака дигоксина на челичним површинама да би се контролисала процедура чишћења. Памучни брисеви, квашени метанолом, коришћени су за уклањање остатака дигоксина са челичне површине, а добијене вредности за прекривање износиле су 85,92, 85,22 и 78,74 %, на три концентрациона нивоа. Прецизност резултата, представљена као релативна стандардна девијација (*RSD*), била је испод 6,3 %. Метода је потврђена у опсегу концентрација 0,05–12,5 $\mu\text{g mL}^{-1}$. Мале количине остатака дигоксина одређене су помоћу HPLC коришћењем Symmetry C18 колоне ((150×4,6) mm, 5 μm), на 20 °C, са мобилном фазом ацетонитрил–вода (28:72, v/v) и протоком од 1,1 mL min⁻¹, инјекционом запремином од 100 μL и таласном дужином за детекцију од 220 nm. Коришћењем поменутих процедуре, развијена је, потврђена и примењена једноставна, селективна и осетљива HPLC–UV метода за одређивање остатака дигоксина на челичним површинама.

(Примљено 25. фебруара, ревидирано 15. Маја 2009)

REFERENCES

1. *Guide to Inspections Validation of Cleaning Processes*, U.S. Food and Drug Administration, (FDA), Office of Regulatory Affairs, Washington, DC, pp. 1–6, http://www.fda.gov/ora/inspect_ref/igs/valid.html (accessed 20 April, 2009)
2. *Cleaning Validation Guidance, Guidance on aspects of cleaning validation in active pharmaceutical ingredient plants*, <http://apic.cefic.org/pub/pub-cleaning-validation.pdf> (accessed 20 April, 2009)
3. *Guide to Cleaning Validation in API plants, Cleaning Validation in Active pharmaceutical ingredient manufacturing plants*, available at: <http://apic.cefic.org/pub/4CleaningVal9909.pdf> (accessed 20 April, 2009)
4. *World Health Organization, Supplementary guidelines on good manufacturing practices (GMP): Validation*, Working document QAS/03.055/Rev.2, pp. 24–33, http://www.who.int/medicines/services/expertcommittees/pharmprep/Validation_QAS_055_Rev2combined.pdf (accessed 20 April, 2009)
5. R. Klinkenberg, B. Strel, A. Ceccato, *J. Pharm. Biomed. Anal.* **32** (2003) 345
6. T. T. Fazio, A. K. Singh, E. R. M. Kedor-Hackmann, M. I. R. M. Santoro, *J. Pharm. Biomed. Anal.* **43** (2007) 1495
7. T. Mirza, M. J. Lunn, F. J. Keeley, R. C. George, J. R. Bodenmiller, *J. Pharm. Biomed. Anal.* **19** (1999) 747
8. D. Belachew, K. M. McErlane, *J. Pharm. Sci.* **71** (1982) 777
9. M. Song, M. Li, X. Hu, *CA* 143:139350 [2005:435677]
10. B. Pekić, B. Slavica, *Memoir of Matica Srpska for natural Sciences* **84** (1993) 73
11. D. M. Popova, T. N. Konyakhina, V. A. Semenova, A. P. Arzamastsev, *Farm. Zhurnal (Kiev)* **3** (1983) 44 (in Russian)
12. D. Belachew, E. Kwong, K. M. McErlane, *J. Chromatogr.* **240** (1982) 137
13. M. C. Castle, *J. Chromatogr.* **115** (1975) 437
14. Q. Zhang, *CA* 144:94565 [2005:1317285]
15. X. Ouyang, Y. He, *CA* 142:397882 [2005:236821]
16. D. Ivanović, M. Medenica, D. Radulović, Z. Djugumović, *Drug Dev. Ind. Pharm.* **21** (1995) 1789
17. T. Hagiwara, K. Nakayama, K. Akiyama, M. Doguchi, *CA* 111:140376 [1989:540376]
18. T. Hagiwara, K. Akiyama, *CA* 106:144053 [1987:144053]
19. T. Sugiyama, R. Matsuyama, S. Usui, Y. Katagiri, K. Hirano, *Biol. Pharm. Bull.* **23** (2000) 274
20. V. S. M. Varma, N. Kapoor, M. Sarkar, R. Panchagnula, *J. Chromatogr. B* **813** (2004) 347
21. E. Reh, H. Jork, *Fres. Zeitsch. Anal. Chem.* **318** (1984) 264
22. A. J. Morais, A. R. Zlotecki, E. Sakmar, L. P. Stetson, G. J. Wagner, *Res. Comm. Chem. Pathol. Pharmacol.* **31** (1981) 285
23. S. Shi, Z. Li, H. Chen, F. Zeng, *J. Chromatogr. B* **875** (2008) 405
24. C. B. Fernao, K. Wolfgang, A. R. Rubens, B. O. Alaide, *Quimica Nova* **20** (1997) 481 (in Portuguese)
25. Y. Ikeda, Y. Fujii, M. Yamazaki, *J. Nat. Prod.* **55** (1992) 748
26. M. J. Nozal, J. L. Bernal, J. J. Jimenez, M. T. Martin, F. J. Diez, *J. Chromatogr. A* **1024** (2004) 115
27. M. J. Nozal, J. L. Bernal, L. Toribio, M. T. Martin, F. J. Diez, *J. Pharm. Biomed. Anal.* **30** (2002) 285

28. M. J. Nozal, J. L. Bernal, L. Toribio, M. T. Martin, F. J. Diez, *J. Chromatogr. A* **919** (2001) 87
29. J. Lambropoulos, G. A. Spanos, N. V. Lazaridis, *J. Pharm. Biomed. Anal.* **23** (2000) 421
30. N. Fakutsu, T. Konse, T. Kawasaki, K. Saito, H. Nakazawa, *J. Pharm. Biomed. Anal.* **41** (2006) 599
31. M. B. Boca, Z. Apostolides, E. Pretorius, *J. Pharm. Biomed. Anal.* **37** (2005) 461
32. D. M. Milenović, M. L. Lazić, V. B. Veljković, Z. B. Todorović, *Acta Chromatogr.* **20** (2008) 183
33. *International Conference on Harmonization Q2 (R1), Validation of Analytical Procedures, Text and Methodology*, <http://www.ich.org/LOB/media/MEDIA417.pdf> (accessed 20 April, 2009).